Miniature treadmills reveal proprioceptive mechanisms in walking *Drosophila*

Brandon Pratt

A dissertation

submitted in partial fulfillment of the

requirements for the degree of

Doctor of Philosophy

University of Washington

2024

Reading Committee:

John C Tuthill, Chair

Chip Asbury

Bing Wen Brunton

Program Authorized to Offer Degree:

Physiology & Biophysics

University of Washington

Abstract

Miniature treadmills reveal proprioceptive mechanisms in walking *Drosophila*

Brandon Pratt

Chair of the Supervisory Committee:
John C Tuthill
Physiology & Biophysics

As animals navigate in an unpredictable and ever-changing world, their movement is bombarded by unanticipated perturbations. Proprioception, the sense of how the body is articulated and moving in space, enables animals to rapidly overcome these perturbations to avoid predators and to find mates, shelter, and food. However, it has been challenging to study the role of proprioception in adaptive movement because of the lack of tools to precisely perturb animal locomotion and the diminishment of spontaneous locomotion after manipulating proprioceptive neural circuits. To overcome these limitations, I engineered miniature treadmill systems for the genetic model organism, *Drosophila melanogaster*, that enable robust locomotion in flies lacking proprioceptive feedback, calibrated perturbations to walking, and quantifications of 3D walking kinematics. Using these systems, I found that proprioceptive feedback controls step kinematics across walking speeds, the middle legs of flies correct for asymmetric perturbations, and a class of proprioceptive neurons, called hair plates, facilitate the swing-to-stance transition, as predicted by the connectome. Overall, my dissertation work makes technical advances to reveal fundamental principles of how proprioception supports adaptive locomotion.

Table of Contents

List of Figures

List of Tables

Acknowledgements

First, John Tuthill, you have my sincerest gratitude. Your kindness, wittiness, and clever (sometimes wild) ideas made it beyond fun to be in your lab. Following your lead, I have become a scientist that I am proud of – one that approaches science with rigor, creativity, and curiosity. I strongly believe that these qualities that you instilled within me will enable me to have a successful scientific career. Overall, I wouldn't change a thing about my experience in your lab and truly feel lucky that you were my PhD mentor. Although I won't be able to barge into your office as easily, I will continue to seek out your advice and mentorship in the years to come.

I also want to thank the rest of the Tuthill lab crew for making my time in the lab so enjoyable. I value the friendships I forged with each one of you and all of the scientific insights I gained through our interactions. Like with John, I aim to stay in touch with you all and wish each one of you the best in your future endeavors.

Additionally, I extend my gratitude to my committee members Bing, Chip, Forrest, Shawn, and Sam for providing me with invaluable feedback over the years that not only led to stronger evidence for my research, but also made it more impactful. I want to specially thank Bing Brunton for the much-needed wisdom, coffee walks, and chocolates. I look forward to our continued interactions in the future.

Next, I want to thank Tom Daniel for not only being the catalyst that got me here, but also for being an amazing life-long mentor and friend. I truly value our catch ups and am excited for the ones to come.

To my entire family and friends, thank you for supporting me throughout this process, being interested in my science, and for all of the unforgettable memories over the years. I love each one of you.

Although he can't read this, I also want to thank my dog, Biscuit, for always putting a smile on my face by being the biggest goof. All of the snuggles, chasing, and toy tug-of-wars helped me to remain positive and optimistic throughout my PhD. I love you Bitty.

Lastly and most importantly, I give immense thanks to the most caring, funny, and smart person I know, my wife, Stephanie. Your support and advice over the years have gotten me to this point and I continue to grow as a person because of you. I cherish every memory that we have made throughout my PhD journey, from our camping and road trips to our wedding day. I'm excited for what the future holds for us and can't wait to talk science with you until the very end. I love you so much Steph and am so grateful for all that you do.

Dedication

I dedicate this work to my late grandfather, Gene Clasen, whose brave battle with Parkinson's inspired my scientific pursuits.

Chapter 1.

Introduction

Evolution has molded the bodies of animals into intricate and complex forms. However, a more complex body becomes more challenging for the nervous system to control. In legged locomotion, for example, both the coordination within multi-jointed limbs and between limbs must be controlled for an animal to execute fluid movements and correct for unexpected perturbations[1–3]. Without such an ability to control the body, animals would be unable to navigate their environment, preventing them from finding food, shelter, and mates. Therefore, adaptive locomotion, that is the ability for an animal to rapidly adjust its movement in response to unanticipated perturbations, is coupled to an animal's survival.

Adaptive motor control is critical for animals to walk in unpredictable and non-uniform environments. For instance, both humans[4] and cockroaches[5] have been shown to use similar locomotor strategies to recover walking after tripping – an event that could have otherwise resulted in injury. Hence, nervous systems enable the rapid recovery of walking in response to unexpected perturbations. Another feature of walking that nervous systems adaptively control is the coordination between the legs, referred to as inter-leg coordination. In both vertebrates[3] and invertebrates, like hexapod insects[6–9], inter-leg coordination is adjusted to enable walking at different speeds. Even microscopic tardigrades, which experience completely different fluid forces than these other animals, display speed-dependent changes in inter-leg coordination[10]. To achieve these changes, animals must alter the coordination and kinematics of single legs. For example, speed-dependent inter-leg coordination changes in six-legged insects are accompanied by spatiotemporal adjustments in leg movement, particularly, a decrease in the stance duration of each leg[6–8,11]. Interestingly, inter-leg coordination changes discretely as a function of walking speed for vertebrates to support optimal energetics[3], but changes along a speed-dependent continuum in invertebrates[7] to enhance moment-to-moment stability[12]. Therefore, the body plan of an animal seems to influence how the nervous system adaptively controls walking.

Proprioception[13,14], the sense of how the body is articulated and moving in space, enables animals to rapidly adjust leg movement during walking. Analogous classes of proprioceptive neurons, called proprioceptors, are found in vertebrates[15,16] and invertebrates[2,17]. Each

proprioceptor type encodes distinct information about the leg. For instance, proprioceptors embedded in vertebrate muscle and within the insect leg, called muscle spindles and the chordotonal organ, encode information about the relative position and movement between two interconnected leg segments. Likewise, both vertebrate Golgi tendon organs and invertebrate campaniform sensilla detect how much load is on the legs. Finally, low threshold mechanoreceptors, such as Ruffini endings, in vertebrates and invertebrate hair plates serve as limit detectors by encoding the extremes of joint movement. Although the encoding properties of these proprioceptors have been characterized, how their proprioceptive information is integrated in central circuits to enable adaptive walking remains unclear. However, technical limitations have historically made it challenging to study the role proprioception in adaptive walking.

First, animals have constrained and reduced spontaneous walking after manipulations of sensorimotor circuits[8,13], creating a confound when investigating the role of proprioception in natural leg motor control. Exacerbated by the diminished walking behavior, it is also challenging to precisely perturb the walking of animals with impaired proprioceptive circuits. Treadmills are a tool that can circumvent these challenges and enable the study of proprioception in adaptive walking. There is a long history in which treadmills have been used to study the neural control of movement in vertebrates[18–20] and invertebrates[21–25]. For example, intact and decerebrated cats were driven to walk using a treadmill, which lead to important insights into how spinal circuits control adaptive[26] and reflexive[27] leg movements. In addition to the treadmills that can be found at a standard gym, split-belt treadmills consisting of two independently controlled belts have been used to perturb the coordination between legs and induce a motor adaptation process, called split-belt adaptation[28]. This form of adaptation occurs by initially driving the left and right legs at the same speed, followed by driving them at different speeds for an extended period of time, and then finally, driving them at the same speed again. As humans[29,30] and mice[31] underwent this process, they learned new inter-leg coordination patterns to cope with the changing environmental conditions (i.e. changing belt speeds). Overall, treadmills are a means to discover fundamental principles of how proprioceptive feedback supports flexible walking behavior.

Another limitation to characterizing the neural control of adaptive walking is capturing the richness of walking itself. During walking, the body and legs dynamically move in a 3D space, however, traditional methods were limited in their ability to accurately obtain this information. For

example, these approaches relied on manual or semi-automatic tracking alogrithms[32] to extract kinematic information from recorded videos of animal movement. In addition to being laborious, these tracking methods lacked the ability to feasibly process large datasets, which is necessary for fully characterizing how proprioception controls the high dimensionality of walking. However, recent advances in deep learning and pose estimation methods have produced tools, such as DeepLabCut[33], Anipose[34], and SLEAP[35], that enable the unprecedented ability to track and reconstruct 3D positions of annotated key points on animals in large, high-speed videography datasets. As an aside, I used these tools to help collaborators characterize the evolution of walking in fruit fly species[36] and to determine how temperature affects walking behavior in snow flies[37]. In addition to these supervised learning methods, other unsupervised learning approaches have been recently developed, like BKinD-3D[38], that enable 3D tracking of animals without the cumbersome process of annotating frames. Overall, the revolution of deep learning tools to track animal movement now makes it possible to determine the exact features of leg movement that are under proprioceptive control in the context of adaptive walking.

The final challenge to understanding how proprioception enables adaptive walking is being able to characterize proprioceptive neural circuits. Although genetic tools, like those in *Drosophila*[39,40], allow for the targeting of specific cells, experiments are still not high throughput enough to reasonably assess the entire connectivity within proprioceptive circuits. Like the revolution in tracking methods, recent advances in deep learning have made it possible to automatically segment[41] neurons within volumes of scanned nervous system tissue[42], resulting in connectomes. The creation of connectomes for *C. elegans*[43], mouse visual cortex[44], and the fruit fly brain[45] and ventral nerve cord (VNC)[41,46] has resulted in unparallelled discoveries about neural circuit architecture and possible function. For example, the connectome of the female fruit fly VNC[41,42], which I assisted in proofreading and analyzing, revealed that premotor networks are organized in such a way to control specific motor modules of the leg[47]. In the same connectomic dataset, it was also discovered that different proprioceptive subtypes of the femoral chordotonal organ connect to distinct neural circuits to potentially aid in motor control or vibration sensing[48]. Altogether, these connectomes and those that will be created enable predictions of how neural circuits that process proprioceptive information support adaptive motor control, which can expedite the rate of scientific discovery by facilitating targeted experimental testing.

In my dissertation work, I combine all of these technical advances to investigate the proprioceptive control of adaptive walking in the fruit fly, *Drosophila melanogaster*. In **Chapter 2**, I introduce the miniature linear and split-belt treadmill systems I engineered and illustrate how they can be used to drive robust walking behavior in flies lacking proprioceptive feedback, perturb the coordination between the legs, and obtain 3D walking kinematics of unconstrained flies when used in tandem with modern pose estimation tools[33,34]. In addition to showing that the walking kinematics of flies on the treadmill are similar to those of freely walking flies, I also discovered that proprioceptive feedback is needed to control step kinematics across all walking speeds. Moreover, by using the split-belt treadmill, I found that the middle legs are adaptive appendages that correct for asymmetric perturbations to keep a fly on a straight walking course. In **Chapter 3**, I used the connectome of the female fruit fly VNC to generate predictions about how hair plates on the fly leg contribute to the adaptive control of leg movement. Using a myriad of experimental approaches, including the treadmill systems, my colleagues and I validated the prediction of one of the hair plates on the coxa, called CxHP8, in controlling the anterior to posterior transition of leg movement. We then used this validation as grounds for prescribing functional roles to the other hair plates in controlling leg movement. Overall, my dissertation work makes innovations in the field of fly systems neuroscience to discover fundamental principles of how proprioceptive feedback enables adaptive locomotor behaviors, like walking.

References

1. Bidaye, S.S., Bockemühl, T., and Büschges, A. (2018). Six-legged walking in insects: how CPGs, peripheral feedback, and descending signals generate coordinated and adaptive motor rhythms. Journal of Neurophysiology *119*, 459–475. 10.1152/jn.00658.2017.

2. Tuthill, J.C., and Wilson, R.I. (2016). Mechanosensation and Adaptive Motor Control in Insects. Current Biology *26*, R1022–R1038. 10.1016/j.cub.2016.06.070.

3. Alexander, R.M. (1989). Optimization and gaits in the locomotion of vertebrates. Physiological Reviews *69*, 1199–1227. 10.1152/physrev.1989.69.4.1199.

4. Eng, J.J., Winter, D.A., and Patla, A.E. (1994). Strategies for recovery from a trip in early and late swing during human walking. Experimental Brain Research *102*, 339–349. 10.1007/BF00227520.

5. Couzin-Fuchs, E., Kiemel, T., Gal, O., Ayali, A., and Holmes, P. (2015). Intersegmental coupling and recovery from perturbations in freely running cockroaches. Journal of Experimental Biology *218*, 285–297. 10.1242/jeb.112805.

6. Strauss, R., and Heisenberg, M. (1990). Coordination of legs during straight walking and turning in Drosophila melanogaster. J. Comp. Physiol. A *167*, 403–412.

7. DeAngelis, B.D., Zavatone-Veth, J.A., and Clark, D.A. (2019). The manifold structure of limb coordination in walking Drosophila. eLife *8*, e46409. 10.7554/eLife.46409.

8. Mendes, C.S., Bartos, I., Akay, T., Márka, S., and Mann, R.S. (2013). Quantification of gait parameters in freely walking wild type and sensory deprived *Drosophila melanogaster*. eLife Sciences *2*, e00231. 10.7554/eLife.00231.

9. Wilson, D.M. (1966). Insect Walking. Annual Review of Entomology *11*, 103–122. https://doi.org/10.1146/annurev.en.11.010166.000535.

10. Nirody, J.A., Duran, L.A., Johnston, D., and Cohen, D.J. (2021). Tardigrades exhibit robust interlimb coordination across walking speeds and terrains. Proceedings of the National Academy of Sciences *118*, e2107289118. 10.1073/pnas.2107289118.

11. Wosnitza, A., Bockemühl, T., Dübbert, M., Scholz, H., and Büschges, A. (2013). Inter-leg coordination in the control of walking speed in Drosophila. Journal of Experimental Biology *216*, 480–491. 10.1242/jeb.078139.

12. Szczecinski, N.S., Bockemühl, T., Chockley, A.S., and Büschges, A. (2018). Static stability predicts the continuum of interleg coordination patterns in Drosophila. Journal of Experimental Biology *221*, jeb189142. 10.1242/jeb.189142.

13. Dietz, V. (2002). Proprioception and locomotor disorders. Nature Reviews Neuroscience *3*, 781–790. 10.1038/nrn939.

14. Tuthill, J.C., and Azim, E. (2018). Proprioception. Current Biology *28*, R194–R203. 10.1016/j.cub.2018.01.064.

15. Proske, U., and Gandevia, S.C. (2012). The Proprioceptive Senses: Their Roles in Signaling Body Shape, Body Position and Movement, and Muscle Force. Physiological Reviews *92*, 1651–1697. 10.1152/physrev.00048.2011.

16. Windhorst, U. (2007). Muscle proprioceptive feedback and spinal networks. Brain Research Bulletin *73*, 155–202. 10.1016/j.brainresbull.2007.03.010.

17. Burrows, M. (1996). The Neurobiology of an Insect Brain (Oxford University Press) 10.1093/acprof:oso/9780198523444.001.0001.

18. Belanger, M., Drew, T., Provencher, J., and Rossignol, S. (1996). A comparison of treadmill locomotion in adult cats before and after spinal transection. Journal of Neurophysiology *76*, 471–491. 10.1152/jn.1996.76.1.471.

19. Hasan, Z., and Stuart, D.G. (1988). Animal Solutions to Problems of Movement Control: The Role of Proprioceptors. Annu. Rev. Neurosci. *11*, 199–223. 10.1146/annurev.ne.11.030188.001215.

20. Wetzel, M.C., and Stuart, D.G. (1976). Ensemble characteristocs of cat locomotion and its neural control. Progress in Neurobiology *7*, 1–98. 10.1016/0301-0082(76)90002-2.

21. Dean, J., and Wendler, G. (1983). Stick Insect Locomotion On A Walking Wheel: Interleg Coordination of Leg Position. Journal of Experimental Biology *103*, 75–94. 10.1242/jeb.103.1.75.

22. Foth, E., and Bässler, U. (1985). Leg movements of stick insects walking with five legs on a treadwheel and with one leg on a motor-driven belt. Biological Cybernetics *51*, 313–318. 10.1007/BF00336918.

23. Foth, E., and Graham, D. (1983). Influence of loading parallel to the body axis on the walking coordination of an insect. Biological Cybernetics *47*, 17–23. 10.1007/BF00340065.

24. Herreid, C.F., and Full, R.J. (1984). Cockroaches on a treadmill: Aerobic running. Journal of Insect Physiology *30*, 395–403. 10.1016/0022-1910(84)90097-0.

25. Watson, J.T., and Ritzmann, R.E. (1997). Leg kinematics and muscle activity during treadmill running in the cockroach, Blaberus discoidalis: II. Fast running. Journal of Comparative Physiology A *182*, 23–33. 10.1007/s003590050154.

26. Buford, J.A., and Smith, J.L. (1993). Adaptive control for backward quadrupedal walking. III. Stumbling corrective reactions and cutaneous reflex sensitivity. Journal of Neurophysiology *70*, 1102–1114. 10.1152/jn.1993.70.3.1102.

27. McCrea, D.A. (2001). Spinal circuitry of sensorimotor control of locomotion. The Journal of Physiology *533*, 41–50. 10.1111/j.1469-7793.2001.0041b.x.

28. Reisman, D.S., Block, H.J., and Bastian, A.J. (2005). Interlimb Coordination During Locomotion: What Can be Adapted and Stored? Journal of Neurophysiology *94*, 2403–2415. 10.1152/jn.00089.2005.

29. Reisman, D.S., Wityk, R., Silver, K., and Bastian, A.J. (2007). Locomotor adaptation on a split-belt treadmill can improve walking symmetry post-stroke. Brain *130*, 1861–1872. 10.1093/brain/awm035.

30. Kambic, R.E., Roemmich, R.T., and Bastian, A.J. (2023). Joint-level coordination patterns for split-belt walking across different speed ratios. Journal of Neurophysiology *129*, 969–983. 10.1152/jn.00323.2021.

31. Darmohray, D.M., Jacobs, J.R., Marques, H.G., and Carey, M.R. (2019). Spatial and Temporal Locomotor Learning in Mouse Cerebellum. Neuron *102*, 217-231.e4. 10.1016/j.neuron.2019.01.038.

32. Hedrick, T.L. (2008). Software techniques for two- and three-dimensional kinematic measurements of biological and biomimetic systems. Bioinspiration & Biomimetics *3*, 034001. 10.1088/1748-3182/3/3/034001.

33. Mathis, A., Mamidanna, P., Cury, K.M., Abe, T., Murthy, V.N., Mathis, M.W., and Bethge, M. (2018). DeepLabCut: markerless pose estimation of user-defined body parts with deep learning. Nature Neuroscience *21*, 1281. 10.1038/s41593-018-0209-y.

34. Karashchuk, P., Rupp, K.L., Dickinson, E.S., Walling-Bell, S., Sanders, E., Azim, E., Brunton, B.W., and Tuthill, J.C. (2021). Anipose: A toolkit for robust markerless 3D pose estimation. Cell Rep *36*, 109730. 10.1016/j.celrep.2021.109730.

35. Pereira, T.D., Tabris, N., Matsliah, A., Turner, D.M., Li, J., Ravindranath, S., Papadoyannis, E.S., Normand, E., Deutsch, D.S., Wang, Z.Y., et al. (2022). SLEAP: A deep learning system for multi-animal pose tracking. Nature Methods *19*, 486–495. 10.1038/s41592-022-01426-1.

36. York, R.A., Brezovec, L.E., Coughlan, J., Herbst, S., Krieger, A., Lee, S.-Y., Pratt, B., Smart, A.D., Song, E., Suvorov, A., et al. (2022). The evolutionary trajectory of drosophilid walking. Current Biology *32*, 3005-3015.e6. 10.1016/j.cub.2022.05.039.

37. Golding, D., Rupp, K.L., Sustar, A., Pratt, B., and Tuthill, J.C. (2023). Snow flies self-amputate freezing limbs to sustain behavior at sub-zero temperatures. Current Biology *33*, 4549-4556.e3. 10.1016/j.cub.2023.09.002.

38. Sun, J.J., Karashchuk, L., Dravid, A., Ryou, S., Fereidooni, S., Tuthill, J.C., Katsaggelos, A., Brunton, B.W., Gkioxari, G., and Kennedy, A. (2023). BKinD-3D: self-supervised 3D keypoint discovery from multi-view videos. In Proceedings of the IEEE/CVF Conference on Computer Vision and Pattern Recognition, pp. 9001–9010.

39. Smith, S.A., and Shepherd, D. (1996). Central afferent projections of proprioceptive sensory neurons in Drosophila revealed with the enhancer-trap technique. Journal of Comparative Neurology *364*, 311–323. 10.1002/(SICI)1096-9861(19960108)364:2<311::AID-CNE9>3.0.CO;2-8.

40. Duffy, J.B. (2002). GAL4 system in drosophila: A fly geneticist's swiss army knife. genesis *34*, 1–15. 10.1002/gene.10150.

41. Azevedo, A., Lesser, E., Mark, B., Phelps, J., Elabbady, L., Kuroda, S., Sustar, A., Moussa, A., Kandelwal, A., Dallmann, C.J., et al. (2022). Tools for comprehensive reconstruction and analysis of *Drosophila* motor circuits. bioRxiv, 2022.12.15.520299. 10.1101/2022.12.15.520299.

42. Phelps, J.S., Hildebrand, D.G.C., Graham, B.J., Kuan, A.T., Thomas, L.A., Nguyen, T.M., Buhmann, J., Azevedo, A.W., Sustar, A., Agrawal, S., et al. (2021). Reconstruction of motor control circuits in adult Drosophila using automated transmission electron microscopy. Cell *184*, 759-774.e18. 10.1016/j.cell.2020.12.013.

43. Cook, S.J., Jarrell, T.A., Brittin, C.A., Wang, Y., Bloniarz, A.E., Yakovlev, M.A., Nguyen, K.C.Q., Tang, L.T.-H., Bayer, E.A., Duerr, J.S., et al. (2019). Whole-animal connectomes of both Caenorhabditis elegans sexes. Nature *571*, 63–71. 10.1038/s41586-019-1352-7.

44. Yao, S., Wang, Q., Hirokawa, K.E., Ouellette, B., Ahmed, R., Bomben, J., Brouner, K., Casal, L., Caldejon, S., Cho, A., et al. (2023). A whole-brain monosynaptic input connectome to neuron classes in mouse visual cortex. Nature Neuroscience *26*, 350–364. 10.1038/s41593-022-01219-x.

45. Dorkenwald, S., Matsliah, A., Sterling, A.R., Schlegel, P., Yu, S., McKellar, C.E., Lin, A., Costa, M., Eichler, K., Yin, Y., et al. (2023). Neuronal wiring diagram of an adult brain. bioRxiv, 2023.06.27.546656. 10.1101/2023.06.27.546656.

46. Takemura, S., Hayworth, K.J., Huang, G.B., Januszewski, M., Lu, Z., Elizabeth C Marin, Stephan Preibisch, C Shan Xu, John Bogovic, Andrew S Champion, et al. (2023). A Connectome of the Male Drosophila Ventral Nerve Cord. bioRxiv, 2023.06.05.543757. 10.1101/2023.06.05.543757.

47. Lesser, E., Azevedo, A.W., Phelps, J.S., Elabbady, L., Cook, A., Mark, B., Kuroda, S., Sustar, A., Moussa, A., Dallmann, C.J., et al. (2023). Synaptic architecture of leg and wing motor control networks in Drosophila. bioRxiv, 2023.05.30.542725. 10.1101/2023.05.30.542725.

48. Lee, S.-Y.J., Dallmann, C.J., Cook, A., Tuthill, J.C., and Agrawal, S. (2024). Divergent neural circuits for proprioceptive and exteroceptive sensing of the Drosophila leg. bioRxiv, 2024.04.23.590808. 10.1101/2024.04.23.590808.

Chapter 2.

Miniature linear and split-belt treadmills reveal mechanisms of adaptive motor control in walking *Drosophila*

Source

This chapter comes from a manuscript that is currently in revision at *Current Biology*.

Authors and Affiliations

Brandon G. Pratt[1], Su-Yee J. Lee[1], Grant M. Chou[1], and John C. Tuthill[1]*

[1]Department of Physiology and Biophysics, University of Washington, Seattle, WA, USA

2.1 Abstract

To navigate complex environments, walking animals must detect and overcome unexpected perturbations. One technical challenge when investigating adaptive locomotion is measuring behavioral responses to precise perturbations during naturalistic walking; another is that manipulating neural activity in sensorimotor circuits often reduces spontaneous locomotion. To overcome these obstacles, we introduce miniature treadmill systems for coercing locomotion and tracking 3D kinematics of walking *Drosophila*. By systematically comparing walking in three experimental setups, we show that flies compelled to walk on the linear treadmill have similar stepping kinematics to freely walking flies, while kinematics of tethered walking flies are subtly different. Genetically silencing mechanosensory neurons alters step kinematics of flies walking on the linear treadmill across all speeds, while inter-leg coordination remains intact. We also found that flies can maintain a forward heading on a split-belt treadmill by adapting the step distance of their middle legs. Overall, these new insights demonstrate the utility of miniature treadmills for studying insect locomotion.

2.2 Introduction

Many animals rely on legged locomotion to move through diverse and unpredictable environments. To achieve behavioral goals in the face of this unpredictability, nervous systems have

evolved to control the body in an adaptive manner. Animals as diverse as cockroaches[1] and humans[2] use similar strategies to recover from unexpected motor outcomes (e.g., tripping), by rapidly adjusting coordination within and between legs. Understanding how sensorimotor neural circuits detect perturbations and generate adaptive motor responses remains a fundamental question in neuroscience[3].

A common method to investigate the neural control of movement is to perturb neurons within candidate circuits and measure the effect on an animal's behavior. For example, past efforts to identify sensorimotor circuits have relied on anatomical lesions[4,5]. While these methods revealed regions of the nervous system that are important for proprioceptive sensing and motor control, they lack cell-type specificity and produce wide-ranging behavioral effects. More recently, genetic methods have enabled targeted manipulation of specific cell-types that sense or control the body. However, these experimental manipulations often decrease the probability and vigor of spontaneous behavior. For example, the loss of feedback from mechanosensory neurons in both mammals[6] and insects[7] reduces walking speed and probability. This confound has made it challenging to dissect the relative roles of mechanosensory feedback vs. feedforward motor commands across different walking speeds[8].

One strategy to overcome this reduction in spontaneous behavior is to compel animals to walk, for example by placing them on an actuated treadmill. Treadmills have been historically used to study the neural basis of motor control and adaptive locomotion in both vertebrates[9–11] and invertebrates[12–18]. For instance, treadmills have been used to drive walking in cats[19] and rodents[20], leading to important insights into spinal circuits for adaptive locomotor control.

Because treadmills are externally controlled, they can also deliver calibrated mechanical perturbations to walking animals. Previous work showed that cats walking on a treadmill learn to increase the height of their steps to avoid being smacked by a paddle[21]. Split-belt treadmills, which consist of two independently controlled belts, are another classic paradigm to investigate walking coordination and motor adaptation. Both humans[22–24] and mice[25] learn new inter-leg coordination patterns when their left and right legs are driven at different speeds on a split-belt treadmill. This phenomenon of split-belt adaptation has been used to investigate behavioral and neural mechanisms of adaptive locomotion[26]. A final advantage of treadmills is that they enable the study of locomotion within a confined space, which is important for capturing body kinematics or physiological signals

from neurons and muscles. For example, one trailblazing study recorded leg joint kinematics and muscle activity in rock lobsters walking on a split-belt treadmill[27].

In recent years, the fruit fly, *Drosophila melanogaster*, has emerged as an important model system for studying proprioceptive sensing and adaptive locomotion[7,28–33]. The key advantages of the fly are a compact, fully-mapped nervous system[34–36] and cell-type specific tools for targeted genetic manipulations. Fly locomotion has been previously studied in tethered animals walking on a floating sphere[37–40], or in freely walking animals constrained to a behavioral arena[7,41–45]. One advantage of the tethered preparation is that it enables 3D tracking of the fly's body and legs[46,47], which has not previously been possible in freely walking flies. It is also possible to record neural signals of tethered flies using optical imaging[48] or electrophysiology[49,50]. However, one disadvantage of studying locomotion in tethered flies is that their posture is constrained, and normal ground reaction forces may be disrupted, which could affect walking kinematics.

To bridge these established methodologies, we introduce a new linear treadmill system that enables long-term 3D tracking of walking *Drosophila*. We systematically compare walking kinematics on the linear treadmill to those of freely walking and tethered flies. We then use the linear treadmill to investigate step kinematics and inter-leg coordination following genetic silencing of mechanosensory neurons. Last, we introduce a novel split-belt treadmill for fruit flies, which we use to uncover behavioral mechanisms of adaptive motor control. We provide open-source software and hardware designs for these treadmill systems as resources for the community.

2.3 Results

A linear treadmill for tracking 3D walking behavior in *Drosophila*

We engineered a miniature linear treadmill system to measure 3D walking kinematics in flies (**Figure 2.1A**). A fly was constrained to walk on the treadmill within a transparent chamber. Its wings were trimmed to discourage flight initiation. We used 5 high-speed video cameras (180 fps) to record fly walking behavior. To test the treadmill system, we used wild-type Berlin flies that had a body length of 2.04 ± 0.10 mm. We used DeepLabCut[51] and Anipose[47] to track and extract 3D kinematics of the fly leg tips and body (**Figure 2.1B**).

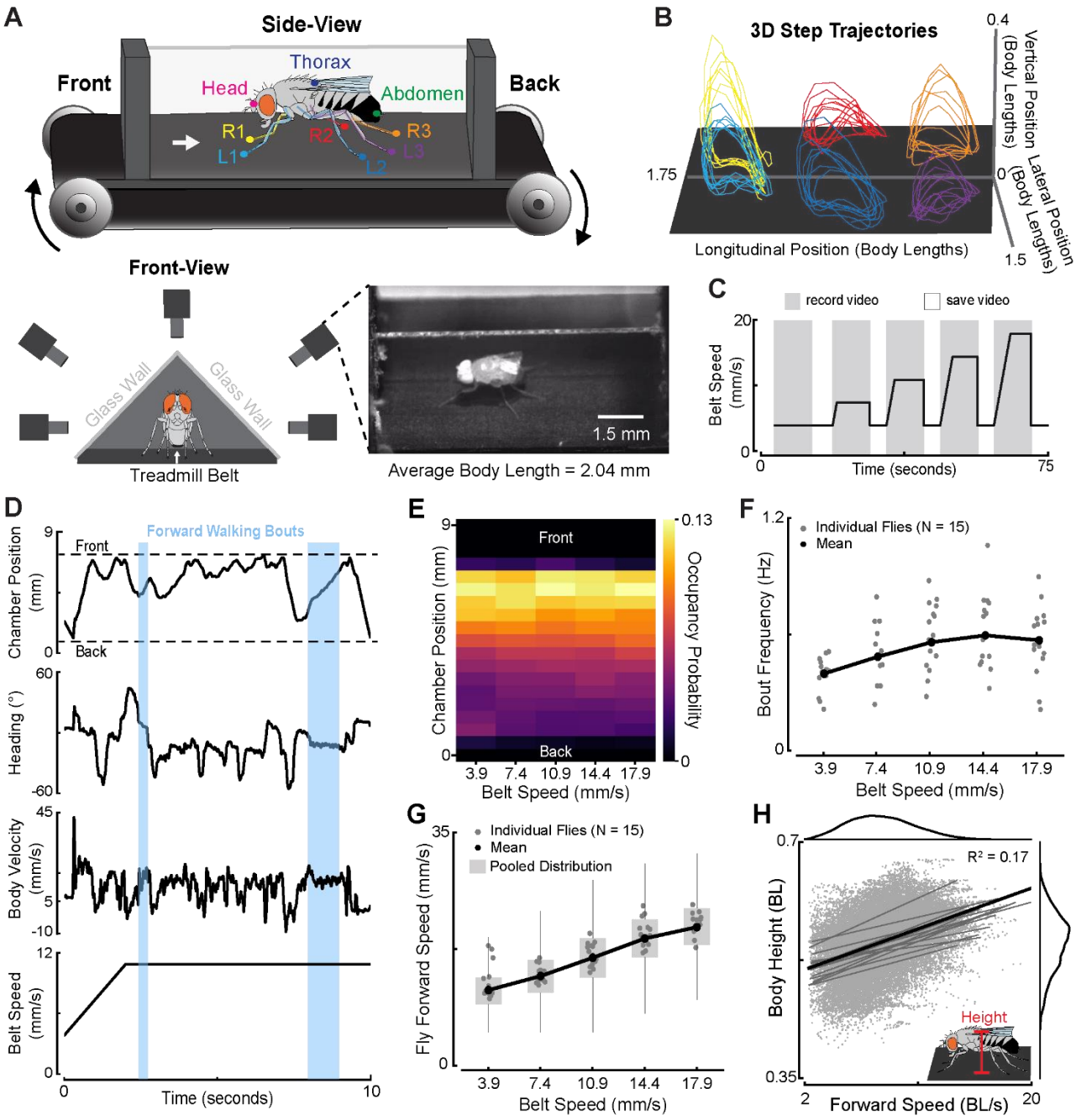

Figure 2.1. The linear treadmill controls locomotor speed and enables tracking of 3D kinematics in walking *Drosophila.* (**A**) Schematic of the linear treadmill setup. Key points associated with the head, thorax, abdomen, and each leg tip were tracked in 3D. Flies were recorded with 5 high-speed cameras as they were driven to walk on the treadmill within an attic-shaped chamber. Flies had an average body length of 2.04 ± 0.10 mm. Note that the schematic flies are not to scale. (**B**) 3D leg tip (tarsi) trajectories during forward walking. Colors correspond to the labels in (A). (**C**) Flies were compelled to walk at different speeds by moving the treadmill belt at one of 5 steady-state speeds. The belt gradually increased in speed to reach steady-state speeds greater than 5 mm/s. Each speed was presented to a fly 10 times, with speeds randomly interleaved. Each trial was composed of a 10 s recording period (gray) followed by a 5s saving period (white) in which the belt speed returned to the baseline speed. (**D**) A representative trial of a fly walking on the treadmill with a belt speed of 10.9 mm/s. The position of the fly along the chamber (measured at the thorax), the fly's heading angle and body velocity, and the belt speed profile are plotted from top to bottom, respectively. Forward walking bouts are highlighted by the light blue shaded regions. Forward walking bouts were classified as periods lasting at least 200 ms where the fly walked in the

middle of the chamber (see Methods), had a heading angle between -15 to 15 degrees with respect to the front of the chamber, and had a body velocity greater than 5 mm/s. (**E**) Flies walked between the middle and front of the chamber across all belt speeds. (**F**) Flies increased their walking bout frequency as the belt speed increased. Gray dots are the mean frequency of individual flies, while the black line denotes the mean across all flies. (**G**) Flies increased their forward walking speed as the belt speed increased. Box plots show the distribution of pooled data. Black line connects the median forward speed across all flies and belt speeds. (**H**) Flies increased their body height (vertical distance between the thorax and ground) as they walked faster (in body lengths per second, or BL/s). Black: population fit; Gray line: individual fit. See also Video 1.

We first measured the 3D kinematics of flies as they walked across a range of belt driving speeds (**Figure 2.1C**). As illustrated by a representative fly walking at an intermediate belt speed, flies on the treadmill displayed forward walking bouts, standing, and other lateral movements (**Figure 2.1D**, **Video 2.1**). Flies traversed the entirety of the chamber but spent most of their time toward the front (**Figure 2.1E**). They typically walked in short bursts, accelerating toward the front of the chamber, where they would walk for a short period, after which they would ride the belt to the back of the chamber; contact with the back of the chamber would then initiate another walking bout. Flies increased their walking bout frequency as the belt speed increased, as measured by the frequency at which they crossed the middle of the chamber from the rear (**Figure 2.1F**). The sporadic structure of fly treadmill walking is similar to that previously reported for freely walking flies[52]. Flies on the treadmill also consistently increased their walking speed to keep up with the treadmill's belt driving speed (**Figure 2.1G**). At the extremes, flies on the treadmill were able to sustain walking at a max belt speed of 40 mm/s (**Video 2.2**) and surpassed an instantaneous walking velocity of 50 mm/s (**Video 2.3**), which is the fastest walking speed ever recorded for *Drosophila melanogaster*. By driving flies to walk across a range of speeds while recording their 3D kinematics, we found that flies increased their body height as they walked faster by 0.007 BL per BL/s (**Figure 2.1H**).

In summary, our engineered treadmill makes it possible to force individual flies to walk for long periods (up to 1 hour) while tracking 3D body and leg kinematics. Flies remained upright 97% of the time on the treadmill and spent an average of 54% of the time walking, enabling collection of large amounts of useful kinematic data from each animal. Using 3D tracking, we discovered that flies elevate their body as they walked faster, a relationship that has been shown in other walking animals, from cockroaches[53] to humans[54], but had not been previously described in *Drosophila*.

Comparison of walking kinematics between treadmill, freely, and tethered walking flies

Multiple previous studies have quantified step kinematics of freely walking flies[7,41,42,44,55–57]. To compare treadmill walking to freely walking kinematics, we tracked and analyzed a new dataset

of wild-type flies walking in a circular arena. We focused our kinematic analyses on forward walking bouts, which were identified from fly heading direction and body velocity. Note that more detailed definitions of all kinematic parameters are included in the Methods.

We found that the key relationships between stepping kinematics and forward walking speed were similar between flies walking on the treadmill (**Figure 2.2i**) and freely walking flies (**Figure 2.2ii**, **Video 2.4**). Flies in both setups increased step frequency as they walked faster (**Figure 2.2Ai-ii**). Correspondingly, stance duration was inversely related to walking speed for flies in both setups (**Figure 2.2Bi-ii**). However, swing duration remained fairly constant across speeds and was of a similar magnitude for treadmill and freely walking flies (**Figure 2.2Ci-ii**). Step length, the distance between the footfalls of each leg, was also comparable between treadmill and freely walking flies (**Figure 2.2Di-ii**). Flies in both setups had similar increases in step length with increasing walking speed. The largest difference between treadmill and freely walking flies was that the step kinematics of freely walking flies were more variable (e.g., step frequency within the walking speed range of 6.5-10.1 BL/s: freely walking $\sigma^2 = 5.18\ s^{-1}$; treadmill walking $\sigma^2 = 1.98\ s^{-1}$). This could be because the treadmill has a single driving axis, which may result in straighter walking bouts. The step kinematics of flies in our freely walking dataset were also consistent with prior work[7,41,44,56,57], even though fly strain and sex were sometimes different in those studies (**Table S2.1**). Overall, the step kinematics of flies walking on the treadmill were similar to freely walking flies.

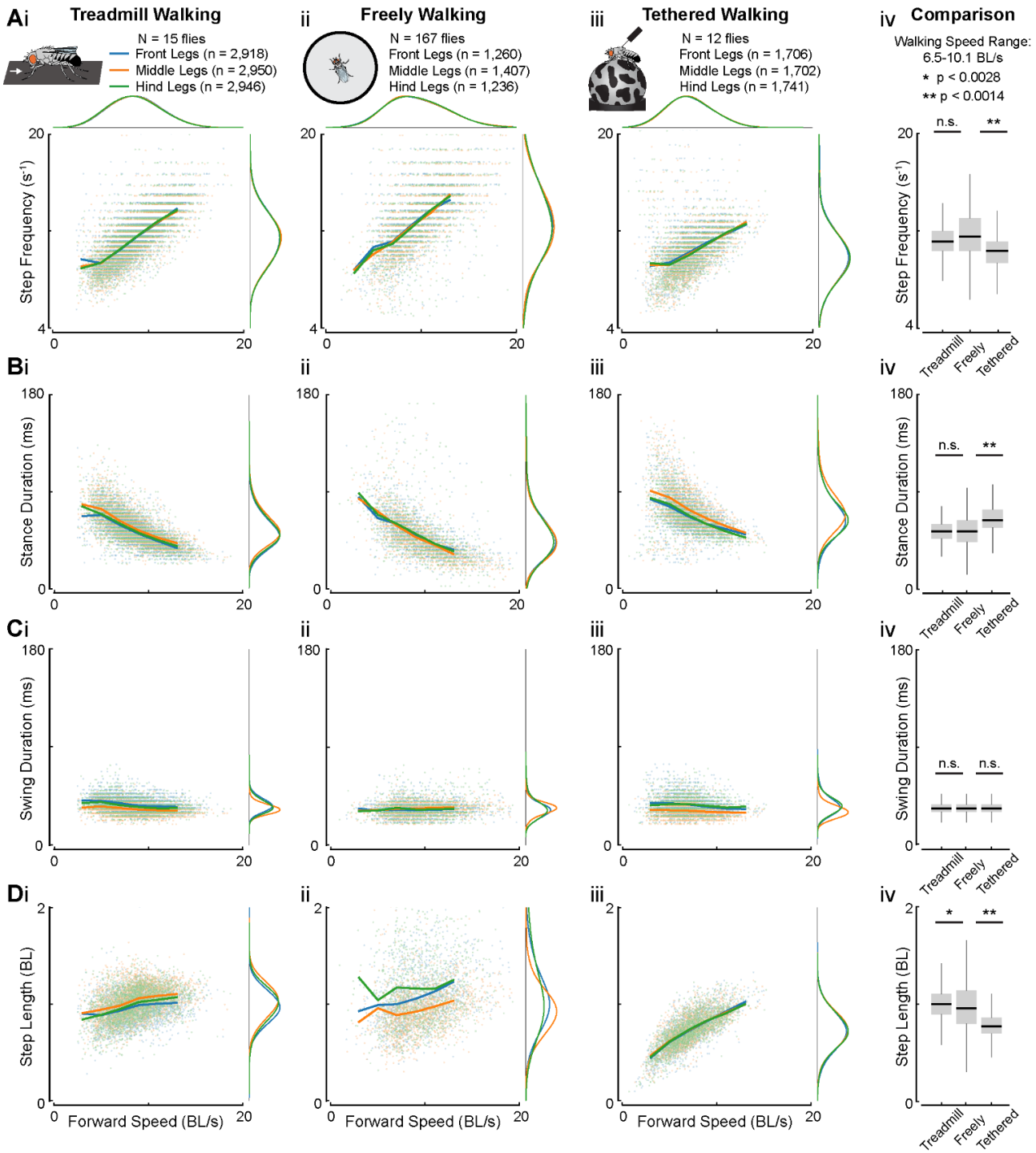

Figure 2.2. Step kinematics are similar across treadmill and freely walking flies, but different from tethered flies. (**A**) Step frequency of the front (blue), middle (orange), and hind (green) legs as a function of forward walking speed for treadmill (i), freely walking (ii), and tethered flies (iii). Distributions (iv; gray box plots) that combine step frequency across leg pairs for treadmill, freely, and tethered walking flies over an overlapping and dense range of walking speeds (6.5-10.1 BL/s). (**B**) Stance duration as a function of forward walking speed for flies in the different setups. (**C**) Swing duration as a function of forward walking speed. (**D**) Step length as a function of forward walking speed. In **A-D,** lines are speed-binned averages (2 BL/s bins between 3 and 13 BL/s) for each kinematic parameter and leg pair. Step frequency, stance duration, and swing duration (**A-C**) were computed on interpolated data for treadmill (i; 180 to 300 fps) and freely walking flies (ii; 150 to 300 fps) to enable the comparison to tethered flies. Distributions associated with

each leg were visually offset from each other for presentation in **A-C**. In **A-C iv**, Chi-squared test for goodness of fit with a Bonferroni correction of 18 was used to statistically compare the distributions across the different walking setups. In **D**, t-test with a Bonferroni correction of 18 was used to compare the distributions. N: number of flies; n: number of steps. See also Figure S1 for comparisons of the similarity between the setups with respect to step kinematics, leg pairs, and walking speeds.

Having developed a framework for comparing walking kinematics across experimental setups, we took the opportunity to extend our analysis to a third setup: tethered flies walking on a floating sphere (**Figure 2.2iii**, **Video 2.5**). The "fly-on-a-ball" setup is commonly used in our lab[28,47,58] and many others (e.g., Berendes et al., 2016; Creamer et al., 2018; Seelig et al., 2010), but leg kinematics of tethered and freely walking flies have not been systematically compared.

In general, we found that the relationships between stepping kinematics and walking speed were similar across all three setups. However, tethered flies differed from untethered ones (i.e. treadmill and freely walking flies) in several key aspects. First, tethered flies didn't reach the faster walking speeds displayed by untethered flies. Step frequency of tethered flies was also significantly lower than that of untethered flies (**Figure 2.2Aiv**), whereas stance duration was significantly longer (**Figure 2.2Biv**). There was no significant difference in swing duration across all setups (**Figure 2.2Civ)**. Therefore, the reduced step frequency in tethered flies resulted from longer stance durations across walking speeds. Tethered flies also had a significantly lower step length than untethered flies (**Figure 2.2Div**). However, the step length of tethered flies was more correlated with walking speed (tethered: $r = 0.41$; freely: $r = 0.05$; treadmill: $r = 0.22$). We also compared step kinematics between the different setups across leg pairs and walking speeds (**Table S2.1**). We found that there was a greater similarity in the step kinematics between treadmill and freely walking flies, especially at fast walking speeds. These differences in step kinematics and walking speed ranges between tethered and untethered flies may be because the tethered flies are walking on a spherical surface and/or because their body weight is supported by a rigid tether.

We next compared inter-leg coordination across the three setups. We quantified the number of legs that were in the stance phase of the step cycle at each point in time, which remains constant for idealized coordination patterns, such as the tripod coordination pattern where 3 legs are in stance[41]. We found that the probability of having a specific number of legs in stance was similar between tethered and untethered flies. Specifically, flies in all three setups showed an increased probability of having 3 legs in stance as walking speed increased (**Figure 2.3A**). This is consistent

with prior work showing that freely walking flies are more likely to use a canonical tripod coordination pattern at higher speeds[7,41,57,59].

Given that flies across all three setups had similar speed-dependent changes in inter-leg coordination, we next asked if the stepping pattern underlying inter-leg coordination was different between tethered and untethered flies. We therefore examined the relative swing and stance relationships across legs. We observed that the order in which legs entered stance conformed to the so-called *Cruse Control* rules for both tethered and untethered flies[8,60,61]. This is illustrated by the anterior progression of ipsilateral leg stepping (diagonal black stripes in **Figure 2.3B**). We also examined the relative phase relationships between the left front leg and all other legs across the different setups. We computed the phase by determining when a leg entered stance within the left front leg's step cycle. We found that the relative phase relationships across all legs were similar for treadmill, freely, and tethered walking flies (**Figure 2.3C**). However, the phase relationships of the ipsilateral front and hind legs and contralateral middle leg that make up the canonical tripod were more coupled for tethered flies.

Finally, we looked at the order in which legs within a tripod entered stance with respect to the left front leg's step cycle. We found differences in the stance onset order between tethered and untethered flies. For example, the front leg within a tripod was usually the first leg to contact the ground for treadmill (**Figure 2.3Di**) and freely walking flies (**Figure 2.3Dii**), whereas the stance order was more variable for tethered flies, having more instances of the middle leg entering stance first (**Figure 2.3Diii**). Tethered flies also had more instances where all legs within a tripod entered stance at the same time, called an "ideal tripod". Therefore, the inter-leg phase coupling of tethered flies was stronger than that of untethered flies. One explanation could be that the added stability from the tether induces a more tightly coupled inter-leg coordination pattern. In summary, we found that although step kinematics were subtly different between tethered and untethered flies (**Figure 2.2**), inter-leg coordination was broadly similar (**Figure 2.3**).

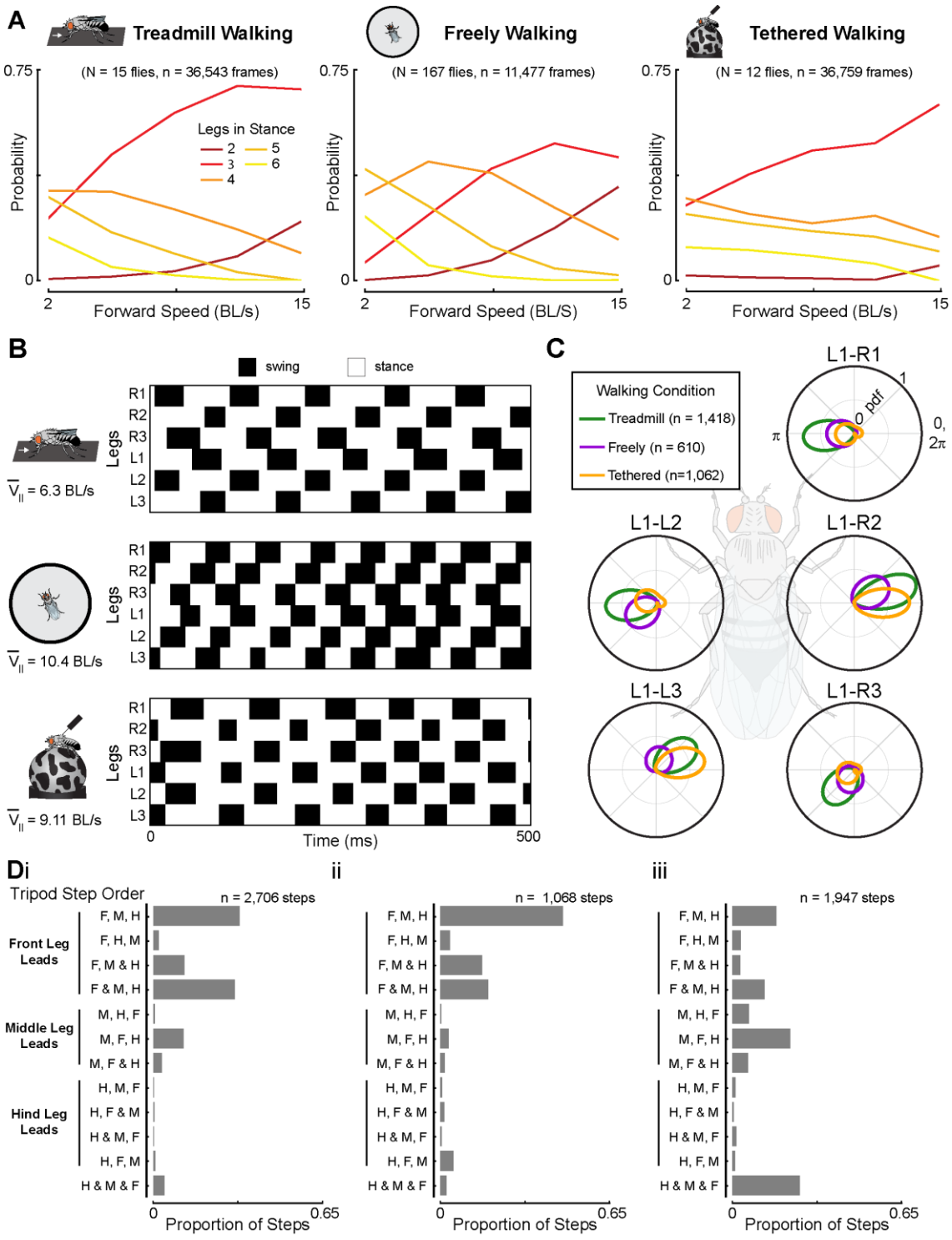

Figure 2.3. Subtle differences in inter-leg coordination between tethered and untethered flies. (**A**) Probability of treadmill, freely walking, and tethered flies exhibiting 2-6 legs in stance across forward walking speeds. Lines are speed-binned averages of the probability of a certain number of legs in stance (3.2 BL/s bins between 2 and 15 BL/s). N: number of flies; n: number of camera frames. (**B**) Representative plots of the swing and stance phases of each leg across all setups. Black: swing; White; stance. **(C)** Polar plots of the relative phase between the left front leg and each other leg for flies in each setup. Kernel density estimations were used to determine the probability density functions. n: number of phase comparisons. (**D**) Bar plot of the proportion of steps attributed to each

step order combination of the legs with a tripod for treadmill (i), freely (ii), and tethered (iii) walking flies. The leading leg is indicated on the left of the graph. '&' denotes legs contacting the ground at the same time. n: number of steps.

Silencing mechanosensory feedback alters step kinematics across walking speeds but not inter-leg coordination

One of our motivations to develop a linear treadmill was to investigate the role of mechanosensory feedback in fly locomotion. This has historically been challenging, because silencing mechanosensory neurons typically leads to a reduction in locomotor probability and speed in flies[7] and other animals[5,6]. To test whether flies lacking mechanosensory feedback will walk on the linear treadmill, we genetically silenced chordotonal neurons (iav-GAL4 > UAS-kir2.1), which are found at multiple joints throughout the fly's body, including in the femur and tibia (**Figure 2.4A**). As expected, silencing chordotonal neurons drastically reduced locomotion in freely walking flies (**Figure 2.4B**). However, flies lacking chordotonal feedback walked a greater proportion of the time and across a wider range of speeds when driven to walk on the linear treadmill (**Figure 2.4C**). Silencing chordotonal neurons altered the structure of fly locomotion on the treadmill compared to genetically-matched controls. In particular, flies with silenced chordotonal neurons spent more time towards the back of the chamber at faster belt speeds (**Figure 2.4D**) and exhibited a lower bout frequency (**Figure 2.4E**).

The leg movements of flies with silenced chordotonal neurons were noticeably different. Qualitatively, the legs appeared less rigid and moved with less precision (**Video 2.6**). Therefore, we next analyzed the impact of silencing chordotonal neurons on step kinematics and inter-leg coordination. We found that flies lacking chordotonal feedback had a lower step frequency across legs and speeds compared to control flies (**Figure 2.4F**). In addition, flies with silenced chordotonal neurons had greater step lengths across speeds, suggesting that they increased the size of their steps to compensate for taking fewer of them (**Figure 2.4G**). However, inter-leg coordination was not significantly different between controls and flies lacking chordotonal feedback (**Figure 2.4H**).

In summary, we found that silencing mechanosensory feedback from chordotonal neurons altered step kinematics across all walking speeds but did not have a significant effect on inter-leg coordination. We conjecture that other proprioceptor classes, such as hair plates and campaniform sensilla[62], may play a more important role than chordotonal neurons in inter-leg coordination. Overall,

these results also demonstrate the advantage of the linear treadmill to investigate the role of sensory feedback in locomotion.

A split-belt treadmill reveals that middle legs correct for rotational perturbations

We next engineered a split-belt treadmill to investigate behavioral mechanisms of adaptive motor control in walking flies (**Figure 2.5A**). We compared the leg kinematics of walking flies while the belts moved at the same speed (tied) vs. when the belts moved at different speeds (split: slow and fast), focusing our analysis on periods of forward, straight walking (see Methods, **Figure 2.5B left**, **Video 2.7**). We tested splits in both directions and pooled symmetric conditions for subsequent analyses.

We found that flies achieved straight walking by modifying spatial rather than temporal step kinematics. For instance, flies significantly altered where the legs contacted or lifted off of the ground (i.e., the anterior and posterior extreme positions (**Figure 2.5B**). Specifically, the mean anterior extreme position (AEP) shifted posteriorly and medially for the front leg on the fast belt, and laterally for the front leg on the slow belt. The front leg's mean posterior extreme position (PEP) also shifted posteriorly when on the fast belt. The middle leg's AEP shifted medially when on the fast belt but translated posteriorly and laterally on the slow belt. Meanwhile, the PEP of the middle legs shifted in the opposite direction. The hind leg shifted its mean PEP in a similar manner along the longitudinal axis. These changes in leg placement produced changes in the total distance that the legs, particularly the middle legs, traveled during a step cycle with respect to the body (i.e., step distance, **Figure 2.5C**). Step frequency, the timing component of the step cycle, did not change (**Figure 2.5D**), which suggests that changes in step distance alone dictated the speed at which legs moved through their step cycle (**Figure 2.5E**). For example, the increased step distance of the middle leg on the fast belt resulted in a faster step speed. Although changes in step speed could in principle have been achieved by altering temporal kinematics, spatial kinematics, or a combination of both, our results suggest that flies overcome the belt asymmetries to maintain forward locomotion by specifically adjusting the step size of the middle legs.

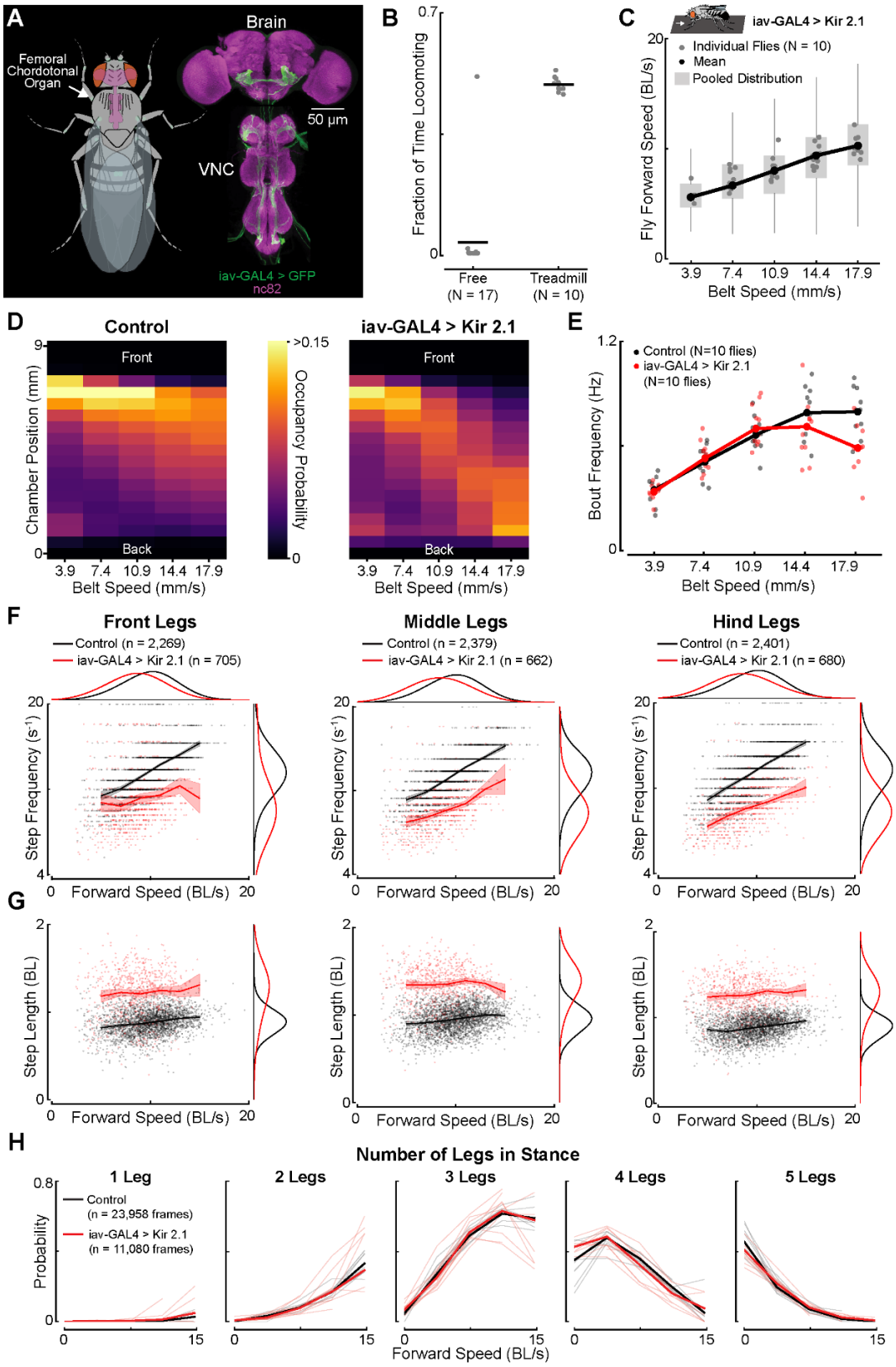

Figure 2.4. Silencing mechanosensory chordotonal neurons alters step kinematics but not inter-leg coordination across walking speeds. (**A**) A schematic of the locations of chordotonal neurons (green), including the femoral chordotonal organ in each leg (white

arrow for left front leg), labeled by the iav-GAL4 driver line. The axons of chordotonal neurons (green) are shown in the max intensity projection of a confocal stack of the fly brain and VNC (magenta). (**B**) Flies with silenced chordotonal neurons (iav-GAL4> Kir 2.1) spent more walking on the treadmill compared to the arena. Gray dots: individual flies; Black lines are means. (**C**) The flies in (B) increased their forward walking speed as the belt speed increased. N: number of flies. Box plots show the distribution of pooled data. Black line connects the median forward speed for all flies for each belt speed. Gray dots are the median forward speed of each fly. (**D**) Heatmap of the occupancy probability along the chamber of genetically-matched controls (R52A01 GAL4-DBD > Kir2.1; left panel) and flies lacking chordotonal feedback (right) shows that the latter has a greater probability of being located towards the back of the chamber at fast belt speeds. (**E**) Bout frequency was lower at fast belt speeds for flies lacking chordotonal feedback (red) compared to controls (black). Dots are the mean bout frequency for each fly. N: number of flies. (**F**) The step frequency of the front (left), middle (center), and hind (right) legs was lower across walking speeds for flies lacking chordotonal feedback (red) compared to genetically-matched controls (black). Lines are speed binned averages (2 BL/s bins from 5-15 BL/s) for each kinematic parameter and the 95% confidence interval is shown by the shaded region. Distributions between control and experimental flies were offset from each other so that they could be visualized. n: number of steps. (**G**) Step length was greater across walking speeds for flies lacking chordotonal feedback (red) compared to controls (black). (**H**) The probability of a certain number of legs in stance (1-5: left-right) was not different across walking speeds between flies with silenced chordotonal neurons (red) and controls (black). Solid lines: pooled data; Thin lines: individual flies. n: number of camera frames.

Split-belt walking had minimal effects on inter-leg coordination. For instance, there was only a small difference in the probability of 3 legs being in stance during asymmetric belt movement compared to when the belts were tied in speed (**Figure 2.5F**). Moreover, the mean phase offsets between legs were either not altered or shifted slightly when the belts were driven at different speeds compared to when they were tied (**Figure 2.5G**). These subtle changes in inter-leg coordination may help correct for the rotational perturbation induced by the treadmill. However, the more substantial changes in the spatial positioning of the middle legs appear to be the primary mechanism that flies use to achieve straight walking during split-belt walking (**Figure 2.5H**).

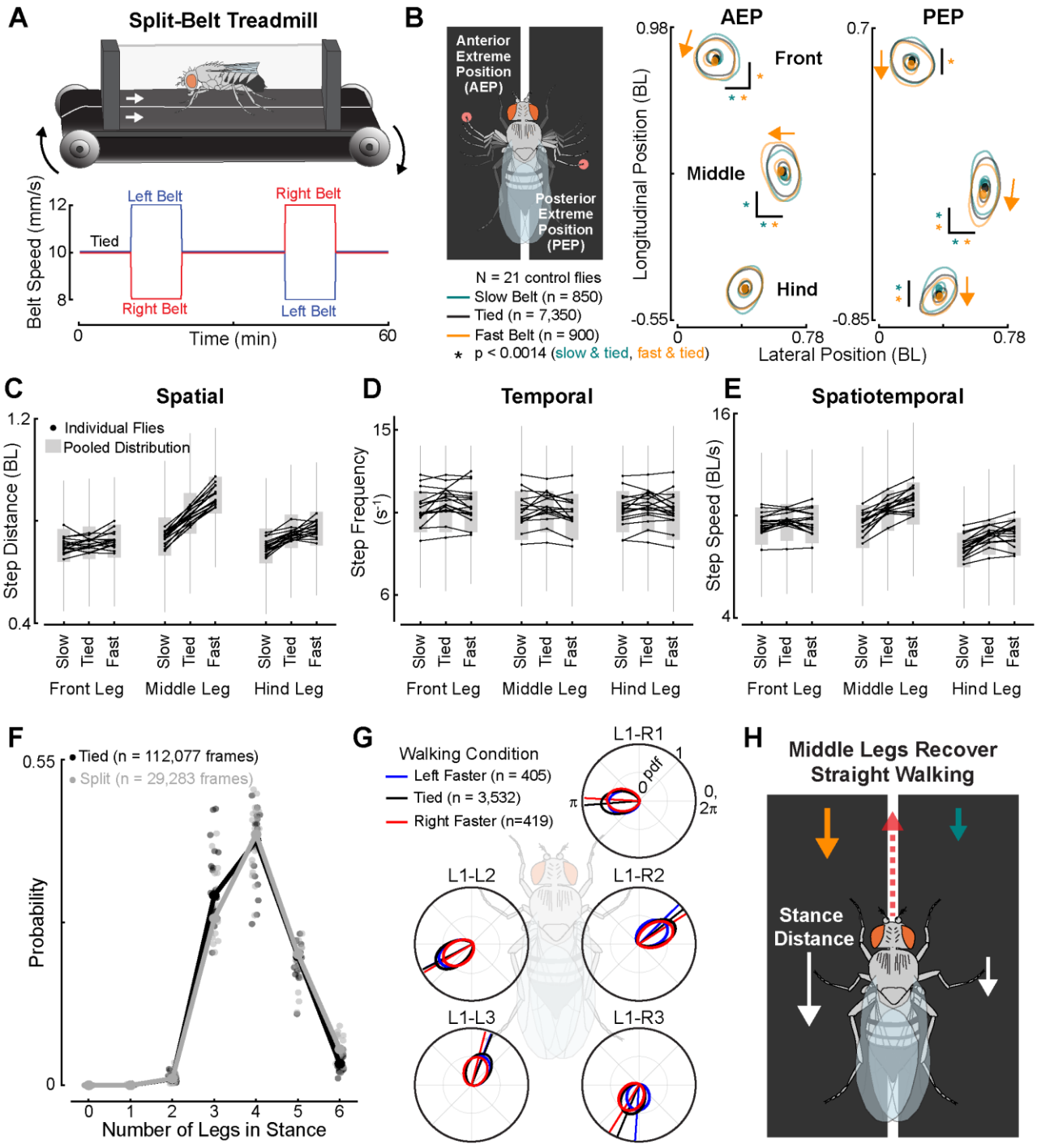

Figure 2.5. A split-belt treadmill reveals that flies adjust spatial kinematics to correct for rotational perturbations. (**A**) A schematic of the split-belt treadmill (top) and the belt speed protocol (bottom). The split-belt treadmill consists of two independently controlled belts, which were initially driven at the same speed (tied). The right (red) and left (blue) belts then differed in speed by 40%, and the direction of the speed change reversed on the subsequent split period. (**B**) We focused our analysis on forward walking bouts where the left and right legs moved on their respective belts (left). The distributions of where the legs first contact the ground, the anterior extreme positions (AEP), and where they takeoff from the ground, the posterior extreme positions (PEP), are shown for when legs walked on belts during the tied condition (black) or on the slow (teal) and fast (orange) belt during the split condition. Distributions are shown by kernel density estimations and means are denoted by dots. Arrows indicate the direction the distributions shifted with respect to the tied distribution. Bootstrapping with a Bonferroni correction of 36 was used to statistically compare the means of the tied

and split distributions. An absence of a "*" indicates no significant difference. N: number of flies; n = number of steps. (**C**) Step distance increased for the middle leg as belt speed increased. The hind leg had a lower step distance when walking on the slow belt. Box plots show the distribution of pooled data. Black lines and dots are the median step distances of individual flies. (**D**) Step frequency did not change across conditions for any leg. (**E**) Step speed increased for the middle leg as belt speed increased and was lower for the hind leg on the slow belt. (**F**) Probability of 0-6 legs being stance when the belts were tied (black) or split (gray) in speed. Dots connected by lines are the global probabilities. Individual dots are the probability that a given fly shows a certain number of legs in stance. (**G**) Polar plots of the relative phase between the left front leg and the other legs when the belts were tied (black) or split (left faster: blue; right faster: red) in speed. n: number of phase comparisons. (**H**) Summary schematic showing that the middle legs adjust their step distance to recover straight walking in the presence of asymmetric belt speeds.

2.4 Discussion

In this study, we engineered miniature linear and split-belt treadmills for walking *Drosophila*. Flies walking on the treadmill exhibited similar walking behavior, step kinematics, and inter-leg coordination to freely walking flies. The treadmill allowed us to achieve the first 3D tracking of untethered fly walking, which revealed that flies elevate their body height as they walk faster. We also used the linear treadmill to show that flies lacking mechanosensory feedback from chordotonal neurons are able to walk at higher speeds if compelled to do so. Across all walking speeds, silencing chordotonal neurons altered motor control of individual legs, but not coordination between legs. Finally, we found that flies can maintain a forward heading on a split-belt treadmill by adjusting the step size of their middle legs. These insights illustrate how treadmills fill an important gap between freely walking and tethered preparations for investigating neural and behavioral mechanisms of fly locomotion.

Although our primary goal was to compare treadmill and freely walking flies, we also took the opportunity to examine walking kinematics of tethered flies. The advantage of tethered walking is that it enables full 3D joint tracking[46,47], spatially targeted optogenetic stimulation[28], and recordings of neural activity with calcium imaging[48] or electrophysiology[49,50]. However, our results suggest that studies of tethered walking should be interpreted with caution, because walking kinematics of tethered flies differ in subtle but important ways from untethered flies (**Figures 2.2-2.3**; **Figure S2.1**). Although speed-dependent changes in walking kinematics and coordination were consistent between tethered and untethered flies, the magnitude of step kinematics and the coupling strength between legs were different. One reason for these differences may be that tethered flies walk on a sphere (i.e., a foam ball), whereas treadmill and freely walking flies walk on a flat surface. Tethered flies also do not support their own body weight, but instead use their legs to rotate the floating sphere, a configuration that is unlikely to mimic normal ground reaction forces. Indeed, prior

work showed that changing the load on the body alters walking kinematics in freely walking flies[63]. On the other hand, it is remarkable that flies and other animals walk at all while tethered on a floating sphere. Given the major mechanical differences between tethered and untethered conditions, the kinematic differences we found are relatively subtle.

One of our primary motivations for developing a treadmill system for flies was to investigate the role of mechanosensory feedback across walking speeds. Prior work has suggested that proprioception is most important at slower walking speeds, and that flies use a more feedforward motor program when walking faster[8]. However, testing this hypothesis has been challenging, because silencing mechanosensory neurons causes flies to walk less and at lower velocities[7]. The linear treadmill makes it possible to drive fly locomotion across a wide range of speeds, including after genetic manipulations to mechanosensory neurons. We found that silencing mechanosensory feedback alters step kinematics across all walking speeds. Indeed, the greatest deviation in step kinematics between control and experimental flies occurred at faster walking speeds. However, the lack of mechanosensory feedback did not impact inter-leg coordination at any walking speed. We chose to use a blunt manipulation with a broad driver line (iav-Gal4) to illustrate the utility of the treadmill for driving walking even when mechanosensory feedback is profoundly altered. One important caveat is that we expressed Kir 2.1 in chordotonal neurons throughout development, so the nervous system could have compensated to maintain normal inter-leg coordination. In the future, it will be interesting to silence mechanosensory feedback of flies walking on the treadmill with more temporal and genetic specificity, for example using optogenetic manipulation of proprioceptor subtypes in the femoral chordotonal organ[29,30]. Our results are consistent with the hypothesis that proprioceptors in the femoral chordotonal organ contribute to individual leg kinematics, whereas descending commands from the brain[8] or feedback signals from other proprioceptor classes may have more influence on inter-leg coordination[62].

In hexapod insects, each pair of legs plays a specialized role in controlling locomotion. In freely walking insects, the front legs are typically used for steering[31], while the hind legs contribute to propulsion and jumping[64–66]. Using the split-belt treadmill, we found that the middle legs play a unique role in correcting for perturbations that displace flies from a forward walking trajectory. The middle legs are ideally positioned to stably pivot the body of the fly about its center of mass, like rowing a boat from its center. In larger insects, the middle legs have been shown to play a role in

executing tight turns[67]. Although the split-belt treadmill puts the fly in artificial circumstances, it mimics many situations in the wild when flies may need to perform rotational body corrections. For example, heterogeneous terrain, meddlesome conspecifics, or unilateral wind gusts could asymmetrically act on the movement of the left and right legs to induce a rotation of the body. In the future, the split-belt treadmill may also provide a useful method to study the neural mechanisms that underlie adaptive heading stabilization in walking flies[68].

In addition to their utility for investigating sensorimotor control of fly walking, we anticipate several additional applications of miniature treadmill systems. One will be to investigate motor adaptation during split-belt walking, a phenomenon which has been extensively studied in mammals[69]. The split-belt treadmill is also used as a clinical tool for diagnosing cerebellar deficits[70] and post-stroke rehabilitation[23] in humans. The linear treadmill may also be useful for the study of insect respiratory physiology, which has previously been studied during flight[71] and in running cockroaches[15] and tarantulas[72]. Finally, because our treadmill system is constructed of simple and inexpensive belts, pulleys, and motors, it can be easily customized to study other walking insects, such as ants[73] and snow flies[74].

2.5 Methods

Fly Husbandry and Genotypes

Adult male *Drosophila melanogaster* between 2-7 days post-eclosion were used for experiments (Table 2.1). Flies were reared in a 25°C incubator with 14:10 light:dark cycle within vials filled with a standard cornmeal and molasses medium.

Stock Name	Genotype	Figure(s)	Stock Source
WT Berlin	+; +; +	1-3	Gifted from Heisenberg Lab
R52A01 DBD > Kir 2.1 (Control)	w[1118]/+ DL; +/+ DL; pJFRC49-10XUAS-IVS-eGFP::Kir2.1(attP2)/P{y[+t7.7]w[+mC]=R52A01-GAL4.DBD}attP2	4	Crossed Dickinson Lab Stock U-111 with Bloomington Stock #69141
Iav-GAL4 > Kir 2.1	w[*]/+ DL; +/+ DL; pJFRC49-10XUAS-IVS-eGFP::Kir2.1(attP2)/P{w[+mC]=iav-GAL4.K}3	4	Crossed Dickinson Lab Stock U-111 with Bloomington Stock #52273
R48A07 AD > Kir 2.1 (Control)	w[1118]/+ DL; P{+t[7.7]w[=mC]=R48A07-p65.AD}attP40/+ DL; pJFRC49-10XUAS-IVS-eGFP::Kir2.1(attP2)/+	5	Crossed Dickinson Lab Stock U-111 with Bloomington Stock #71070
R39B11 AD > Kir 2.1 (Control)	w[1118]/+ DL; P{+t[7.7]w[=mC]=R39B11-p65.AD}attP40/+ DL; pJFRC49-10XUAS-IVS-eGFP::Kir2.1(attP2)/+	5	Crossed Dickinson Lab Stock U-111 with Bloomington Stock #71040

Table 2.1. *Drosophila melanogaster* genotypes used for experiments.

Miniature Treadmills

Linear treadmill and experiments

The key components of the linear treadmill system are a custom 3D-printed chamber, pulleys, a belt, a DC motor controlled programmatically with a PID controller, and 5 high-speed cameras. The chamber was designed using 3D CAD software (Autodesk Fusion 360: *Treadmill_Chamber.stl* in GitHub repository) and printed with black resin using a high spatial resolution 3D printer (Formlabs Form 2; black resin RS-F2-GPBK-04). The region of the chamber where a fly walked had transparent, sloped walls, a length of 8.929 mm, a max width of 6.5 mm, and a max height of 1.5 mm. Coverslips that were 22m x 22m and size #1 were used as the transparent walls of the chamber (Electron Microscopy Sciences: #72200-10). Rain-X was applied to the inner surface of the coverslips to limit flies from walking on the glass. The pullies (B & B Manufacturing: 28MP025M6FA6) were attached to steel bars which rotated with bearings (AST Bearings: SMF126ZZ) that were mounted on custom fabricated brackets. The distance between the brackets was adjustable, which enabled the belt (B & B Manufacturing: 100MXL025UK) held between the pullies to be tensioned. A mounted DC motor (Phidgets: 12V/0.8Kg-cm/46RPM 50:1 DC Gear Motor w/ Encoder ID: 3256E_0) actuated the belt. An infrared ring-light (Olympus Controls: R130-850) was used to illuminate flies on the belt. 5 high-speed cameras (Machine Vision Store; USB 3.0 Basler camera acA800 x 600, Basler AG) with adjustable lenses (Computar: MLM3X-MP) and IR filters

(Olympus Controls: FS03-BP850-34) recorded flies walking on the belt and within the chamber at 180 fps. The DC motor and high-speed cameras were controlled using a microcontroller (Phidgets: PhidgetMotorControl 1-Motor ID: 1065_1B) and DAQ (National Instruments: BNC-2110), respectively, and a custom Python script (*linear_treadmill_belt_stim_videography.py* in GitHub repository).

Male *Drosophila* (specific genotypes in Table 1) were driven to walk on the linear treadmill while the belt's steady state speed was either 3.9, 7.4, 10.9, 14.4, or 17.9 mm/s. To smoothly reach steady-state belt speeds above 3.9mm/s, the belt linearly increased in speed with a slope of 3.5 mm/s^2. Wild-type Berlin and iav-GAL4 > Kir 2.1 flies were subjected to each belt speed 10 times, whereas R52A01 DBD > Kir 2.1 flies were presented each belt speed 15 times. Trials in which flies walked at a given belt speed were 10 seconds. There was a 5 second period between trials where the belt moved at 3.9 mm/s and the high-speed videos were saved. DeepLabCut and Anipose[47,51] were used track the fly's leg tips (i.e. tarsi), head, thorax, abdomen, and key points on the chamber in 3D using 2,250 annotated frames as the training dataset. The test prediction error of the tracking was 5.45 pixels and the reprojection error was 2.88 pixels. Walking kinematics were analyzed and visualized using custom Python scripts (*linear_treadmill_walking_analysis.ipynb* & *linear_treadmill_visualization_walking_comparisons.ipynb* in GitHub repository).

We also tried driving tethered flies to walk on the linear treadmill. Occasionally, the front legs moved with the belt, but the overall movement between legs was uncoordinated. We typically observed legs being dragged along the surface of the belt. It should be noted that we tried many different tether designs, from rigid ones to light-weight, low-resistance ones inspired from a treadmill used for desert ants[73]. Overall, we were unable to drive coordinated walking in tethered flies using the treadmill.

Split-belt treadmill and experiments

The construction of the split-belt chamber was similar to the linear treadmill. The key difference was the addition of a second independently actuated belt. Therefore, we used smaller belts (B & B Manufacturing: 100MXL012UK) and pullies (B & B Manufacturing: 28MP012M6FA6), while the chamber size remained the same. We also used DC motors (Phidgets: 12V/3.0Kg-

cm/78RPM 51:1 DC Gear Motor w/ Encoder ID: 3263E_1) that were of a newer model. Finally, the frame rate of the high-speed cameras was increased to 200 fps. A custom Python script controlled the motors and cameras (*splitbelt_treadmill_belt_stim_videography.py* in GitHub repository).

Only male flies were used in split-belt experiments (specific genotype in Table S1). Flies initially walked on belts that were tied in speed (i.e. 10 mm/s) for 10 minutes. Then, one belt increased in speed by 20% (i.e. 12 mm/s) while the other belt decreased in speed by 20% (i.e. 8 mm/s). This split period also lasted 10 minutes. Following the split period, the belts again moved at 10 mm/s for 10 minutes. At the end of the 10 minutes, this trial structure was repeated, but the belts switched which increased or decreased in speed during the split period. 5 high-speed cameras recorded the movement of the fly during this task and the same key points in the linear treadmill experiments were tracked and reconstructed in 3D. The training dataset consisted of 4,140 annotated frames and the DeepLabCut network achieved a test error of 6.13 pixels. The reprojection error was 1.82 pixels. Custom Python scripts were used to analyze and visualize walking kinematics (*splitbelt_walking_analysis.ipynb* and *splitbelt_walking_visualization.ipynb* in GitHub repository).

Freely Walking Experiments

Groups of 10, 2-7 day old, male wild-type Berlin flies were placed in a 10 cm circular arena with sloped walls (i.e. fly bowl) and allowed to freely walk[43]. A high-speed camera (Machine Vision Store: USB 3.0 Basler camera acA1300-200um, Basler AG) recorded a 2.4 cm x 2.7 cm region of the arena from above at 150 fps in 10s bouts. Leg tips, head, thorax, and abdomen of flies were tracked using SLEAP, which is optimized for multi-animal pose estimation[76]. Custom Python scripts quantified and visualized walking kinematics (*freely_walking_analysis_visualization.ipynb* in GitHub repository).

Tethered Experiments

De-winged male wild-type Berlin flies, 2-5 days old, were attached to a thin tungsten tether (0.1 mm) with UV curing glue (KOA 300). Flies were then positioned with a micromanipulator on a spherical foam ball (weight: 0.13 g; diameter: 9.08 mm) suspended by a regulated air supply. The 2D trajectory, and forward, rotational, and side-slip velocities of the fly were measured from the movement of the ball with FicTrac[77]. 6 high-speed cameras (Machine Vision Store: USB 3.0 Basler

camera acA800 x 600, Basler AG) recorded flies walking on the ball at 300 fps over 2 second bouts. Custom python and MATLAB scripts were used to acquire the high-speed videos. The leg joints, tips, head, and abdomen were tracked and reconstructed in 3D using DeepLabCut and Anipose, respectively. Walking kinematics were analyzed and visualized using Python (*tethered_walking_analysis_visualization.ipynb* in GitHub repository).

Statistical and KL Divergence Analyses

Chi-squared test and t-tests were used to test for differences in step kinematics between the different experimental setups (**Figure 2.2**). Statistics were conducted on kinematic distributions containing data from all leg pairs and that were associated with a walking speed between 6.5-10.1 BL/s. This walking speed range was chosen because it contained 50% of the data across setups given their overlapping speed ranges. The chi-squared test determined whether the proportion of values of a given discretely measured step metric (i.e. step frequency, stance duration, and swing duration) was the same between freely walking flies and those in the other two setups. A Bonferroni correction of 18 was added to account for multiple comparisons (6 legs and 3 setups). Therefore, a significant difference was determined to be $p < 0.0028$. Note that to make the statistical comparisons of step frequency, stance duration, and swing duration between all three setups, we had to interpolate the underlying signal for treadmill and freely walking flies from 180 fps and 150 fps, respectively, to 300 fps (i.e. the tethered setup sampling rate). Finally, a t-test was used to determine significant differences between the mean step lengths of freely, treadmill, and tethered walking flies. A Bonferroni correction of 18 was also applied.

To determine whether step kinematics of freely walking flies were more similar to those of treadmill or tethered walking flies, we computed the relative KL divergence (**Figure S2.1**). KL divergence computes an unbounded similarity, in the form of entropy, between two distributions, where a value closer to zero indicates greater similarity. Thus, we computed the KL divergence between freely and treadmill step kinematic distributions, and freely and tethered distributions. Then, we calculated a relative similarity score between the two sets of distributions by using the following equation:

$$Similarity = 1 - \frac{KL_{freely-treadmill}}{(KL_{freely-treadmill} + KL_{freely-tethered})}$$

A value of 1 indicated that freely and treadmill walking step kinematics were more similar than freely and tethered ones, and vice versa.

Finally, a bootstrap statistical analysis was used to test if there were significant shifts in the mean anterior and posterior extreme positions across the different belt conditions (i.e. tied, slow, and fast belt) of the split-belt task. A Bonferroni correction of 36 was applied (6 legs, 3 belt conditions, and 2 axes of comparison), requiring a $p < 0.0014$ for a significant difference.

Kinematic Classification and Parameters

Swing and stance classification

Leg tip velocity was used to classify leg swing and stance phases in all walking setups. We first computed the instantaneous speed of each leg tip from their allocentric positions along the longitudinal and lateral body axes. For the treadmill and tethered walking setups, a rotation matrix had to be applied to the position data to align all flies to a common reference frame and to ensure symmetric contralateral leg movement with respect to the defined axes. The instantaneous speed was then transformed into velocity by applying a negative sign to instances where the leg moved backward along the longitudinal body axis in an egocentric reference frame. This forced the stance to be negative. To achieve this sign application for freely and treadmill walking setups, where the heading of the fly is constantly changing, we rotated the fly in each frame to a common heading. This made it easier to distinguish the period when the leg moved along the body. The instantaneous velocities of the leg tips were then smoothed with a Gaussian kernel. The width of the kernel was chosen such that the signal wasn't oversmoothed, but instantaneous tracking errors were mitigated. Swing was classified as periods where the smoothed leg tip velocities were above and below manually chosen upper (treadmill: 5 mm/s, freely: 15 mm/s, tethered: 0 mm/s) and lower thresholds (all setups: -25 mm/s). Stance was classified as the period where the leg tip velocities were between these thresholds. Finally, we corrected blips in the classification (e.g. converting a swing period consisting of 1 frame into stance) and matched the stance and swing onsets of a given step.

We checked the accuracy of the swing and stance classifications by manually inspecting the raw high-speed videos. Note that we also tried to perform swing and stance classification by thresholding the Hilbert transformed longitudinal body axis position signal of each leg tip, and doing peak detection on that signal, but both methods performed more poorly than the method described above. The Hilbert transform assumes that a signal is non-stationary, which is invalid when using a leg position signal that dynamically moves in 3D. Peak detection also fails to compensate for the richness of leg movement. Overall, our accurate classifications of swing and stance enabled precise quantifications of step kinematics and inter-leg coordination.

Forward walking bout classification

Different forward walking bout classifiers were used for each walking setup. In the linear and split-belt setups, forward walking bouts were periods lasting 200 ms where the fly walked in the middle of the chamber, had a heading angle within -15 to 15 degrees with respect to the front of the chamber, and had a forward walking velocity (aligned to the driving axis of the treadmill) greater than 5 mm/s. Flies were classified as walking in the middle of the chamber if their abdomen was 1.85 mm in front of the back of the chamber and the tarsi of their front legs were 1.08 mm behind the front of the chamber. For freely walking flies, the thorax position, specifically the angle between sets of 3 position sample points, was used to first isolate straight body trajectories in allocentric coordinates. A straight trajectory was defined as one where the angles between thorax position sample points were less than 4.5 degrees. Once a straight trajectory was isolated, we classified it as a forward walking bout if the corresponding fly's average body velocity was greater than 5 mm/s, the inter-quartile range of the heading angles was less than 20 degrees, and the duration of the trajectory was greater than 200 ms. Lastly, forward walking bouts of tethered flies were first identified by using a previously described behavioral classifier [47], but later refined to those greater than 200 ms in duration, having an average forward velocity greater than 5 mm/s, a minimum instantaneous forward velocity of 0.5 mm/s, an average absolute rotational velocity less than 25 degrees/s, and an absolute instantaneous rotational velocity less than 100 degrees/s. Across all setups, the first and last steps of all legs were trimmed within identified forward walking bouts to compensate for the transitions into and out of them.

Forward walking step filtering

Forward walking steps were filtered based on step frequency, stance duration, and swing duration in all walking setups. Forward walking steps were considered to be those that had a step frequency between 5 and 20 steps/s, a swing duration between 15 and 75 ms, and a stance duration less than 200 ms. These filtering thresholds were empirically determined and based on previously published results of forward walking step kinematics in fruit flies[41,56,57,63].

Glossary of kinematic parameters

Body length: the distance between the head and distal part of the abdomen.

Body height: the vertical distance between the ground and thorax.

Step frequency: the number of steps completed within a second.

Stance duration: the duration that a leg contacts the ground while walking.

Swing duration: the duration of the aerial phase of leg movement during walking.

Step length: the total distance a leg travels within a step (i.e. stance onset to the subsequent stance onset) in allocentric coordinates.

Step distance: the total distance a leg travels within a step (i.e. stance onset to the subsequent stance onset) in egocentric coordinates.

Step speed: the total distance a leg travels within a step in egocentric coordinates divided by the duration of the step.

Anterior extreme position: the position where a leg first contacts the ground (i.e. stance onset) in egocentric coordinates.

Posterior extreme position: the position where a leg first takes off from the ground (i.e. swing onset) in egocentric coordinates.

Number of legs in stance: the number of legs contacting the ground at a given moment in time.

L1 relative phase: the relative offset in the stance onsets between the left front leg and the leg of interest with respect to the left front leg's step cycle.

Tripod step order: the order in which the legs within a tripod group (i.e. ipsilateral front and hind legs and the contralateral middle leg) first enter stance with respect to the left front leg's step cycle.

Acknowledgements

We thank Max Mauer for engineering the first prototype of the treadmill, Sarah Walling-Bell and Srinidhi Naidu for performing some of the initial treadmill experiments, Eric Martinson for valuable advice and technical support throughout the development of the treadmill systems, Tom Daniel and Jeff Riffell for letting us use their 3D printing equipment and providing advice on the development of the treadmill chamber, Michael Dickinson for designing the fly cartoons many years ago and reminding us of it often, Anne Sustar for the brain and VNC images in Figure 4A, and members of the Tuthill and B.W. Brunton labs for feedback on the manuscript. B.G.P was supported by an NSF Graduate Research Fellowship (Fellow ID: 2018261272). S.J.L. was supported by T32 NS 99578-3. Other support was provided by National Institutes of Health grants R01NS102333 and U19NS104655, a Searle Scholar Award, a Klingenstein-Simons Fellowship, a Pew Biomedical Scholar Award, a McKnight Scholar Award, a Sloan Research Fellowship, the New York Stem Cell Foundation, and a UW Innovation Award to J.C.T. J.C.T is a New York Stem Cell Foundation – Robertson Investigator.

Author Contributions

B.G.P. and J.C.T. conceived of the study. B.G.P. engineered the linear and split-belt treadmills. B.G.P. developed high-speed videography acquisition scripts and code to control the treadmill belts. B.G.P. collected and analyzed linear and split-belt treadmill data. S.J.L. collected and analyzed freely walking data. G.M.C. collected and analyzed tethered walking data. B.P. and G.M.C. performed the statistical analyses. B.G.P. and J.C.T. wrote the manuscript with input from other authors.

Data and Code Availability

Data is available on Dryad (https://doi.org/10.5061/dryad.mpg4f4r73). Code for analyzing and visualizing treadmill, freely, and tethered walking kinematics is located on GitHub

(https://github.com/Prattbuw/Treadmill_Paper). The .stl file used for the 3D printed treadmill chamber and Python scripts to acquire high-speed video and control the treadmills are also located there.

Video Legends

Video 2.1. A representative fruit fly walking on the linear treadmill with a steady-state belt speed of ~11 mm/s. Top-down and side views of a wild-type Berlin fly walking on the treadmill within the chamber are shown by the top left and right videos, respectively. The videos were recorded at 180 fps. Below, in descending order, are the position of the fly within the chamber, its heading angle, its body velocity, and the belt speed throughout the video. The light blue regions indicates forward walking bouts. This data is displayed in **Figure 1D**.

Video 2.2. Fruit flies are capable of walking across a wide range of treadmill belt speeds. Top-down and side views of a wild-type Berlin fly walking on the linear treadmill within a chamber are shown by the top left and right videos, respectively. The tracked head (red), thorax (green), and abdomen (blue) are displayed for each camera view, as well as the belt speed profile contained within the video. Note that this early chamber design differs from that used in the rest of the paper.

Video 2.3. The linear treadmill forces high-speed walking in flies. Top-down and side views of a control (R52A01 DBD > tnt) fly walking on the linear treadmill within a chamber are shown by the top left and right videos, respectively. The fly was driven at a belt speed of about 18 mm/s and achieved walking velocities greater than 50 mm/s, which is the fastest walking velocity reported for *Drosophila melanogaster*. Note that flies of this genotype are not used elsewhere in the paper.

Video 2.4. A fruit fly walking freely and forward in an arena. The top-down view shows a wild-type Berlin fly walking in an arena (i.e. the fly bowl). The forward walking bout is indicated by the appearance of the "Forward Walking" label. The video was recorded at 150 fps and was slowed down 10x. This data is contained in **Figures 2.2 & 2.3**.

Video 2.5. A representative tethered fruit fly walking on a sphere suspended by air. Side and top-down views (left and right, respectively) show a wild-type Berlin fly walking on a floating sphere while tethered. The forward walking bout is indicated by the appearance of the "Forward Walking" label. The video was recorded at 300 fps and was slowed down by 5x. This data is contained in **Figures 2.2 & 2.3**.

Video 2.6. Silencing chordotonal neurons alter walking in flies. Top-down and side views (left and right, respectively) are shown for the same genetically-matched control fly (R52A01 DBD > Kir 2.1; top) and fly with chordotonal neurons broadly silenced (iav-GAL4 > Kir 2.1) as each walked on the linear treadmill. The belt speed was 17.9 mm/s for both flies. Videos were recorded at 180 fps and were slowed down by 2x. This data is contained in **Figure 2.4**

Video 2.7. Flies use their middle legs to correct for rotational perturbations induced by asymmetric belt speeds on the split-belt treadmill. Top-down views of the same control (R48A07 AD > Kir 2.1) fly walking on the split-belt treadmill when the left and right belts were tied in speed (10 mm/s) and when the left belt moved faster (12 mm/s) than the right (8 mm/s). The period of asymmetric belt movement is called the "split" period. During the representative split period, a forward walking bout is shown where the left and right legs of the fly walked on the corresponding belts. Videos were recorded at 200 fps and the video showing the forward walking bout was slowed 5x. This data is contained in **Figure 2.5.**

2.6 Supplemental information

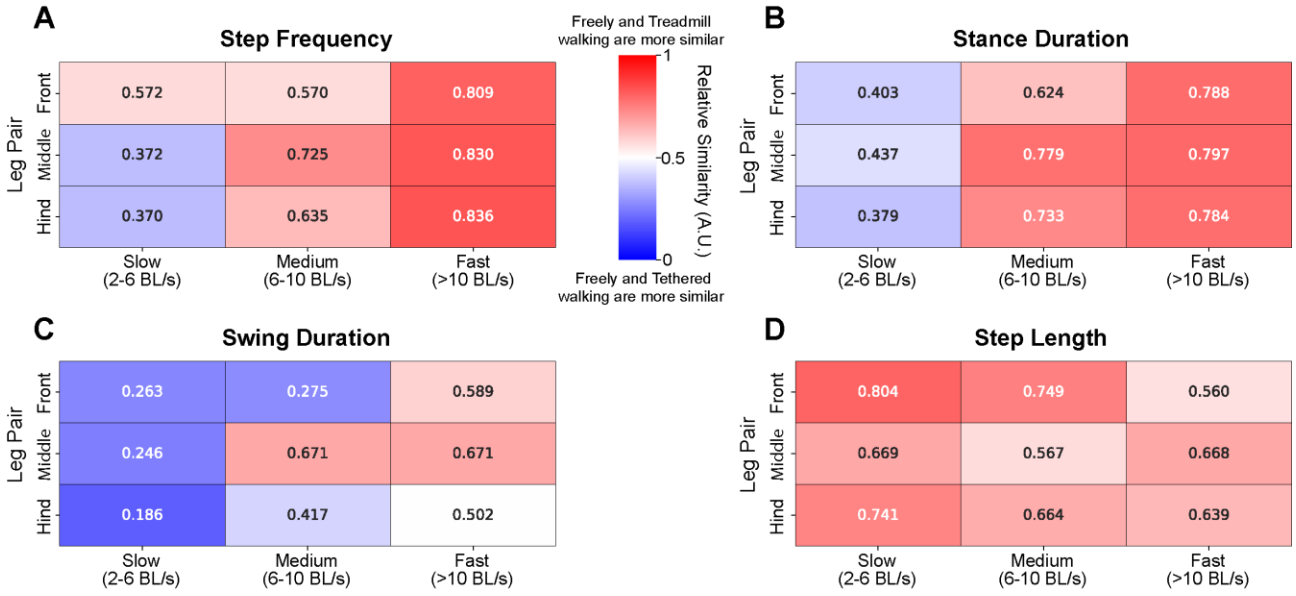

Figure S2.1. Distributions of step kinematics are more similar between freely and treadmill walking flies than between freely walking and tethered flies. (**A**) Step frequency was more similar between treadmill and freely walking flies, especially at medium (6-10 BL/s) and fast (>10 BL/s) walking speeds. At slow (2-6 BL/s) walking speeds, freely and tethered walking step frequencies were more similar. Relative similarity was determined by dividing the KL divergence of freely and treadmill walking kinematic distributions by the sum of the KL divergences between freely and treadmill walking, and freely and tethered walking kinematic distributions. We then reversed the similarity scale by computing 1 minus these values. A value close to 1 indicates that freely and treadmill step kinematics are more similar than freely and tethered walking kinematics for a given walking speed range. The opposite is true for values close to 0. (**B**) Stance duration was more similar between freely and treadmill walking. At slow walking speeds, freely and tethered walking stance durations were slightly more similar than that of treadmill walking. (**C**) Swing duration was more similar between freely and treadmill walking flies at fast speeds, whereas the swing duration of freely and tethered walking flies was more similar at slower speeds. (**D**) Step length was most similar between freely and treadmill walking flies across all speeds and legs.

Kinematics Parameter	Source	Fly Strain	Sex	Mean Value @ 10 mm/s	Mean Value @ 20 mm/s	Mean Value @ 30 mm/s
Step Frequency (s^{-1})	Szczecinski et al., 2018	WT Berlin, Canton S, w^{1118}	Male	9	12.5	15
	Present Study – Treadmill Walking	WT Berlin	Male	9	12.5	15
	Present Study – Freely Walking	WT Berlin	Male	10	13	15.5
	Present Study – Tethered Walking	WT Berlin	Male	9	11	N.A.
Stance Duration (ms)	Szczecinski et al., 2018	WT Berlin, Canton S, w^{1118}	Male	80	50	45
	DeAngelis et al., 2019	WT flies from Gohl et al., 2011	Female	80	50	40
	Mendes et al., 2013	Oregon R	Female	100	60	45
	Present Study – Treadmill Walking	WT Berlin	Male	75	50	37.5
	Present Study – Freely Walking	WT Berlin	Male	75	50	37.5
	Present Study – Tethered Walking	WT Berlin	Male	80	55	N.A.
Swing Duration (ms)	Szczecinski et al., 2018	WT Berlin, Canton S, w^{1118}	Male	35	30	28
	Wosnitza et al., 2013 (data used in above ref.)	WT Canton S	Male	35	30	25
	DeAngelis et al., 2019	WT flies from [75]	Female	30	35	40
	Mendes et al., 2013	Oregon R	Female	35	32.5	30
	Strauβ and Heisenberg, 1990	WT Berlin	Female	35	30	28
	Present Study – Treadmill Walking	WT Berlin	Male	37.5	35	32.5
	Present Study – Freely Walking	WT Berlin	Male	35	35	35
	Present Study – Tethered Walking	WT Berlin	Male	37.5	35	N.A.
Step Length (mm)	DeAngelis et al., 2019	WT flies from Gohl et al., 2011	Female	1	1.5	2
	Mendes et al., 2013	Oregon R	Female	1.25	1.75	2.25
	Strauβ and Heisenberg, 1990	WT Berlin	Female	1.5	2.25	2.5
	Present Study – Treadmill Walking	WT Berlin	Male	1.8	2.1	2.125
	Present Study – Freely Walking	WT Berlin	Male	1.8	2.05	2.2
	Present Study – Tethered Walking	WT Berlin	Male	1.3	1.75	N.A.

Table S2.1. Summary of previously reported relationships between step kinematics and forward walking speed in *Drosophila melanogaster* and those reported in this study. Mean values were determined through visual inspection of fits within relevant plots of previous literature. The mean values for the relationships obtained in this study were approximated through visual inspection of the fits in Figure 2, as we did for the other papers.

2.7 References

1. Couzin-Fuchs, E., Kiemel, T., Gal, O., Ayali, A., and Holmes, P. (2015). Intersegmental coupling and recovery from perturbations in freely running cockroaches. Journal of Experimental Biology *218*, 285–297. 10.1242/jeb.112805.

2. Eng, J.J., Winter, D.A., and Patla, A.E. (1994). Strategies for recovery from a trip in early and late swing during human walking. Experimental Brain Research *102*, 339–349. 10.1007/BF00227520.

3. Tuthill, J.C., and Wilson, R.I. (2016). Mechanosensation and Adaptive Motor Control in Insects. Curr Biol *26*, R1022–R1038. 10.1016/j.cub.2016.06.070.

4. Andersson, O., and Grillner, S. (1983). Peripheral control of the cat's step cycle. Acta Physiologica Scandinavica *118*, 229–239. 10.1111/j.1748-1716.1983.tb07267.x.

5. Dietz, V. (2002). Proprioception and locomotor disorders. Nature Reviews Neuroscience *3*, 781–790. 10.1038/nrn939.

6. Chesler, A.T., Szczot, M., Bharucha-Goebel, D., Čeko, M., Donkervoort, S., Laubacher, C., Hayes, L.H., Alter, K., Zampieri, C., Stanley, C., et al. (2016). The Role of PIEZO2 in Human Mechanosensation. N Engl J Med *375*, 1355–1364. 10.1056/NEJMoa1602812.

7. Mendes, C.S., Bartos, I., Akay, T., Márka, S., and Mann, R.S. (2013). Quantification of gait parameters in freely walking wild type and sensory deprived Drosophila melanogaster. eLife Sciences *2*, e00231. 10.7554/eLife.00231.

8. Bidaye, S.S., Bockemühl, T., and Büschges, A. (2018). Six-legged walking in insects: how CPGs, peripheral feedback, and descending signals generate coordinated and adaptive motor rhythms. Journal of Neurophysiology *119*, 459–475. 10.1152/jn.00658.2017.

9. Belanger, M., Drew, T., Provencher, J., and Rossignol, S. (1996). A comparison of treadmill locomotion in adult cats before and after spinal transection. Journal of Neurophysiology *76*, 471–491. 10.1152/jn.1996.76.1.471.

10. Hasan, Z., and Stuart, D.G. (1988). Animal Solutions to Problems of Movement Control: The Role of Proprioceptors. Annu. Rev. Neurosci. *11*, 199–223. 10.1146/annurev.ne.11.030188.001215.

11. Wetzel, M.C., and Stuart, D.G. (1976). Ensemble characteristocs of cat locomotion and its neural control. Progress in Neurobiology *7*, 1–98. 10.1016/0301-0082(76)90002-2.

12. Dean, J., and Wendler, G. (1983). Stick Insect Locomotion On A Walking Wheel: Interleg Coordination of Leg Position. Journal of Experimental Biology *103*, 75–94. 10.1242/jeb.103.1.75.

13. Foth, E., and Bässler, U. (1985). Leg movements of stick insects walking with five legs on a treadwheel and with one leg on a motor-driven belt. Biological Cybernetics *51*, 313–318. 10.1007/BF00336918.

14. Foth, E., and Graham, D. (1983). Influence of loading parallel to the body axis on the walking coordination of an insect. Biological Cybernetics *47*, 17–23. 10.1007/BF00340065.

15. Herreid, C.F., and Full, R.J. (1984). Cockroaches on a treadmill: Aerobic running. Journal of Insect Physiology *30*, 395–403. 10.1016/0022-1910(84)90097-0.

16. Herreid, C.F., II, Full, R.J., and Prawel, D.A. (1981). Energetics of Cockroach Locomotion. Journal of Experimental Biology *94*, 189–202. 10.1242/jeb.94.1.189.

17. Watson, J.T., and Ritzmann, R.E. (1998). Leg kinematics and muscle activity during treadmill running in the cockroach, Blaberus discoidalis: II. Fast running. J. Comp. Physiol. A *182*, 23–33.

18. Watson, J.T., and Ritzmann, R.E. (1997). Leg kinematics and muscle activity during treadmill running in the cockroach, Blaberus discoidalis: II. Fast running. Journal of Comparative Physiology A *182*, 23–33. 10.1007/s003590050154.

19. Whelan, P.J. (1996). Control of locomotion in the decerebrate cat. Progress in Neurobiology *49*, 481–515. 10.1016/0301-0082(96)00028-7.

20. Fujiki, S., Aoi, S., Funato, T., Sato, Y., Tsuchiya, K., and Yanagihara, D. (2018). Adaptive hindlimb split-belt treadmill walking in rats by controlling basic muscle activation patterns via phase resetting. Scientific Reports *8*, 17341. 10.1038/s41598-018-35714-8.

21. McVea, D.A., and Pearson, K.G. (2007). Long-Lasting, Context-Dependent Modification of Stepping in the Cat After Repeated Stumbling-Corrective Responses. Journal of Neurophysiology *97*, 659–669. 10.1152/jn.00921.2006.

22. Kambic, R.E., Roemmich, R.T., and Bastian, A.J. (2023). Joint-level coordination patterns for split-belt walking across different speed ratios. Journal of Neurophysiology *129*, 969–983. 10.1152/jn.00323.2021.

23. Reisman, D.S., Wityk, R., Silver, K., and Bastian, A.J. (2007). Locomotor adaptation on a split-belt treadmill can improve walking symmetry post-stroke. Brain *130*, 1861–1872. 10.1093/brain/awm035.

24. Reisman, D.S., Block, H.J., and Bastian, A.J. (2005). Interlimb Coordination During Locomotion: What Can be Adapted and Stored? Journal of Neurophysiology *94*, 2403–2415. 10.1152/jn.00089.2005.

25. Darmohray, D.M., Jacobs, J.R., Marques, H.G., and Carey, M.R. (2019). Spatial and Temporal Locomotor Learning in Mouse Cerebellum. Neuron *102*, 217-231.e4. 10.1016/j.neuron.2019.01.038.

26. Torres-Oviedo, G., Vasudevan, E., Malone, L., and Bastian, A.J. (2011). Chapter 4 - Locomotor adaptation. In Progress in Brain Research, A. M. Green, C. E. Chapman, J. F. Kalaska, and F. Lepore, eds. (Elsevier), pp. 65–74. 10.1016/B978-0-444-53752-2.00013-8.

27. Clarac, F. (1984). Spatial and temporal co-ordination during walking in crustacea. Trends in Neurosciences *7*, 293–298. 10.1016/S0166-2236(84)80199-X.

28. Agrawal, S., Dickinson, E.S., Sustar, A., Gurung, P., Shepherd, D., Truman, J.W., and Tuthill, J.C. (2020). Central processing of leg proprioception in Drosophila. Elife *9*, e60299. 10.7554/eLife.60299.

29. Chen, C., Agrawal, S., Mark, B., Mamiya, A., Sustar, A., Phelps, J.S., Lee, W.-C.A., Dickson, B.J., Card, G.M., and Tuthill, J.C. (2021). Functional architecture of neural circuits for leg proprioception in Drosophila. Current Biology *31*, 5163–5175. 10.1016/j.cub.2021.09.035.

30. Chockley, A.S., Dinges, G.F., Di Cristina, G., Ratican, S., Bockemühl, T., and Büschges, A. (2022). Subsets of leg proprioceptors influence leg kinematics but not interleg coordination in Drosophila melanogaster walking. Journal of Experimental Biology *225*, jeb244245. 10.1242/jeb.244245.

31. Isakov, A., Buchanan, S.M., Sullivan, B., Ramachandran, A., Chapman, J.K.S., Lu, E.S., Mahadevan, L., and de Bivort, B. (2016). Recovery of locomotion after injury in *Drosophila* depends on proprioception. Journal of Experimental Biology, jeb.133652. 10.1242/jeb.133652.

32. Mamiya, A., Sustar, A., Siwanowicz, I., Qi, Y., Lu, T.-C., Gurung, P., Chen, C., Phelps, J.S., Kuan, A.T., Pacureanu, A., et al. (2023). Biomechanical origins of proprioceptor feature selectivity and topographic maps in the Drosophila leg. Neuron *111*, 3230-3243.e14. 10.1016/j.neuron.2023.07.009.

33. Mamiya, A., Gurung, P., and Tuthill, J.C. (2018). Neural Coding of Leg Proprioception in Drosophila. Neuron *100*, 636-650.e6. 10.1016/j.neuron.2018.09.009.

34. Azevedo, A., Lesser, E., Mark, B., Phelps, J., Elabbady, L., Kuroda, S., Sustar, A., Moussa, A., Kandelwal, A., Dallmann, C.J., et al. (2022). Tools for comprehensive reconstruction and analysis of Drosophila motor circuits. bioRxiv, 2022.12.15.520299. 10.1101/2022.12.15.520299.

35. Takemura, S., Hayworth, K.J., Huang, G.B., Januszewski, M., Lu, Z., Elizabeth C Marin, Stephan Preibisch, C Shan Xu, John Bogovic, Andrew S Champion, et al. (2023). A Connectome of the Male Drosophila Ventral Nerve Cord. bioRxiv, 2023.06.05.543757. 10.1101/2023.06.05.543757.

36. Dorkenwald, S., Matsliah, A., Sterling, A.R., Schlegel, P., Yu, S., McKellar, C.E., Lin, A., Costa, M., Eichler, K., Yin, Y., et al. (2023). Neuronal wiring diagram of an adult brain. bioRxiv, 2023.06.27.546656. 10.1101/2023.06.27.546656.

37. Berendes, V., Zill, S.N., Büschges, A., and Bockemühl, T. (2016). Speed-dependent interplay between local pattern-generating activity and sensory signals during walking in Drosophila. Journal of Experimental Biology *219*, 3781–3793. 10.1242/jeb.146720.

38. Buchner, E. (1976). Elementary movement detectors in an insect visual system. Biological Cybernetics *24*, 85–101. 10.1007/BF00360648.

39. Creamer, M.S., Mano, O., and Clark, D.A. (2018). Visual Control of Walking Speed in Drosophila. Neuron *100*, 1460-1473.e6. 10.1016/j.neuron.2018.10.028.

40. Götz, K.G., and Wenking, H. (1973). Visual control of locomotion in the walking fruitflyDrosophila. J. Comp. Physiol. *85*, 235–266. 10.1007/BF00694232.

41. DeAngelis, B.D., Zavatone-Veth, J.A., and Clark, D.A. (2019). The manifold structure of limb coordination in walking Drosophila. eLife *8*, e46409. 10.7554/eLife.46409.

42. Fujiwara, T., Brotas, M., and Chiappe, M.E. (2022). Walking strides direct rapid and flexible recruitment of visual circuits for course control in Drosophila. Neuron *110*, 2124-2138.e8. 10.1016/j.neuron.2022.04.008.

43. Simon, J.C., and Dickinson, M.H. (2010). A New Chamber for Studying the Behavior of Drosophila. PLOS ONE *5*, e8793. 10.1371/journal.pone.0008793.

44. Strauss, R., and Heisenberg, M. (1990). Coordination of legs during straight walking and turning in Drosophila melanogaster. J. Comp. Physiol. A *167*, 403–412.

45. York, R.A., Brezovec, L.E., Coughlan, J., Herbst, S., Krieger, A., Lee, S.-Y., Pratt, B., Smart, A.D., Song, E., Suvorov, A., et al. (2022). The evolutionary trajectory of drosophilid walking. Curr Biol *32*, 3005-3015.e6. 10.1016/j.cub.2022.05.039.

46. Günel, S., Rhodin, H., Morales, D., Campagnolo, J., Ramdya, P., and Fua, P. (2019). DeepFly3D, a deep learning-based approach for 3D limb and appendage tracking in tethered, adult Drosophila. eLife *8*, e48571. 10.7554/eLife.48571.

47. Karashchuk, P., Rupp, K.L., Dickinson, E.S., Walling-Bell, S., Sanders, E., Azim, E., Brunton, B.W., and Tuthill, J.C. (2021). Anipose: A toolkit for robust markerless 3D pose estimation. Cell Rep *36*, 109730. 10.1016/j.celrep.2021.109730.

48. Seelig, J.D., Chiappe, M.E., Lott, G.K., Dutta, A., Osborne, J.E., Reiser, M.B., and Jayaraman, V. (2010). Two-photon calcium imaging from head-fixed Drosophila during optomotor walking behavior. Nature Methods *7*, 535–540. 10.1038/nmeth.1468.

49. Fujiwara, T., Cruz, T.L., Bohnslav, J.P., and Chiappe, M.E. (2017). A faithful internal representation of walking movements in the Drosophila visual system. Nature Neuroscience *20*, 72–81. 10.1038/nn.4435.

50. Turner-Evans, D., Wegener, S., Rouault, H., Franconville, R., Wolff, T., Seelig, J.D., Druckmann, S., and Jayaraman, V. (2017). Angular velocity integration in a fly heading circuit. eLife *6*, e23496. 10.7554/eLife.23496.

51. Mathis, A., Mamidanna, P., Cury, K.M., Abe, T., Murthy, V.N., Mathis, M.W., and Bethge, M. (2018). DeepLabCut: markerless pose estimation of user-defined body parts with deep learning. Nature Neuroscience *21*, 1281. 10.1038/s41593-018-0209-y.

52. Sorribes, A., Armendariz, B.G., Lopez-Pigozzi, D., Murga, C., and de Polavieja, G.G. (2011). The Origin of Behavioral Bursts in Decision-Making Circuitry. PLOS Computational Biology *7*, e1002075. 10.1371/journal.pcbi.1002075.

53. Full, R.J., and Tu, M.S. (1991). Mechanics of A Rapid Running Insect: Two-, Four-and Six-Legged Locomotion. Journal of Experimental Biology *156*, 215–231. 10.1242/jeb.156.1.215.

54. Struzik, A., Karamanidis, K., Lorimer, A., Keogh, J.W.L., and Gajewski, J. (2021). Application of Leg, Vertical, and Joint Stiffness in Running Performance: A Literature Overview. Applied Bionics and Biomechanics *2021*, 9914278. 10.1155/2021/9914278.

55. Chun, C., Biswas, T., and Bhandawat, V. (2021). Drosophila uses a tripod gait across all walking speeds, and the geometry of the tripod is important for speed control. eLife *10*, e65878. 10.7554/eLife.65878.

56. Szczecinski, N.S., Bockemühl, T., Chockley, A.S., and Büschges, A. (2018). Static stability predicts the continuum of interleg coordination patterns in Drosophila. Journal of Experimental Biology *221*, jeb189142. 10.1242/jeb.189142.

57. Wosnitza, A., Bockemühl, T., Dübbert, M., Scholz, H., and Büschges, A. (2013). Inter-leg coordination in the control of walking speed in Drosophila. Journal of Experimental Biology *216*, 480–491. 10.1242/jeb.078139.

58. Azevedo, A.W., Dickinson, E.S., Gurung, P., Venkatasubramanian, L., Mann, R.S., and Tuthill, J.C. (2020). A size principle for recruitment of Drosophila leg motor neurons. eLife *9*, e56754. 10.7554/eLife.56754.

59. Pereira, T.D., Aldarondo, D.E., Willmore, L., Kislin, M., Wang, S.S.-H., Murthy, M., and Shaevitz, J.W. (2019). Fast animal pose estimation using deep neural networks. Nature Methods *16*, 117–125. 10.1038/s41592-018-0234-5.

60. Cruse, H. (1990). What mechanisms coordinate leg movement in walking arthropods? Trends in Neurosciences *13*, 15–21. 10.1016/0166-2236(90)90057-H.

61. Cruse, H. (1985). Which Parameters Control the Leg Movement of a Walking Insect?: II. The Start of the Swing Phase. Journal of Experimental Biology *116*, 357–362. 10.1242/jeb.116.1.357.

62. Tuthill, J.C., and Azim, E. (2018). Proprioception. Curr. Biol. *28*, R194–R203. 10.1016/j.cub.2018.01.064.

63. Mendes, C.S., Rajendren, S.V., Bartos, I., Márka, S., and Mann, R.S. (2014). Kinematic Responses to Changes in Walking Orientation and Gravitational Load in Drosophila melanogaster. PLOS ONE *9*, e109204. 10.1371/journal.pone.0109204.

64. Burrows, M. (2013). Jumping mechanisms of treehopper insects (Hemiptera, Auchenorrhyncha, Membracidae). Journal of Experimental Biology *216*, 788–799. 10.1242/jeb.078741.

65. Burrows, M. (2007). Anatomy of the hind legs and actions of their muscles during jumping in leafhopper insects. Journal of Experimental Biology *210*, 3590–3600. 10.1242/jeb.009100.

66. Card, G., and Dickinson, M.H. (2008). Visually Mediated Motor Planning in the Escape Response of Drosophila. Current Biology *18*, 1300–1307. 10.1016/j.cub.2008.07.094.

67. Cruse, H., Ehmanns, I., Stübner, S., and Schmitz, J. (2009). Tight turns in stick insects. Journal of Comparative Physiology A *195*, 299–309. 10.1007/s00359-008-0406-3.

68. Haberkern, H., Chitnis, S.S., Hubbard, P.M., Goulet, T., Hermundstad, A.M., and Jayaraman, V. (2022). Maintaining a stable head direction representation in naturalistic visual environments. bioRxiv, 2022.05.17.492284. 10.1101/2022.05.17.492284.

69. Hinton, D.C., Conradsson, D.M., and Paquette, C. (2020). Understanding Human Neural Control of Short-term Gait Adaptation to the Split-belt Treadmill. Neuroscience *451*, 36–50. 10.1016/j.neuroscience.2020.09.055.

70. Hoogkamer, W., Bruijn, S.M., Sunaert, S., Swinnen, S.P., Van Calenbergh, F., and Duysens, J. (2015). Adaptation and aftereffects of split-belt walking in cerebellar lesion patients. Journal of Neurophysiology *114*, 1693–1704. 10.1152/jn.00936.2014.

71. Lehmann, F.-O. (2001). Matching Spiracle Opening to Metabolic Need During Flight in Drosophila. Science *294*, 1926–1929. 10.1126/science.1064821.

72. Shillington, C., and Peterson, C.C. (2002). Energy metabolism of male and female tarantulas (Aphonopelma anax) during locomotion. Journal of Experimental Biology *205*, 2909–2914. 10.1242/jeb.205.18.2909.

73. Dahmen, H., Wahl, V.L., Pfeffer, S.E., Mallot, H.A., and Wittlinger, M. (2017). Naturalistic path integration of Cataglyphis desert ants on an air-cushioned lightweight spherical treadmill. Journal of Experimental Biology *220*, 634–644. 10.1242/jeb.148213.

74. Golding, D., Rupp, K.L., Sustar, A., Pratt, B., and Tuthill, J.C. (2023). Snow flies self-amputate freezing limbs to sustain behavior at sub-zero temperatures. Current Biology *33*, 4549-4556.e3. 10.1016/j.cub.2023.09.002.

75. Gohl, D.M., Silies, M.A., Gao, X.J., Bhalerao, S., Luongo, F.J., Lin, C.-C., Potter, C.J., and Clandinin, T.R. (2011). A versatile in vivo system for directed dissection of gene expression patterns. Nature Methods *8*, 231–237. 10.1038/nmeth.1561.

76. Pereira, T.D., Tabris, N., Matsliah, A., Turner, D.M., Li, J., Ravindranath, S., Papadoyannis, E.S., Normand, E., Deutsch, D.S., Wang, Z.Y., et al. (2022). SLEAP: A deep learning system for multi-animal pose tracking. Nature Methods *19*, 486–495. 10.1038/s41592-022-01426-1.

77. Moore, R.J.D., Taylor, G.J., Paulk, A.C., Pearson, T., van Swinderen, B., and Srinivasan, M.V. (2014). FicTrac: A visual method for tracking spherical motion and generating fictive animal paths. Journal of Neuroscience Methods *225*, 106–119. 10.1016/j.jneumeth.2014.01.010.

Chapter 3.

Leg proprioception controls joint limits in behaving *Drosophila*

Source

This chapter is from a manuscript that is currently in preparation to be submitted at *Neuron*.

Authors and Affiliations

Brandon G. Pratt[1], Chris J. Dallmann[1,2], Grant M. Chou[1], Igor Siwanowicz[3], Sarah Walling-Bell[1], Andrew Cook[1], Anne Sustar[1], Anthony Azevedo[1], and John C. Tuthill[1]*

[1]Department of Physiology and Biophysics, University of Washington, Seattle, WA, USA

[2]Department of Neurobiology and Genetics, Julius-Maximilians-University of Würzburg, Würzburg, Germany

[3]Janelia Research Campus, Howard Hughes Medical Institute, Ashburn, VA, USA

3.1 Abstract

To control a complex body in a dynamic environment, animals rely on their sense of proprioception to continuously monitor the state of their body and react to unexpected perturbations. How central circuits process proprioceptive information to control naturalistic behaviors remains an open question. Here, we used an electron microscopy dataset of the fruit fly VNC to characterize the downstream circuitry and predict the role of hair plate proprioceptors in leg motor control. Equipped with a specific driver line, we tested the prediction that CxHP8, a hair plate on the coxa, facilitates the transition to posterior leg movement through a reflex circuit. Using a variety of experimental methods, we showed that, as predicted, CxHP8 neurons encode the extremes of anterior joint movement, drive posterior leg movement when activated, and aid in the precision of the swing-to-stance transition during forward walking. Therefore, the connectome provides credible predictions of neural circuit function, like those for other hair plates.

3.2 Introduction

Animals must coordinate various aspects of their body to perform rich behaviors, such as navigating dynamic and unpredictable environments. Although animals appear to do this with ease, orchestrating body movement and posture is challenging because not only are there many body segments that need to be coordinated, but also the joints that link them have variable degrees of freedom[1–3]. In walking, for example, vertebrates[4] and invertebrates[5,6] both need to coordinate the movement of each segment within the same leg as well as between legs. Proprioception, the sense of how the body is positioned and moving in space, is critical for coordinating the body[7,8]. However, it remains unclear how different types of proprioceptive neurons (i.e. proprioceptors) enable this coordination across behaviors.

Analogous proprioceptors exist for vertebrates[9,10] and invertebrates[11–13], each monitoring a specific component of body state, such as position, velocity, and/or vibration. For instance, the vertebrate muscle spindles that are embedded in muscle, and the invertebrate chordotonal organ neurons both encode the relative position or velocity about adjoining limb segments. Similarly, Golgi tendon organs in vertebrates and campaniform sensilla in invertebrates extract information about the load experienced by the body. The last general type of proprioceptor consists of those that are position-tuned and situated to detect the extremes of joint movement. In vertebrates, low threshold mechanoreceptors called Ruffini endings and Pacinian corpuscles act as joint "limit detectors" by having peak activity towards the end of joint movement. The invertebrate analog, hair plates, which consists of a field of cuticular hairs innervated by mechanosensory neurons, also signals the extremes of joint movement. Although these proprioceptor classes have specific tuning, they likely act in redundant and parallel pathways to enable robust control of behavior[7,14,15]. The gap that remains is understanding how each class contributes to the control of naturalistic behaviors, such as walking and postural maintenance.

In "big" insects, there is a long history of research on hair plates[12]. On the legs of insects, such as locusts[16–20], cockroaches[21–24], and stick insects[25–30], hair plates are concentrated at the proximal leg joints. The length of the cuticular hairs of a given hair plate are often categorized as short or long[12]. Even though the purpose of the short hairs in motor control remains an enigma, the long hairs have been well characterized. Prior electrophysiological recordings of hair plate neurons

in the cockroach[21,22] and locust[16,17] revealed two types – one that rapidly adapts to displacements of the hairs and another that slowly adapts and is tonically active during sustained deflections. Hair plate neuron activity was also shown to be proportional to the magnitude[20,22,30] and dependent on the rate[27] of hair displacement. Beyond encoding the extremes of joint movement, hair plates were found to drive resistance reflex circuits in these insects. Multiple studies involving different hair plates and organisms showed that hair plate neurons make monosynaptic, excitatory chemical synapses onto motor neurons, while also indirectly exerting inhibition onto antagonistic motor neurons[16,19,21,23,27,29] through non-spiking interneurons[23,31]. Therefore, it has been suggested that during behaviors like walking, the activation of hair plate neurons is important for switching the movement direction of the leg, such as transitioning the leg from the swing phase of the step cycle to the stance phase. Manipulations to hair plates, like shaving hairs or chronically deflecting them, provide further evidence for this notion. For example, chronically deflecting the hairs of a hair plate in the stick insect resulted in such a dramatic repositioning of the operated leg throughout the step cycle of walking that it would sometimes become entangled with an ipsilateral leg[26]. Interestingly, the kinematic effect depended on the behavioral context because the same operated leg was unimpaired during reaching behavior. Given its established and intimate role in motor control, the reflex circuit that hair plates participate in serves as a great model for elucidating how the nervous system coordinates the body during different behaviors.

Unlike big insects, the small fruit fly, *Drosophila melanogaster*, has a suite of genetic tools[32] and a mapped nervous system[33–36] that enables unprecedented access to the neurons within these circuits and correspondingly, a full description of their role in behavior. In the fly, proximal leg joints each contain multiple hair plates[37–40]. On the front legs, for example, there are 3 hair plates that wrap the thorax-coxa joint, 4 hair plates on the trochanter (3 surrounding the coxa-trochanter joint), and a hair plate on the tibia near the femur-tibia joint. The number of hairs contained in each hair plate varies, but intriguingly, all hairs are roughly the same length of about 15 μm. As observed in larger insects, a hair plate on the fly's front leg called, CxHP8, which is located on the coxa (Cx) and contains 8 hairs, was also found to directly excite a motor neuron through chemical synapses[41]. However, the connectivity of this hair plate and others with all motor neurons and premotor interneurons making up the reflex circuits controlling leg movement remained unattainable until recent advances in connectomics and x-ray imaging. By combining a x-ray holographic nano-tomography dataset of the fly's front leg[40] with a serial section electron microscopy (EM) dataset of

the female ventral nerve cord (FANC)[36], coarsely traced hair plate axons were able to be identified in the ventral nerve cord. The application of automatic segmentation and synapse predication algorithms[34] to FANC then made it possible to assess connectivity between networks of neurons.

We therefore reconstructed all identified hair plates axons projecting from the left front leg in the automatically segmented FANC dataset. Being equipped with a specific CxHP8 driver line[42], we first focused on characterizing the downstream connectivity of CxHP8 neurons in FANC, especially in the framework of reflex circuits. Given its reflex circuit structure, we hypothesized that CxHP8 is involved in transitioning the front leg from moving anterior to posterior. To test this hypothesis, we started by characterizing the joint angles that activate CxHP8 neurons by combining 3D tracking with 2-photon calcium imaging while we passively moved the left front leg. We further used this setup to determine CxHP8 activity during an assortment of behaviors. We found that the inward rotation and adduction of the coxa resulted in increased activity of CxHP8 neurons, and that these neurons were active during specific behaviors. We next used optogenetic activation to show that we could engage the predicted reflex circuit that involves CxHP8. Finally, we used spatiotemporally precise optogenetic silencing in tethered flies and chronic silencing in unconstrained flies on a treadmill to demonstrate that CxHP8 feedback is important for the swing-to-stance transition during walking and for postural control. The validation of the predicted motor function of CxHP8 neurons from the connectome provides credence for the motor control predictions of other hair plates on the fly leg. Thus, we used the connectome to prescribe function to these other hair plates and highlight the power of this approach in generating testable hypotheses of neural circuit function.

3.3 Results

CxHP8 neurons participate in reflex circuits that are predicted to drive posterior leg movement

In the fruit fly, one or more hair plates are found at the proximal joints of all legs[38–40] (**Figure S3.1A**). On the front leg, for example, three hair plates are located at the junction between the coxa (Cx) and thorax (**Figure 3.1A**). These hair plates, called CxHP8, CxHP3, and CxHP4, wrap the joint along the medial-lateral axis. Given this arrangement at the joint, these hair plates seem well-positioned to encode the extremes of joint movement, which has been previously shown in larger insects[22]. To understand the role of hair plates in motor control, we generated and screened through

Split-GAL4 driver lines with the goal of finding lines that only labeled the neurons of one hair plate on the leg (**Table S3.1**). Fortunately, we received a driver line used in a prior study[42] that labeled 6 of the 8 mechanosensory neurons associated with CxHP8 on the front leg, and 3 of 8 CxHP8 neurons on the middle leg, which hereafter is referred to as CxHP8-GAL4 (**Figure 3.1B; Figure S3.1B**). In the ventral nerve cord (VNC), CxHP8 axons project dorsally and along the perimeter of the leg neuromere, which is consistent with the arborization pattern depicted for hair plates in prior studies[32,36,43,44]. Being equipped with a specific driver line for CxHP8 neurons, we next investigated the connectivity of CxHP8 neurons to downstream neurons.

We characterized this connectivity within a segmented EM dataset of the female VNC (FANC) in which synapses have been predicted[34]. We used previous manual annotations[36] of the backbone of CxHP8 neurons to reconstruct all of its axons (**Figure 3.1C**). We next proofread and classified downstream cells of CxHP8 neurons. Surprisingly, we found that CxHP8 neurons allocate 75% of their total output synapses (2,279 ± 482) to neurons within motor circuits (17% motor neurons; 58% premotor neurons) indicating that the function of these neurons is primarily for motor control (**Figure 3.1D**). For example, CxHP8 neurons directly synapse onto motor neurons within the coxa posterior motor module[34,45], which has not been previously described. We further assessed the connectivity of CxHP8 neurons onto motor neurons and found that all CxHP8 neurons make the most synapses onto coxa posterior motor neurons and weaker connections onto motor neurons controlling the movement of more distal leg segments (**Figure 3.1F**). Given this connectivity, the signaling of CxHP8 neurons is likely to drive posterior leg movement through the actuation of the coxa.

Additionally, the direct connectivity of CxHP8 neurons onto specific motor neurons suggests that these neurons are involved in reflex circuits, like those previously described in larger insects[16] and fruit flies[41] through electrophysiological means. In congruence with a reflex circuit, CxHP8 neurons synapse onto both excitatory and inhibitory premotor neurons, which were identified by their hemilineage[46] (**Figure 3.1G**). Therefore, the connectivity of CxHP8 neurons with premotor and motor neurons provides all of the components for a classical reflex circuit motif (**Figure 3.1H**). In the reflex circuit framework, CxHP8 neurons signal to motor neurons directly and indirectly through excitatory premotor neurons to drive posterior leg movement, while also inhibiting the motor neurons that would impede such movement through inhibitory premotor neurons. By filtering for just the strongest connections (10 or greater synapses) between hair plate, premotor, and motor neurons,

we revealed that CxHP8 neurons provide direct and indirect excitatory connections to coxa posterior motor neurons, while also indirectly connecting to antagonistic coxa promote motor neurons through inhibitory premotor neurons (**Figure 3.1I**). CxHP8 neurons also indirectly connect to other motor modules that actuate different leg segments, suggesting that CxHP8 signaling may aid in orchestrating coordinated movement across the entirety of the leg. Overall, from this reflex circuit infrastructure, we predict that CxHP8 neurons control the anterior to posterior transition of leg movement – a transition important for behaviors like walking.

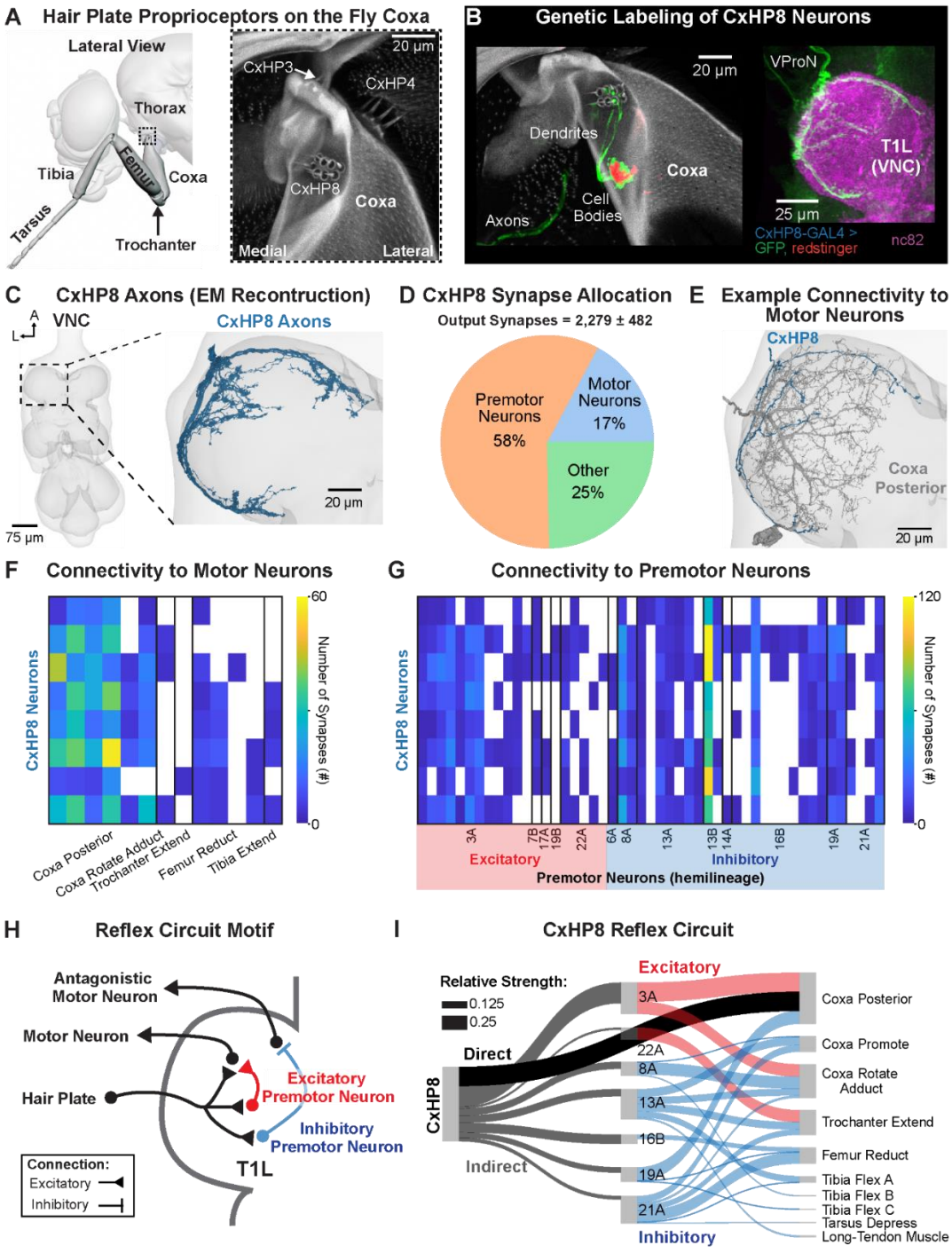

Figure 3.1. Synaptic connectivity predicts that CxHP8 neurons participate in a reflex circuit to drive posterior leg movement. (**A**) A confocal image of the three hair plates, CxHP3, CxHP4, and CxHP8, at the thorax-coxa joint (black dotted box) of the front leg. The fly was rendered in Blender and based on high-resolution confocal images. (**B**) Confocal images of genetically labeled CxHP8 neurons (6 of 8) in the coxa of the front leg and ventral nerve cord (VNC). The ultrastructure (autofluorescence: gray) of CxHP8 consists of 8 cuticular hairs located on the coxa. Each hair is innervated by a single mechanosensory neuron (GFP: green), which projects through the ventral prothoracic nerve (VProN) into the VNC (nc82: magenta). The cell bodies of CxHP8 neurons are labeled red (redstinger). (**C**) All CxHP8 axons were reconstructed within the left front leg neuromere of an automatically segmented serial section electron microscopy (EM) dataset of a *Drosophila* female VNC (i.e. FANC). (**D**) Percent of total output synapses of CxHP8 axons onto motor neurons, premotor neurons, and other cell classes (e.g. ascending, descending, and sensory neurons). (**E**) CxHP8 axon (blue) synapses onto a motor neuron within the coxa posterior motor module (gray). (**F**) Connectivity matrix showing the number

of synapses that motor neurons, defined by their motor module, receive from each CxHP8 axon. Motor neurons within a motor module are arranged according to the proportion of input synapses they receive from each CxHP8 axon. (**G**) Connectivity matrix illustrating the number of synapses that CxHP8 axons supply to premotor neurons. Premotor neurons are classified as excitatory (red) or inhibitory (blue) based on their identified hemilineage. The connectivity matrix was sorted in the same manner as **F**. (**H**) A schematic of a reflex circuit motif showing that hair plate signaling could drive specific joint movement by directly and indirectly exciting motor neurons while indirectly inhibiting the antagonistic set of motor neurons. (**I**) CxHP8 neurons are predicted to participate in reflex circuits based on their connectivity with premotor and motor neurons. The CxHP8 reflex circuit contains direct (black) and indirect (gray) connections onto motor neurons. Indirect connections are mediated by inhibitory (blue) or excitatory (red) premotor neurons that are classified by their hemilineage. The strength of the connection is relative to the maximum number of synapses that hair plate axons provide to a downstream partner within the reflex circuit. Only premotor and motor neurons that received at least 10 synapses from CxHP8 axons are displayed. Moreover, only premotor neurons that supply at least 10 synapses to motor neurons are analyzed.

CxHP8 neurons are active during the adduction and inward rotation of the coxa

To assess if CxHP8 neurons control leg movement in the manner predicted from the connectome, we first needed to determine the joint angles in which these neurons were active. We used a previously described setup[47] that combined 2-photon calcium imaging with high-speed videography to simultaneously record the activity of CxHP8 axons and leg movement in CxHP8-GAL4 flies expressing GCaMP7f and tdTomato (**Figure 3.2A**). To overcome the slow temporal dynamics of GCaMP7f relative to the dynamics of active leg movement in flies, we gradually moved the left front leg using a manually controlled 3-axis platform. We then used DeepLabCut[48] and Anipose[1] to compute the 3 angles corresponding to the rotation, adduction, and flexion of the front leg thorax-coxa joint (**Figure 3.2B**). These angles were defined in the following manner: an increase in the rotation, adduction, and flexion angles corresponded to the coxa rotating inward, moving medially, and flexing, respectively (**Figure S3.2A**). Altogether, this setup enabled us to characterize the thorax-coxa joint angles encoded by CxHP8 neurons (**Figure 3.2C**).

Given that CxHP8 is located medially at the thorax-coxa joint, we hypothesized that its hairs would be deflected during medial movements and inward rotations of the coxa, resulting in the neurons becoming active. As exemplified by a representative trial, CxHP8 axons indeed showed the largest calcium signal when the coxa rotated inwards and adducted medially (**Figure 3.2D**). We further found similar calcium responses to coxa rotation and adduction across all flies (**Figure 3.2E**). Although more variable across flies, CxHP8 axons also showed greater activity when the coxa was extended. Because coxa rotation and adduction produced strong calcium responses, we next investigated how the two angles jointly influenced the activity of CxHP8 neurons. We found that the combination of both inward rotation and medial adduction resulted in maximal calcium activity of

CxHP8 axons (**Figure 3.2F**). Taken together with the prediction from the connectome, CxHP8 neurons appear to encode the thorax-coxa joint angles associated with the extremes of anterior leg movement (**Video 3.1**) to drive posterior leg movement.

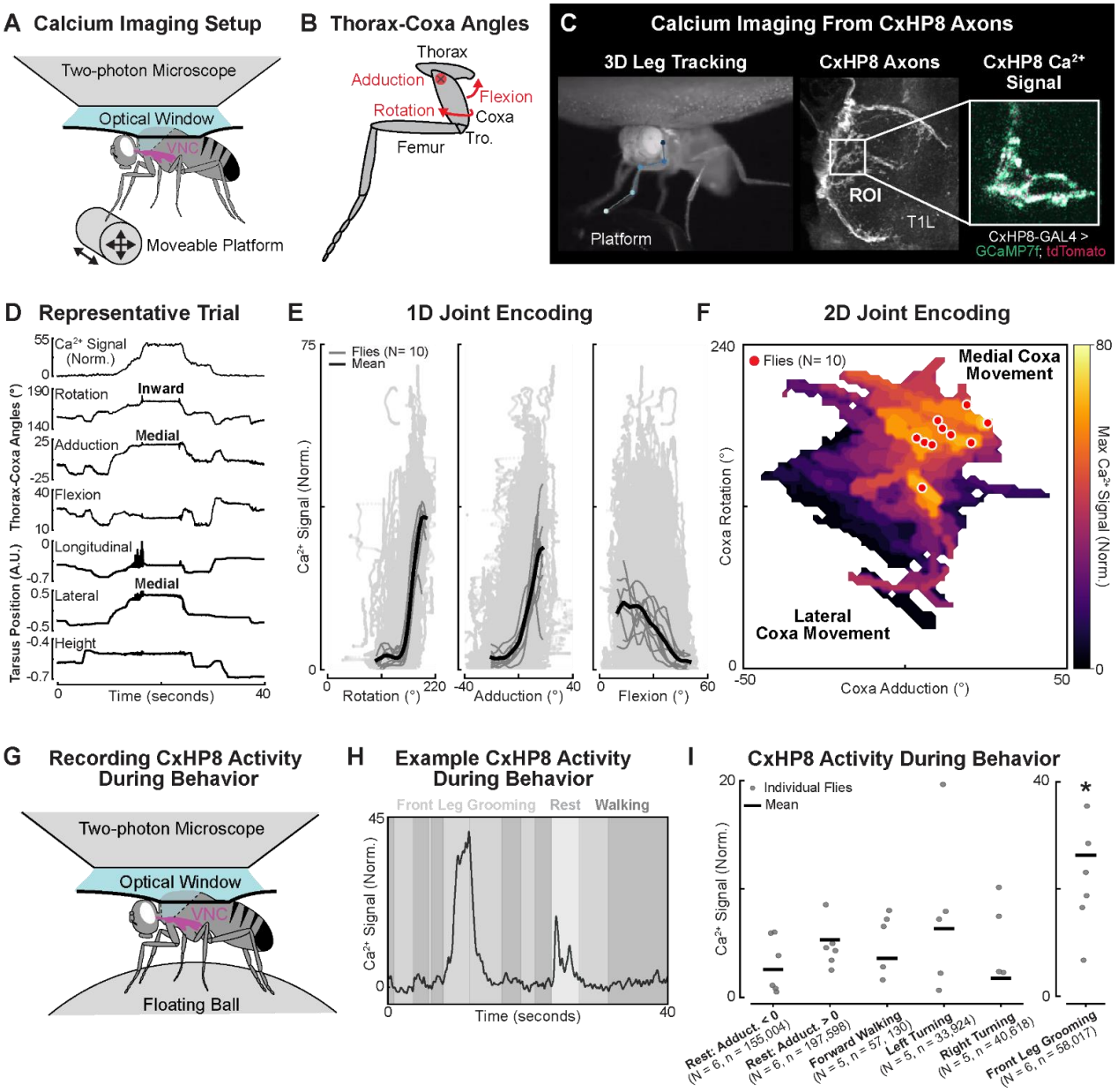

Figure 3.2. Thorax-coxa joint angle encoding of CxHP8 neurons. (**A**) Schematic of the setup used to measure calcium signals from CxHP8 axons as the left front leg was passively moved on a platform. (**B**) Schematic of the rotation, adduction, and flexion thorax-coxa joint angles. (**C**) Example recording of calcium activity of CxHP8 axons. Joint angles were quantified by tracking the joints of the left front leg in 3D. In addition to GCaMP7f (green), CxHP8 axons expressed tdTomato (red) for motion correction and signal normalization. (**D**) Representative trial showing the normalized calcium signal for CxHP8 axons, the thorax-coxa rotation, adduction, and flexion angles, and the 3D position of the tarsus while the left front leg was passively moved. (**E**) Normalized calcium activity of CxHP8 axons with respect to the thorax-coxa rotation, adduction, and flexion angles. Black line: bin averaged mean calcium activity across all flies; Gray lines: bin averaged mean calcium activity for each fly; Silver dots: normalized calcium activity pooled across all flies. (**F**) Contour plot showing the maximum 2D calcium activity across all flies with respect to thorax-coxa rotation and adduction.

Red dots: the rotation and adduction angles at which the normalized calcium activity was maximum for each fly. (**G**) Schematic of the calcium imaging setup used to determine CxHP8 activity during behavior. (**H**) Example trial showing the normalized calcium activity during front leg grooming, rest, and walking. (**I**) CxHP8 activity during rest (when the adduction angle was less than or greater than 0 degrees), forward walking, left and right turns, and front leg grooming. Compared to rest periods where the coxa had an adduction angle less than 0, normalized calcium activity was significantly greater for front leg grooming (*: $p < 0.01$) and non-significantly elevated for forward walking and left turns. t-tests were used for statistical comparisons. Black line: mean normalized calcium activity across all flies; Gray dots: mean normalized calcium activity for each fly; N: number of flies; n: number of frames.

CxHP8 neurons are active during grooming and locomotion

Having characterized the thorax-coxa joint angles encoded by CxHP8 neurons, we next sought to determine the behaviors in which CxHP8 neurons were active. We used a similar setup[47] but replaced the platform with a ball suspended by air and allowed the fly to behave (**Figure 3.2G**). We observed the strongest calcium signals of CxHP8 axons during front leg grooming, but slightly elevated calcium activity during walking compared to resting periods in which the fly was quiescent (**Figure 3.2H**). After quantifying the calcium activity across all selected behaviors, we found that CxHP8 activity was only significantly greater for front leg grooming compared to resting periods where the coxa was positioned laterally away (i.e. adduct < 0) from the body (**Figure 3.2I**). However, mean calcium activity was elevated for resting periods where the coxa was medially positioned, during forward walking, and left turns. The mean calcium activity was lowest during right turns. Although unexpected, we likely didn't see strong calcium signals during forward walking and turning because of the slow temporal dynamics of GCaMP7f relative to the frequency of stepping as well as the transient activity of CxHP8 axons at the extremes of joint movement during the step cycle. Moreover, the elevated activity during rest periods where the coxa was positioned medially suggests that there was context-dependent modulation of the CxHP8 reflex circuit as not to drive posterior leg movement. In summary, CxHP8 axons are strongly active during front leg grooming sequences and likely transiently active during locomotor behaviors, like forward walking.

CxHP8 activation drives posterior leg movement and silencing impairs swing-to-stance transitions during walking

We next determined if we could engage the connectome derived reflex circuit through the optogenetic activation of CxHP8 neurons. Like prior studies in the lab[49,50], we employed a setup that enables spatiotemporally precise optogenetic activation or silencing of neurons within the left front leg of tethered flies behaving of a ball suspended by air (**Figure 3.3A**). To optogenetically activate CxHP8 neurons, we drove the expression of ChrimsonR within the CxHP8 neurons labeled by CxHP8-GAL4 driver line and illuminated the neurons with a red laser. Upon doing this in a

representative standing fly, we observed that its left front leg retracted shortly after the onset of the laser (**Figure 3.3B, *upper***). We then investigated which thorax-coxa joint angles (**Figure 3.3B, *lower***) facilitated the posterior leg movement and found that it resulted from the outward rotation, lateral movement, and flexion of the coxa in response to the optogenetic stimulation of CxHP8 neurons (**Figure 3.3C**). Across trials in which flies were standing, optogenetic activation of CxHP8 neurons resulted in a similar outward rotation and flexion of the coxa (**Figure 3.3D**). However, the effect of optogenetic activation on the adduction angle was less clear but appeared to generally displace the coxa laterally. These joint angle changes were accompanied by the posterior and lateral displacement of the distal tarsus (**Figure 3.3E**). Overall and consistent with the reflex circuit obtained from connectome, the activation of CxHP8 neurons led to a reflexive posterior and lateral movement of the leg as mediated by the outward rotation, lateral displacement, and flexion of the coxa.

Having confirmed that the CxHP8 reflex circuit elicits posterior and lateral leg movement, we then investigated which behaviors use this reflex. We used the same experimental setup, but instead optogenetically silenced CxHP8 neurons expressing the light-gated chloride channel, GtACR1, during various behaviors. We primarily focused on the role of CxHP8 signaling during forward walking because of the cyclical nature and inherent need to control the transitions of leg movement during walking. When CxHP8 feedback was disrupted, the thorax-coxa adduction angle was significantly more medial, especially at the swing-to-stance transition of the step cycle, compared to non-laser control trials (**Figure 3.3F**). Moreover, the distal tarsus was positioned more medially near the swing-to-stance transition and during the stance phase of the step cycle given optogenetic silencing of CxHP8 neurons (**Figure 3.3G**). Thus, the lack of CxHP8 signaling resulted in the coxa to overshoot the normal kinematic range associated with the swing-to-stance transition, which led to the medial displacement of the entire leg. It is important to note that CxHP8 feedback is not necessary for the swing-to-stance transition, but instead aids in its precision. Descending commands from the brain[6] and parallel proprioceptive feedback pathways[7] likely all contribute to the control of the swing-to-stance transition. We also assessed the role of CxHP8 feedback in left (**Figure S3.3A**) and right turns (**Figure S3.3B**), and front leg grooming (**Figure S3.3C**) and found no significant influence when its feedback was silenced. In summary, CxHP8 helps guide the transition between the swing and stance phases of forward walking, which supports the prediction from the connectome.

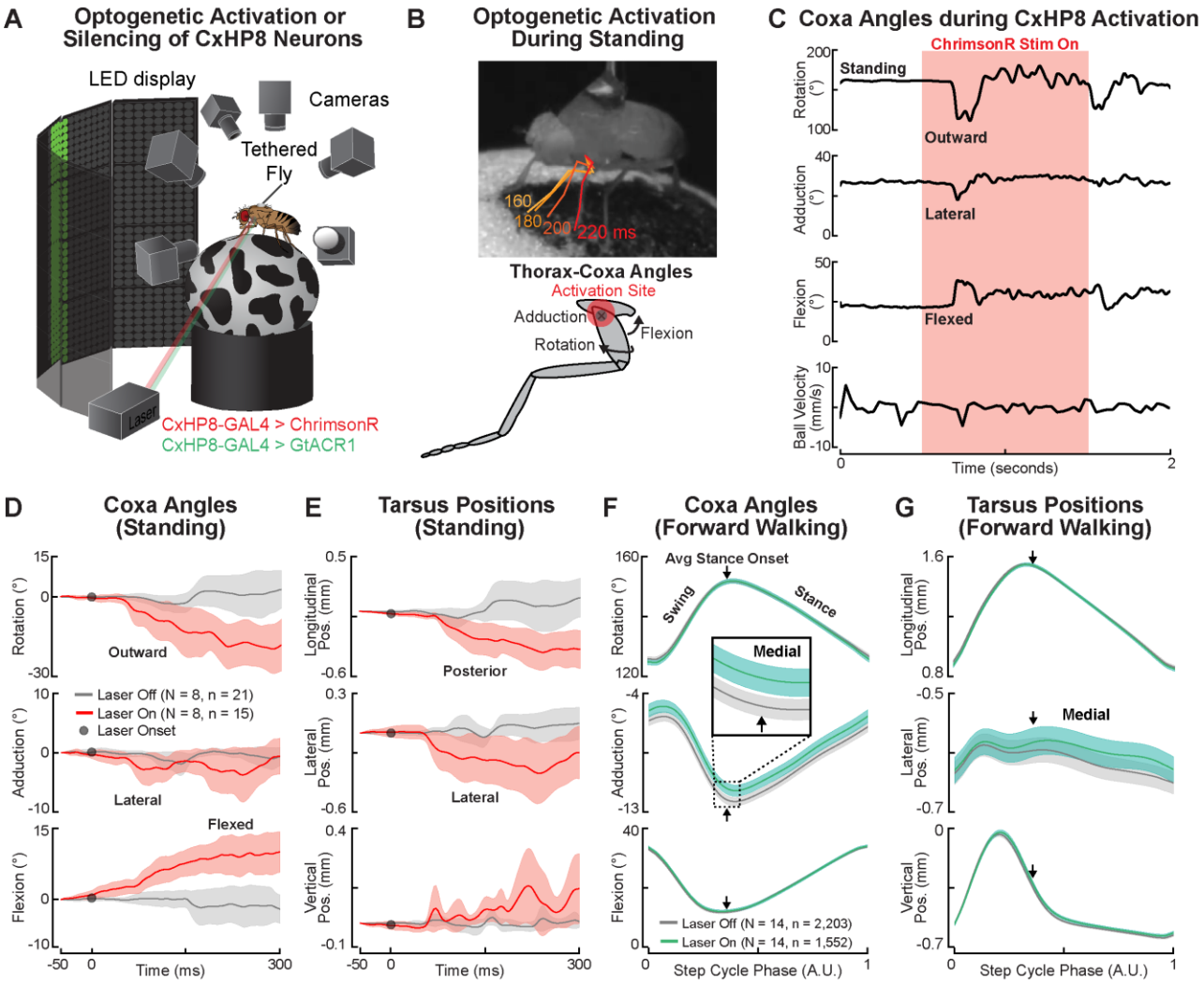

Figure 3.3. CxHP8 neurons drive coxa flexion and posterior leg movement. (**A**) Schematic of setup for optogenetic activation and silencing. 6 high-speed cameras (300 fps) recorded the behavior of a tethered fly on a ball and a laser focused on the left front leg was used to excite or inhibit CxHP8 neurons expressing the light-gated ion channel ChrimsonR (red) or GtACR1 (teal). Trials were 2 seconds in duration and the laser was presented (experimental group) or not (controls) 500 ms on each 1s trial. (**B**) Top: example trial in which CxHP8 activation resulted in the flexion and lateral movement of the coxa in a standing fly. The amount of time, in milliseconds, passed after the onset of the laser is displayed in the same color as the corresponding skeletonized leg. Bottom: the rotation, adduction, and flexion thorax-coxa joint angles. (**C**) For the same trial shown in **B**, the thorax-coxa rotation, adduction, and flexion angles, and the ball velocity in response to the optogenetic activation of CxHP8 neurons. (**D**) Optogenetic activation (red) of CxHP8 neurons in standing flies resulted in significant flexion and outward rotations of the coxa compared to trials in which the laser remained off (gray). Although more variable, the coxa laterally upon CxHP8 stimulation. Shaded region: 95% confidence interval; N: number of flies; n: number of trials. (**E**) Optogenetic activation (red) of CxHP8 neurons in standing flies also resulted in significant lateral and posterior movements of the tarsus compared to trials in which the laser remained off. Shaded region: 95% confidence interval; N: number of flies; n: number of trials. (**F**) Optogenetic silencing (teal) of CxHP8 neurons in flies walking forward produced a significant medial movement of the coxa near the swing-to-stance transition compared to forward walking steps when the laser was off. Arrow: the average onset of the stance phase of the step cycle; Shaded region: 95% confidence interval; N: number of flies; n: number of steps. (**G**) Optogenetic silencing (teal) of CxHP8 neurons in flies walking forward also resulted in a more medial tarsus position following the swing-to-stance transition compared to forward walking steps when the laser was off. Arrow: the average onset of the stance phase of the step cycle; Shaded region: 95% confidence interval; N: number of flies; n: number of steps.

CxHP8 facilitates the swing-to-stance transition and controls posture in unconstrained flies

Given that tethered flies don't need to support their body weight and have different walking kinematics than untethered ones[51], we wanted to confirm that CxHP8 feedback is also important for the control of the swing-to-stance transition in unconstrained flies. Therefore, we characterized the step kinematics and inter-leg coordination of unconstrained flies, with or without impaired CxHP8 feedback, walking in a previously described treadmill system[51]. The inward rectifying potassium channel, Kir 2.1, was used to chronically silence the CxHP8 neurons labeled by the CxHP8-GAL4 driver line throughout development. As flies walked on a split-belt treadmill, in which both belts moved at 10 mm/s, we recorded the movement of each fly at 200 fps with 5 high-speed cameras (**Figure 3.4A**). From the high-speed videos, we reconstructed the 3D positions of the head, thorax, abdomen, and each leg tip using DeepLabCut[48] and Anipose[1]. We then used these reconstructed 3D positions to quantify kinematics and posture during classified walking and rest periods, respectively (see methods for details; **Figure 3.4B**). With this approach, we were uniquely able to determine how the lack of CxHP8 feedback influenced 3D walking kinematics and posture in untethered flies.

Like tethered flies, we also found that CxHP8 silenced flies walking on the treadmill had impaired step kinematics near the swing-to-stance transition. In particular, the anterior extreme position (AEP), where a leg first enters stance, was significantly displaced medially and posteriorly for the front legs in flies with CxHP8 neurons silenced compared to controls (**Figure 3.4C**). The posterior extreme position (PEP), where a leg first enters swing, was also significantly displaced in a similar manner as the AEP. Given that the AEP marks the swing-to-stance transition and that changes in the AEP could drive changes in the PEP, we focused on understanding the kinematic changes that facilitated the displacement of the AEP in CxHP8 silenced flies. We first examined the average swing trajectories of the front legs and found a significant medial deviation of the trajectory near the swing-to-stance transition between CxHP8 silenced flies and controls (**Figure 3.4D**). Although this deviation did not result in a significantly longer mean swing duration (**Figure 3.4E**), the mean swing distance was significantly greater in flies with CxHP8 neurons silenced (**Figure 3.4F**). Unlike front leg step kinematics, inter-leg coordination was not significantly altered in flies with CxHP8 neurons silenced (**Figure 3.4G**). Overall, the silencing of CxHP8 neurons in both tethered and unconstrained flies resulted in the front leg being more medial at the swing-to-stance transition suggesting that CxHP8 feedback is important for the reflexive transitioning of leg movement.

Another advantage of the treadmill setup is the ability to study the role of CxHP8 neurons in postural control. Hair plates in larger insects have been shown to be important in controlling the height of the body[25] and legs[26]. We quantified the posture of flies during rest periods on the treadmill. Even though the silencing of CxHP8 neurons didn't significantly affect body height (**Figure S3.4A**) or the angle of the body (**Figure S3.4B**), the resting positions of the tarsi were more spread out than those of controls (**Figure 3.4H**). We further quantified this by calculating the area of the polygon formed by the positions of each tarsus (**Figure 3.4I**). The mean polygon area of CxHP8 silenced flies was significantly greater than controls providing further support that CxHP8 neurons control the resting position of the legs. In addition to participating in a reflex circuit to control the swing-to-stance transition, CxHP8 neurons also likely signal to non-reflex circuits to control posture.

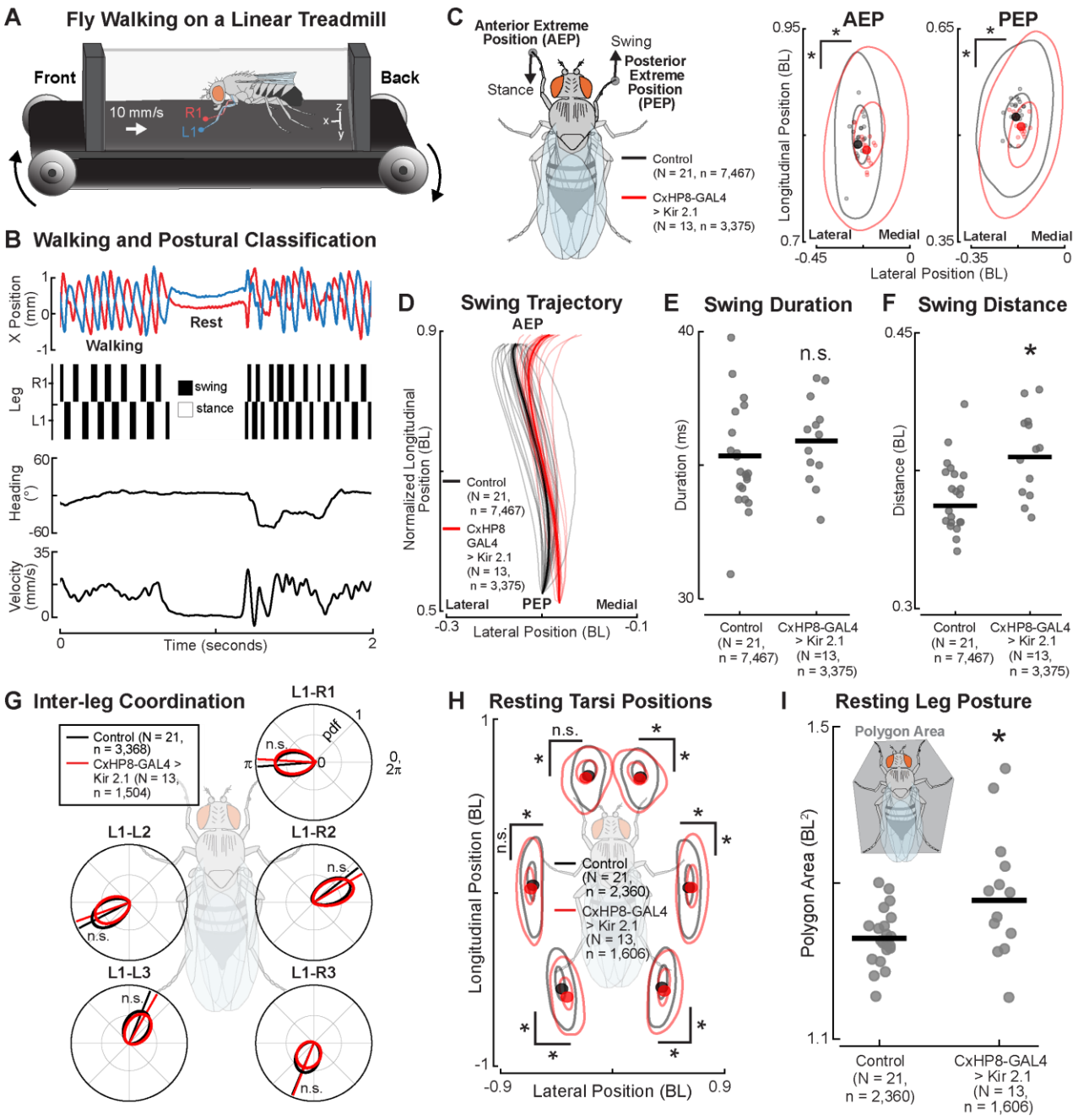

Figure 3.4. CxHP8 neurons control swing-to-stance transitions and contribute to resting posture in unconstrained flies. (**A**) Schematic of the treadmill system. Flies were recorded with 5 highspeed cameras (200 fps) as they walked on a treadmill moving at 10 mm/s. The 3D positions of each distal leg tip and the head, thorax, and abdomen were reconstructed using pose estimation methods. (**B**) Example trial period illustrating that both walking kinematics and resting posture can be obtained using the treadmill system. Shown are the longitudinal ("X") position and the classification of swing and stance of the left and right front leg as the fly walked and rested on the treadmill belt. Walking and resting periods were classified using the heading and body velocity of the fly. (**C**) Left: Schematic of the anterior and posterior extreme positions. Right: Kernel density estimation plots of the anterior and posterior extreme positions significantly shifted medially and posteriorly in flies with CxHP8 neurons chronically silenced (red) with the inward rectifying potassium channel, Kir 2.1. N: number of flies; n: number of steps. Bootstrapping with a Bonferroni correction was used to statistically compare CxHP8 silenced and control flies (*: $p < 0.004$). (**D**) Swing trajectories of CxHP8 silenced (red) and control (black) flies demonstrate the medial overshoot near the swing-to-stance transition. Each trajectory was scaled by the average swing distance and began at the average posterior extreme position. Solid line: mean trajectory; Thin lines: mean trajectory of each fly; Shaded region: 95% confidence interval; N: number of flies; n: number of steps. (**E**) Swing duration was not statistically different between

CxHP8 silenced and control flies, based on conducting a t-test on the means of flies (n.s.: $p > 0.025$). (**F**) Swing distance was significantly greater for CxHP8 silenced flies compared to controls (*: $p < 0.025$). (**G**) Inter-leg coordination (relative step cycle phase) between the left front leg and each other leg was not significantly different between CxHP8 silenced and control flies. t-test on the means of flies with a Bonferroni correction determined significance (n.s.: $p > 0.01$). N: number of flies; n: number of phase comparisons. (**H**) Resting position of the tarsi during periods of standing were significantly different between CxHP8 silenced (red) and control (black) flies. Distributions were determined by kernel density estimation. Dot: mean position; N: number of flies; n: number of resting bouts. Bootstrapping with a Bonferroni correction was used to test for statistical differences (*: $p < 0.001$). (**I**) As quantified by polygon area, the resting posture of the legs was significantly more spread out for flies with CxHP8 neurons silenced compared to controls (t-test; *: $p < 0.05$). N: number of flies; n: number of resting bouts.

The connectome enables functional predictions for other hair plates on the fly leg

From the connectome, we predicted that CxHP8 neurons participate in a reflex circuit to drive posterior coxa and leg movement. Through a series of experiments using a driver line that specifically labels CxHP8 neurons, we were able to show that these neurons indeed engage a reflex circuit to drive posterior leg movement at the extremes of anterior leg movement. However, the lack of specific driver lines for other hair plates on the leg (**Table S3.1**) and the laborious nature of the experiments make it challenging to determine the role of other hair plates in motor and postural control. Having validated the predicted role of CxHP8 neurons and gained confidence in the functional hypotheses generated by the connectome, we turned to the connectome to understand the role of other hair plates in the control of leg movement.

In addition to CxHP8, we focused on predicting the motor control function of the two other hair plates on the coxa, CxHP3 and CxHP4, along with the three hair plates located at the coxa-trochanter joint, TrHP5, TrHP6, and TrHP7 (**Figure 3.5A**). To determine their connectivity with reflex circuits, we reconstructed the axons of each hair plate in FANC (**Figure 3.5B**). Of the thousands of outputs synapses (**Figure S3.5A**), the axons of each hair plate allocate the majority for local premotor and motor neuron connectivity (**Figure 3.5C**), like what was previously shown for CxHP8 axons (**Figure 3.1D**). Interestingly, we found that hair plate axons synapse onto glia suggesting that their signaling may be used for non-motor related computations (**Figure S3.5B**). Like CxHP8 axons, the axons of the other hair plates also primarily connect to distinct populations of motor neurons that actuate the leg segment they are located on (**Figure 3.5D**). For instance, CxHP4 axons provide strong connectivity to motor neurons of the coxa rotate adduct motor module, whereas the antagonistically positioned hair plate, CxHP8, strongly synapses onto an antagonistic set of motor neurons that drive posterior movements of the coxa. To predict the role of each hair plate in the control of leg movement, we further characterized the connectivity of hair plates onto premotor

neurons (**Figure S3.5C**) and constructed reflex circuits for each hair plate. From the generated reflex circuits (**Figure 3.5E**), we predict the following: CxHP4 drives anterior leg movement, CxHP3 reinforces both anterior and posterior leg movement, TrHP5 and TrHP7 supports posterior leg movement, and TrHP6 drives anterior leg movement. Overall, these functional predications indicate that each hair plate may be specialized for controlling specific leg movements, which may arise from encoding different extremes of joint movement because of their physical placement at the joint.

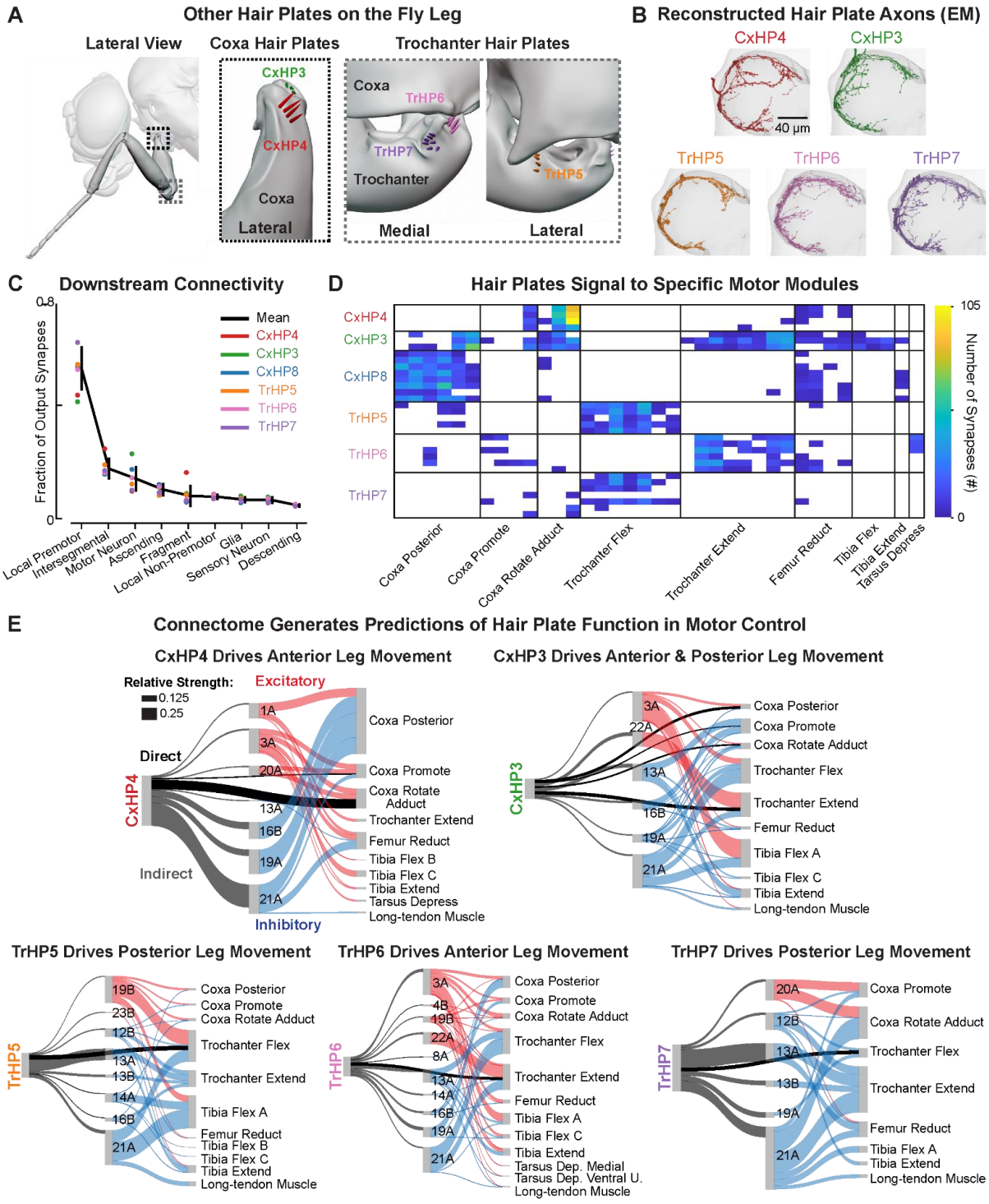

Figure 3.5. Synaptic connectivity of hair plate axons indicates distinct roles in leg motor control. (**A**) Morphologically accurate schematics of hair plates located at the thorax-coxa (black dotted box) and coxa-trochanter (gray dotted box) joints of the front leg. Schematics were rendered in blender and based on high-resolution confocal images. We focused on two additional hair-plates located at the thorax-coxa joint (CxHP4: red; CxHP3: green) and three at the coxa-trochanter joint (TrHP5: orange; TrHP7: purple; TrHP6: pink). (**B**) Reconstructed hair plate axons within the left front leg neuromere of FANC. (**C**) Fraction of hair plate axon output synapses onto VNC cell classes. Black line: mean fraction of output synapses across all hair plate axons; Color dot: mean fraction of output synapses for the axons of each hair plate. (**D**) Connectivity matrix showing the number of synapses that motor neurons receive from hair plate axons. Axons from the same hair plate are grouped together (rows) while motor neurons within their defined motor module

are arranged according to the proportion of input synapses they receive from specific hair plate axons. (**E**) Based on their connectivity with premotor and motor neurons, the neurons of each hair plate are predicted to participate in reflex circuits that control distinct aspects of leg movement. Above each reflex circuit is the prediction for the associated hair plate in controlling leg movement. Only connections of at least 10 synapses were used to construct each reflex circuit.

3.4 Discussion

In this study, we used the connectome to turn connectivity into functional predictions for hair plates on the fly front leg. Having a specific driver line for the neurons of CxHP8, we focused on testing the connectome derived prediction that CxHP8 neurons participate in a reflex circuit to drive posterior coxa and leg movement (**Figure 3.1**). We first revealed that CxHP8 neurons encode inward rotation and medial adduction of the coxa (**Figure 3.2**), which is associated with the extremes of anterior leg movement (**Video 3.1**) and supports the notion that CxHP8 feedback transitions the leg to moving posteriorly. CxHP8 neurons also showed the largest activity during front leg grooming and slightly elevated activity during locomotion compared to rest. Importantly, optogenetic stimulation of CxHP8 neurons was sufficient to drive reflexive posterior and lateral leg movement (**Figure 3.3**). Finally, we sought to understand the role of CxHP8 feedback during behavior and focused on forward walking because of the necessity to transition the movement direction of the leg during the step cycle. We found that both optogenetic silencing in tethered flies (**Figure 3.3**) and chronic silencing in unconstrained flies (**Figure 3.4**) of CxHP8 neurons resulted in the leg to overshoot the swing-to-stance transition and become more medial at the onset of stance. In addition to its role in walking, CxHP8 feedback was also important for setting the resting position of the legs. Taken together, these results provided strong support for the CxHP8 prediction generated from the connectome and gives credibility to the functional predictions of the other hair plates on the front leg (**Figure 3.5**). Therefore, the connectome can be used as a tool to prescribe neural circuit function in cases where experimental testing is not feasible.

When investigating the CxHP8 reflex circuit, we found evidence of context-dependent modulation of the circuit. For example, the optogenetic silencing of CxHP8 neurons had no effect on the thorax-coxa joint angles during front leg grooming (**Figure S3.3C**) even though they showed the greatest activity during the same behavior (**Figure 3.2I**). Moreover, CxHP8 neurons had elevated activity during rest periods in which the coxa was positioned medially (**Figure 3.2I**), however, the coxa remained stationary. In both cases, CxHP8 neurons were active, but the reflex to drive posterior leg movement was not engaged suggesting that the reflex circuit activity was suppressed. Presynaptic

inhibition[52], a mechanism shown to modulate proprioceptive signaling in flies[47], doesn't seem to play a role here because the activity of CxHP8 neurons themselves was not modulated during these behaviors. Instead, gain modulation[53] at the level of premotor neurons likely shapes the overall reflex circuit activity in response to different internal and/or behavioral states[54]. Future work should therefore use similar methods employed here to determine which premotor neurons within the CxHP8 reflex circuit have their activity modulated in a behavior-dependent manner.

In addition to CxHP8 neurons, other hair plates and proprioceptive neuron subtypes also likely contribute to controlling the extremes of anterior leg movement. This is evidenced by the ability of the leg to still execute swing-to-stance transitions after CxHP8 neurons were silenced (**Figures 3.3 & 3.4**). In stick insects, for example, the ablation of additional hair plates on the middle leg resulted in non-linear and greater shifts in the AEP of the ipsilateral hind leg[28]. Therefore, information encoded across hair plates may be integrated to achieve a more precise representation of the state of an individual leg and between legs during different behaviors. Even though the integration of hair plate information with that of other proprioceptors, like campaniform sensilla and femoral chordotonal organ neurons[11], remains experimentally unexplored, multisensory integration has been shown in these other proprioceptors. More recent work in the stick insect has shown that the load and movement information encoded by campaniform sensilla and femoral chordotonal organ neurons, respectively, is integrated in premotor networks to control the femur-tibia joint[55]. Similarly, in the fly, electrophysiological recordings revealed that the distinct information encoded by the three subtypes of the femoral chordotonal organ[13] (i.e. claw, hook, and club neurons) is integrated in downstream neurons[49]. Connectomic analyses further provided evidence for multisensory integration across proprioceptors by showing that specific femoral chordotonal organ subtypes have sharded downstream connectivity as well as connectivity with the downstream neurons of hair plates and campaniform sensilla[56]. Multisensory integration may therefore be a key feature of proprioceptive circuits that enables robust motor control and may explain why silencing CxHP8 neurons didn't have a more profound effect on leg movement.

The emergence of biologically realistic neuromechanical models of the fruit fly[2,57] provides an unprecedented way of investigating the role of feedback from hair plates and other proprioceptors in various behaviors. Each model fly is instantiated within an environment governed by physics thereby enabling simulations of naturalistic behavior. For example, using reinforcement

learning, one model fly was able to execute a visual and olfactory guided navigation task[58], whereas the other was capable of visually guided flight[57]. However, these models are devoid of proprioceptors. Given that the location of hair plates at leg joints is known and their morphology is characterized, they can be added to these models (**Figures 3.1 & 3.5**). Once equipped, the joint angles encoded by each hair plate can be predicted by playing realistic leg movements to the model and determining when the hairs of each hair plate are deflected. Therefore, this modeling approach can overcome experimental hurdles, like finding specific driver lines, and provide insights into neural encoding and function. In addition to adding proprioceptors to these models, connectomes[34,35] can be incorporated to enable predictions of proprioceptive neural circuit activity during simulations of naturalistic fly behavior. Such a connectome-constrained model was used to predict activity and biophysical properties of neurons to visual motion within the fly visual system[59]. Altogether, a neuromechanical model of a fruit fly imbued with a connectome and proprioceptors would overcome experimental limitations and provide an in silico means for investigating how proprioceptive feedback from CxHP8 neurons and others is used by neural circuits to control different behaviors.

In summary, we conducted a series of experiments to validate the prediction derived from the connectome that CxHP8 neurons participate in a reflex circuit to transition the leg from moving anterior to posterior. Having gained confidence in the functional predictions of the connectome, we prescribed a functional role in motor control to the other hair plates on the front leg, which otherwise would have been experimentally challenging because of the lack of driver lines to target those neurons. This highlights the power of the connectome in enabling unparalleled predictions of neuronal circuit function. The credibility of these predictions will continue to grow with further experimental validation and the instantiation of connectomes within neuromechanical models.

3.5 Methods

Fly Husbandry and Genotypes

Experiments were performed on adult male flies, *Drosophila melanogaster*, between 2-5 days post-eclosion. Flies were reared in a 25°C incubator with 14:10 light:dark cycle within vials filled with a standard cornmeal and molasses medium. Genotypes used in experiments are listed in Table 3.1.

Stock Name	Genotype	Figure(s)	Stock Source
R48A07 AD: R20C06 DBD > mCD8GFP; Redstinger	w[1118]/ yw, hs flp, UAS-mCD8-GFP; P{+t[7.7]w[=mC]=R48A07-p65.AD}attP40/ UAS-stingerRed; P{y[+t7.7]w[+mC]=R20C06-GAL4.DBD}attP2/+	1	UAS-mCD8GFP; Redstinger was gifted from the Parrish lab, University of Washington and crossed with split-GAL4 gifted from Moon Lab, Yonsei University (Bloomington Stocks #69841 and #71070)
R48A07 AD: R20C06 DBD > pJFRC7-20XUAS-IVS-mCD8::GFP	w[1118]/w[*]; P{+t[7.7]w[=mC]=R48A07-p65.AD}attP40/ +; P{y[+t7.7]w[+mC]=R20C06-GAL4.DBD}attP2/P{pJFRC7-020XUAS-IVS-mCD8::GFP}attP2	1	20X UAS-mCD8::GFP was gifted from the Rubin lab and crossed with split-GAL4 gifted from Moon Lab, Yonsei University (Bloomington Stocks #69841 and #71070)
R48A07 AD: R20C06 DBD > GCaMP6f; tdTomato	w[1118]/+ DL; P{+t[7.7]w[=mC]=R48A07-p65.AD}attP40/ P{w[+mC] = UAS-tdTom.S}2; P{y[+t7.7]w[+mC]=R20C06-GAL4.DBD}attP2/ PBac{y[+mDint2]w[+mC]=20xUAS-IVS-jGCaMP7f}VK00005	3	UAS-GCaMP7f; tdTomato were contrusted from Bloomington stocks #36327 and #79031, and crossed with split-GAL4 gifted from Moon Lab, Yonsei University (Bloomington Stocks #69841 and #71070)
R48A07 AD: R20C06 DBD > ChrimsonR (CxHP8 optogenetic activation)	w[1118]/+ DL; P{+t[7.7]w[=mC]=R48A07-p65.AD}attP40/+ DL; P{y[+t7.7]w[+mC]=R20C06-GAL4.DBD}attP2/10X UAS ChrimsonR mCherry (attp2)/TM3 Sb	4	UAS-ChrimsonR was gifted from Janelia (outcrossing was done by Anne Sustar, University of Washington) and crossed with split-GAL4 gifted from Moon Lab, Yonsei University (Bloomington Stocks #69841 and #71070)
R48A07 AD: R20C06 DBD > GtACR1 (CxHP8 optogenetic silencing)	w[1118]/+ DL; P{+t[7.7]w[=mC]=R48A07-p65.AD}attP40/+ DL; P{y[+t7.7]w[+mC]=R20C06-GAL4.DBD}attP2/20X-UAS-GtACR1-EYFP (III) attp2	4	UAS-GtACR1 stock was created by Anne Sustar in the Tuthill Lab at the University of Washington and was crossed with split-GAL4 gifted from Moon Lab, Yonsei University (Bloomington Stocks #69841 and #71070)
R48A07 AD: R20C06 DBD > Kir 2.1 (CxHP8 chronic silencing)	w[1118]/+ DL; P{+t[7.7]w[=mC]=R48A07-p65.AD}attP40/+ DL; P{y[+t7.7]w[+mC]=R20C06-GAL4.DBD}attP2/pJFRC49-10XUAS-IVS-eGFP::Kir2.1(attP2)	5	Crossed Dickinson Lab Stock U-111 with split-GAL4 gifted from Moon Lab, Yonsei University (Bloomington Stocks #69841 and #71070)
R48A07 AD > Kir 2.1 (Control)	w[1118]/+ DL; P{+t[7.7]w[=mC]=R48A07-p65.AD}attP40/+ DL; pJFRC49-10XUAS-IVS-eGFP::Kir2.1(attP2)/+	5	Crossed Dickinson Lab Stock U-111 with Bloomington Stock #71070
R39B11 AD > Kir	w[1118]/+ DL; P{+t[7.7]w[=mC]=R39B11-p65.AD}attP40/+ DL; pJFRC49-10XUAS-IVS-	5	Crossed Dickinson Lab Stock U-111 with

2.1 (Control)	eGFP::Kir2.1(attP2)/+		Bloomington Stock #71040

Table 3.1. *Drosophila melanogaster* genotypes used for experiments.

Blender Model of *Drosophila* Body and Front Leg Hair Plates

A morphologically accurate model of an adult *Drosophila melanogaster* containing the hair plates at the thorax-coxa and coxa-trochanter joints of the front leg was constructed using the 3D rendering and modeling software, Blender. The body of the fly, and the anatomy and location of hair plates in the model were based on high-resolution confocal images. We replayed the 3D walking kinematics of the left front leg coxa measured from a tethered fly walking on the ball to this model to illustrate the phases during the step cycle when the hairs of each coxa hair plate would be deflected (**Video 3.1**).

Confocal Imaging for Proprioceptor Expression

Peripheral expression of proprioceptors in legs

Front, middle, and/or hind legs of male flies associated with the driver lines in **Table S3.1** crossed with the UAS-mcD8GFP; redstinger reporter line were fixed in a 4% formaldehyde (PFA) PBS solution for 20 minutes and then washed three times in a 0.2% Triton X-100 PBS solution. Legs were then cleared with FocusClear (CelExplorer) and mounted on slides in MountClear (CelExplorer). The expression at each hair plate was assessed using an Olympus FV1000 confocal microscope. The number of proprioceptor cells labeled by each driver line was then determined through visual inspection of the volumetric imaging stacks in FIJI[60]

Central expression of proprioceptors in the brain and VNC

The brain and VNC were dissected from male flies associated with the split-GAL4 driver lines that showed interesting peripheral expression in hair plates, such as the CxHP8 split-GAL4 driver line (i.e. R48A07 AD; R20C06 DBD). Unlike above, the GAL4 driver resulted in the expression of pJFRC7-20XUAS-IVS-mCD8::GFP. The brains and VNCs were fixed in the same manner as legs, but then were put into a blocking solution (5% goat serum, PBS, 0.2% Triton-X) for 20 minutes, followed by being incubated in a blocking and primary antibody solution (1:50 concentration of anti-GFP chicken antibody, 1:50 concentration of anti-brp mouse) for 24 hours at

room temperature. The brains and VNCs were then washed three times in PBS with 0.2% Triton-X and incubated in a blocking and secondary antibody solution (1:250 concentration of anti-chicken-Alexa 488, 1:250 concentration of anti-mouse-Alexa 633). After this, the brains and VNCs were washed three times with PBST and mounted on a slide in Vectashield (Vector Laboratories). The brains and VNCs were imaged with the same Olympus confocal microscope as legs and image stacks were analyzed in FIJI[60].

Reconstruction of Hair Plate Axons in FANC EM dataset

Hair plate axons were reconstructed in the electron microscopy dataset of the female ventral nerve cord, FANC[36], through manual proofreading of the automatically segmented cell fragments in Neuroglancer[61]. Hair axons were identified from previously traced backbones and annotations in CATMAID[36,40]. Annotations containing information about the reconstructed hair plate axons, such as what hair plate they project from, we uploaded to the Connectome Annotation Versioning Engine (CAVE) and are publicly available to those that have access to the FANC dataset. We then determined and proofread the cell fragments that received or provided at least 3 synapses from or onto hair plate axons. In addition to proofreading the upstream and downstream partners of hair plates, we classified them, if possible, into general cell types and specific cell classes using pre-existing CAVE annotation tables and/or expert knowledge[34,45,46,62]. The annotations of these neurons were also uploaded to CAVE and are publicly available. We determined the downstream and upstream partners of hair plates and performed connectivity analyses using a custom Python script. Note that only neurons in which had 10 output synapses onto individual downstream neurons were used in the reflex circuit analyses.

Calcium Imaging of Hair Plate Axons

We used as previously described preparation, setup, and analysis pipeline[47] to image calcium signals in hair plate axons in the neuromere of the left front leg during active and passive leg movements.

Preparation

We attached a fly to a custom-made holder, removed a rectangular piece of cuticle from the dorsal thorax, removed the underlying indirect flight muscles, and used an insect pin to displace the digestive system. This provided a dorsal view on the hair plate axons entering the VNC from the left front leg.

Two-photon image acquisition

Calcium signals in hair plate axons were recorded with a two-photon Movable Objective Microscope (MOM; Sutter Instruments) with a 20x water-immersion objective (Olympus XLUMPlanFI, 0.95 NA, 2.0 mm wd; Olympus). Hair plate neurons expressed the calcium indicator GCaMP7f (green fluorescence) and the structural marker tdTomato (red fluorescence). Fluorophores were excited at 920 nm by a mode-locked Ti:sapphire laser (Chameleon Vision S; Coherent). We used a Pockels cell to keep the power at the back aperture of the objective below ~35 mW. Emitted fluorescence was directed to two high-sensitivity GaAsP photomultiplier tubes (Hamamatsu Photonics) through a 705 nm edge dichroic beamsplitter followed by a 580 nm edge image-splitting dichroic beamsplitter (Semrock). Fluorescence was band-passed filtered by either a 525/50 (green) or 641/75 (red) emission filter (Semrock). Image acquisition was controlled with ScanImage 5.2 (Vidrio Technologies) in Matlab (MathWorks). The microscope was equipped with a galvo-resonant scanner, and the objective was mounted onto a piezo actuator (Physik Instrumente; digital piezo controller E-709). We acquired volumes of three 512 x 512 pixel images spaced 5 μm apart in depth (10 μm total) at a speed of 8.26 volumes per second.

Two-photon image analysis

Two-photon images were smoothed with a Gaussian filter (sigma = 3 pixels; size = 5 x 5 pixels). Each tdTomato image was aligned to the average tdTomato signal of the recorded trial using a cross-correlation-based image registration algorithm[63]. The same alignment was used for the GCaMP images. We averaged the three GCaMP and tdTomato images per volume. Then, we extracted the mean fluorescence in manually drawn regions of interest (ROIs). To correct for vertical movement of the VNC, we computed the ratio of GCaMP fluorescence to tdTomato fluorescence in each frame. To facilitate comparisons across trials and flies, ratio values were z-scored by subtracting the mean of a baseline ratio and dividing by the standard deviation of that baseline ratio. The baseline was defined in each trial as the 10% smallest ratio values. Finally, z-scored ratio values were

upsampled to the sampling rate of leg tracking (300 Hz) using cubic spline interpolation and then low-pass filtered using a moving average filter with a time window of 0.2 s.

Platform and treadmill

The platform consisted of a metal pin (0.5 mm diameter, 4.4 mm length) mounted onto a three-axis micromanipulator (MP-225; Sutter Instruments). The pin was wrapped in black sandpaper to provide sufficient grip for the flies' tarsi. The micromanipulator was controlled manually.

The treadmill consisted of a patterned Styrofoam ball (9.1 mm diameter; 0.12 g) floating on air in an aluminum holder. The air flow was set to ~500 ml/min. The ball was illuminated by two infrared LEDs (850-nm peak wavelength; ThorLabs) via optical fibers. Ball movements were recorded at 30 Hz with a camera (Basler acA1300-200um; Basler AG) equipped with a macro zoom lens (Computar MLM3X-MP; Edmund Optics). Ball rotations around the fly's cardinal body axes (forward, rotational, sideward) were reconstructed offline using FicTrac[64]. Rotational velocities of the fly were calculated based on the known diameter of the ball. Velocities were upsampled to the sampling rate of leg tracking (300 Hz) using cubic spline interpolation and low-pass filtered using a moving average filter with a time window of 0.2 s.

Leg tracking

Movement of the left front leg was recorded at 300 Hz with two cameras (Basler acA800-510um; Basler AG) equipped with 1.0x InfiniStix lenses (68 mm wd; Infinity) and 875 nm short pass filters (Edmund Optics). The leg was illuminated by an infrared LED (850-nm peak wavelength; ThorLabs) via an optical fiber. We used a previously trained[47] deep neural network[48] to automatically track all leg joints in each camera view. 2D tracking data from both camera views were then combined to reconstruct leg joint positions and angles in 3D using Anipose[1].

Behavior classification

Fly behavior was classified semi-automatically based on thresholds on the velocity of the front and middle leg tarsi as described previously[47]. Flies on the platform were classified as resting or actively moving. Flies on the treadmill were classified as resting, walking, or grooming. All classifications were reviewed and manually corrected if necessary.

Data selection

Frames were manually excluded from the analysis if the front leg was involved in movements other than walking or grooming on the treadmill (e.g., extended downward pushing), the femur-tibia joint of the front leg was not tracked correctly, or the two-photon image registration failed (e.g., the VNC moved out of the imaging volume).

Optogenetic Activation and Silencing Experiments

Optogenetic experiments were performed on adult male flies that were raised on ATR for 1-3 days, were 2-5 days old, de-winged, and fixed to a rigid tether (0.1 mm thin tungsten rod) with UV glue (KOA 300). These flies were placed onto a spherical foam ball (weight: 0.13 g; diameter: 9.08mm) suspended by air within a visual arena. A dark bar with a width of 30 degrees with respect to the fly oscillated at 2.7 Hz in front of the fly. A spatially precise red (638 nm; 1200 Hz pulse rate; 30% duty cycle, Laserland) or green (532 nm; 1200 Hz pulse rate; 60% duty cycle, Laserland) laser was then positioned on the thorax-coxa joint of the left front leg. Optogenetic activation experiments were conducted on flies in which their CxHP8 neurons expressed ChrimsonR, whereas silencing experiments were performed on those that expressed GtACR1 in those neurons (**Table 3.1**). Trials were 2 seconds in duration and consisted of turning the laser on (experimental trials) or keeping it off (control trials) 0.5 seconds into the trial for 1 second. During each trial, the behavior each fly was recorded with 6 high-speed cameras (300 fps; Basler acA800-510 µm; Balser AG) and the movement of the ball was recorded at 30 fps with a camera (FMVU-03MTM-CS) and processed using FicTrac[64]. The 3D positions of each leg joint and the corresponding joint angles were determined by using DeepLabCut[48] and Anipose[1]. Kinematic analyses were performed in a custom Python script.

Treadmill Experiments

Treadmill experiments were performed on 2-5 day old CxHP8 silenced and genetically-matched control male flies (**Table 3.1**) using a previously described treadmill system and experimental protocol[51]. The inward rectifying potassium channel, Kir 2.1, was used to silence the activity of CxHP8 neurons throughout development. In short, trials consisted of placing a de-winged fly into a chamber and moving the belts of the split-belt treadmill at a steady-state speed of 10 mm/s for 20 minutes in total. During which, we recorded the behavior of the fly at 200 fps and in 20 second

bouts with 5 high-speed cameras (Basler acA800-510 µm; Balser AG). We then used DeepLabCut[48] and Anipose[1] to reconstruct the 3D positions of head, thorax, abdomen, and each leg tip. Custom Python scripts were used to analyze and visualize walking kinematics and posture.

Kinematic Classification and Parameters

The classification and quantification of behavior, swing and stance, and most walking kinematic parameters for tethered flies and flies walking on the treadmill were conducted in the same manner as a prior study[51]. For tethered flies in both the calcium imaging and optogenetic experiments, steps or frames were classified as forward walking if the instantaneous forward velocity and absolute rotational velocity of the ball was greater than 5 mm/s and less than 25 degrees/s, respectively. Left and right turns were classified as periods where the rotational velocity was less than -25 degrees/s or greater than 25 degrees/s, respectively. Other behaviors, like rest/sanding and front leg grooming, were determined by using a previously published behavioral classifier[1]. For flies walking on the treadmill, forward walking was classified as periods where the body velocity had a forward velocity greater than 5 mm/s and the absolute heading angle with respect to the front of the chamber was less than 15 degrees. Rest periods are classified as those where the instantaneous velocity of the body and all tarsi was less than 5 mm/s (i.e. all legs in stance; see below for the description of swing and stance classification).

During walking, the classification of each leg into swing and stance was based on the smoothed (i.e. with a Gaussian Kernel) instantaneous velocity of the tarsus of each leg. Instantaneous values were negative during periods where the tarsus moved posteriorly along the longitudinal axis of the body. A leg was classified as being in swing if its tarsus had an instantaneous velocity greater than 5 mm/s or less than -25 mm/s. Otherwise, the leg was classified as being in stance. Short, 1 video frame, classifications of swing or stance were corrected and reclassified as the other phase of the step cycle.

Classified forward walking steps were further filtered to remove steps that occurred during the transition into forward walking or produced kinematics that were inconsistent with what was previously published[65–68]. Any step that didn't meet the following criteria for a forward walking step was removed: step frequency between 5 and 20 steps/s, a swing duration between 15 and 75 ms, and

a stance duration less than 200 ms. Steps that passed these filtering criteria were used for further kinematic analyses and comparisons.

All kinematic analyses and visualizations were done in custom Python scripts, which a publicly available on GitHub (GitHub link).

Statistical Analyses

Bootstrapping or t-tests were performed to determine statistical significance. If multiple comparisons were performed, a Bonferroni correction was employed to adjust the threshold of significance. A t-test on the mean CxHP8 calcium activity across flies was used to determine which behaviors had significantly different mean activity compared to rest periods where the coxa was abducted medially. T-tests were also used to compare posture, step kinematics and inter-leg coordination between CxHP8 silenced and control flies. Finally, bootstrapping was used to statistically compare the anterior and posterior extreme positions between these flies.

Glossary of Kinematic Parameters

Body length (BL): the distance between the head and distal part of the abdomen.

Body height: the vertical distance between the ground and thorax.

Body Angle: the angle made by the body frame.

Anterior extreme position: the position where a leg first contacts the ground (i.e. stance onset) in egocentric coordinates.

Posterior extreme position: the position where a leg first takes off from the ground (i.e. swing onset) in egocentric coordinates.

Swing duration: the total lateral and longitudinal distance a leg travels during the swing phase of the step cycle.

Swing duration: the duration of the aerial phase of leg movement during walking.

L1 relative phase: the relative offset in the stance onsets between the left front leg and the leg of interest with respect to the left front leg's step cycle.

Polygon Area: The area in BL^2 of the polygon formed by the tarsi tip positions of the legs in stance.

Acknowledgements

We thank Seok Jun Moon for generously sending us the hair plate split-GAL4 driver line used in this paper (R48A07 AD: R20C06 DBD). B.G.P was supported by an NSF Graduate Research Fellowship (Fellow ID: 2018261272). Other support was provided by National Institutes of Health grants R01NS102333 and U19NS104655, a Searle Scholar Award, a Klingenstein-Simons Fellowship, a Pew Biomedical Scholar Award, a McKnight Scholar Award, a Sloan Research Fellowship, the New York Stem Cell Foundation, and a UW Innovation Award to J.C.T. J.C.T is a New York Stem Cell Foundation – Robertson Investigator.

Author Contributions

B.G.P. and J.C.T. conceived of the study and wrote the manuscript. I.S. created the gorgeous blender model of a fruit fly with hair plates as well as video 1. B.G.P and A.S. performed confocal imaging of hair plates. B.G.P. and A.C. proofread the hair plate axons on their downstream and upstream partners in FANC. C.J.D. collected and processed the calcium imaging data for CxHP8. G.M.C. and S.W.B. collected optogenetic activation and silencing datasets for CxHP8. B.G.P. analyzed the connectivity, calcium imaging, and optogenetic datasets. B.G.P collected and analyzed the kinematics and posture of flies walking in the treadmill setup. A.A. provided valuable feedback about the connectivity of hair plates onto motor circuits.

Data and Code Availability

Data is available on Dryad (TBD). Code for analyzing and visualizing hair plate connectivity in the EM dataset, calcium activity of CxHP8 neurons, kinematics during optogenetic experiments, and walking kinematics and posture during treadmill experiments is located on GitHub (TBD).

Video Legends

Video 3.1. Animation of hair plates on the front leg of a fly walking on a treadmill. The fly and hair plates were rendered in Blender and based on high resolution confocal images. Depicted are the three hair-plates located at the thorax-coxa joint (CxHP4: red; CxHP3: green; CHP8: blue) and three at the coxa-trochanter joint (TrHP5: orange; TrHP7: purple; TrHP6: pink).

3.6 Supplemental information

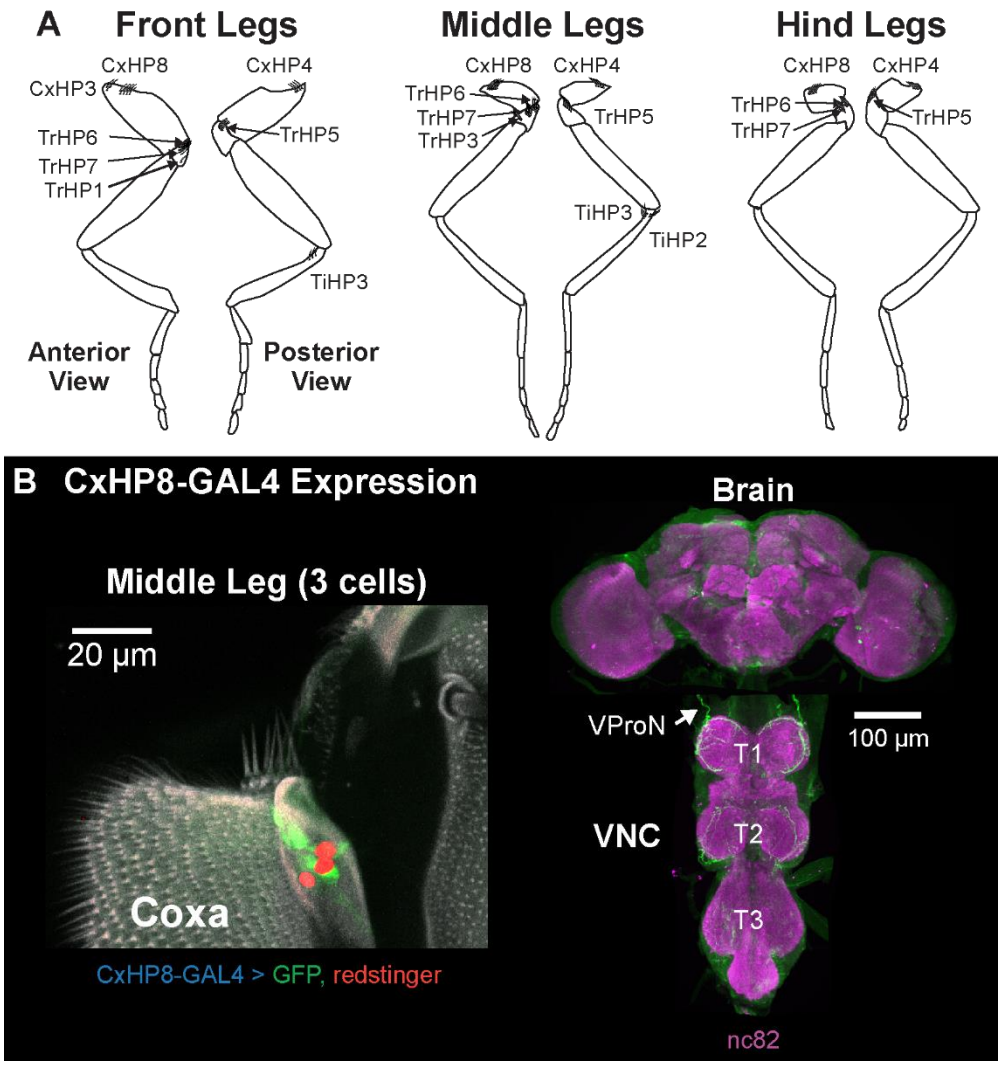

Figure S3.1. Hair plate locations on the legs of *Drosophila* and CxHP8 expression in a specific driver line. (**A**) Schematics of the front, middle, and hind legs showing the locations of hair plates. (**B**) Confocal images showing the expression of the CxHP8 split-GAL4 in the middle leg (3 of 8 neurons labeled), brain, and VNC. The ultrastructure (autofluorescence: gray) of CxHP8 consists of 8 cuticular hairs located on the coxa. Labeled mechanosensory neuron (GFP: green) project through the ventral prothoracic nerve (VProN) into the VNC (nc82: magenta). The cell bodies of CxHP8 neurons are labeled by the nuclear marker, redstinger (red).

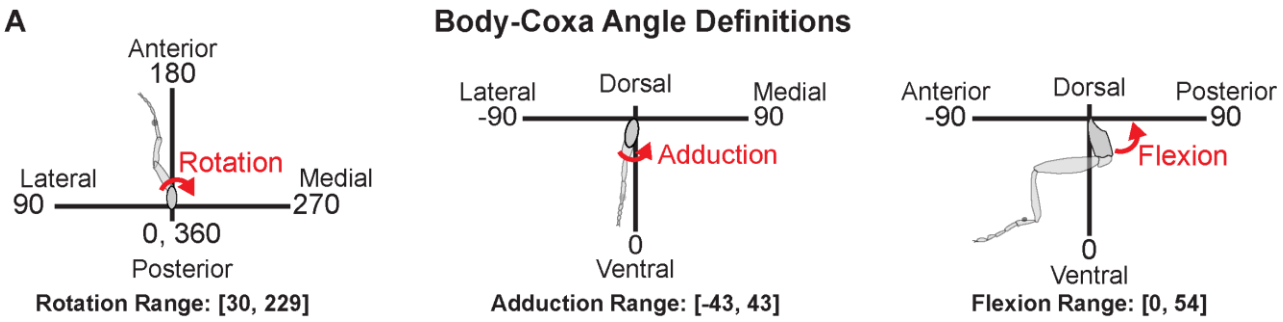

Figure S3.2. Thorax-coxa joint angle definitions. (**A**) Reference frame for the rotation, adduction, and flexion thorax-coxa angles of the front leg. The measured range of each angle is displayed at the bottom.

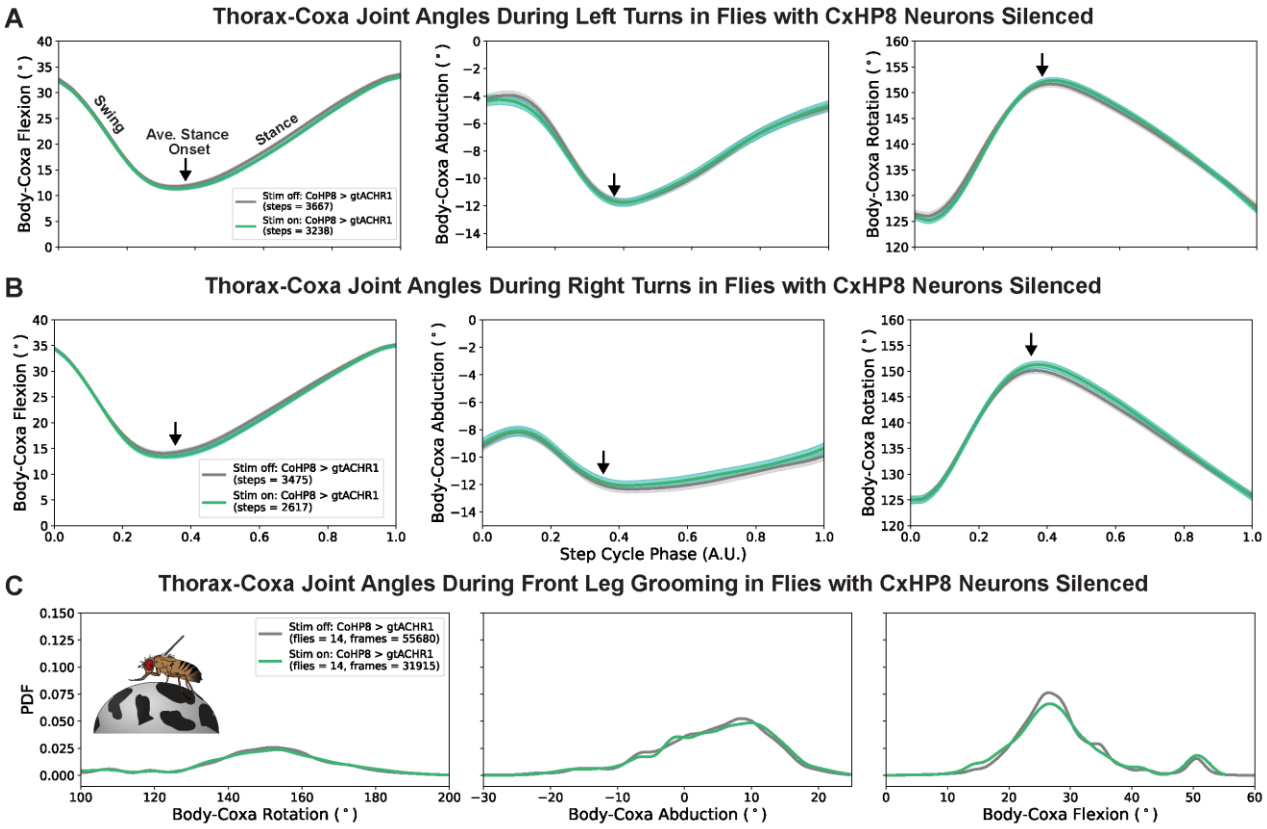

Figure S3.3. CxHP8 silencing had a minimal effect on thorax-coxa joint angles during turning and front leg grooming. (**A**) Optogenetic silencing (teal) of CxHP8 neurons in flies turning left didn't have a significant effect on thorax-coxa angles compared to turning steps when the laser was off. Arrow: the average onset of the stance phase of the step cycle; Shaded region: 95% confidence interval; N: number of flies; n: number of steps. (**B**) Optogenetic silencing of CxHP8 neurons also didn't have a significant effect during right turns. (**C**) Optogenetic silencing (teal) of CxHP8 neurons did not significantly alter the distributions of the thorax-coxa joint angles during front leg grooming compared to grooming when the laser was off (gray). N: number of flies; n: number of frames.

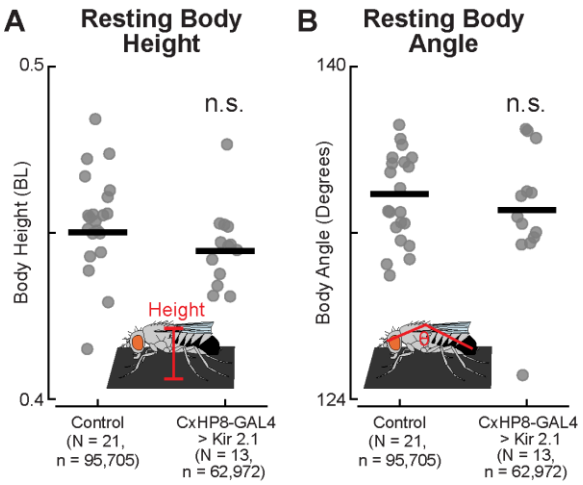

Figure S3.4. CxHP8 feedback does not control body height or angle. (**A**) Body height was not significantly different between CxHP8 silenced and control flies (t-test; $p > 0.05$). N: number of flies; n: number of frames. (**B**) Body angle was also not significantly different between CxHP8 silenced and control flies (t-test; $p > 0.05$). N: number of flies; n: number of frames.

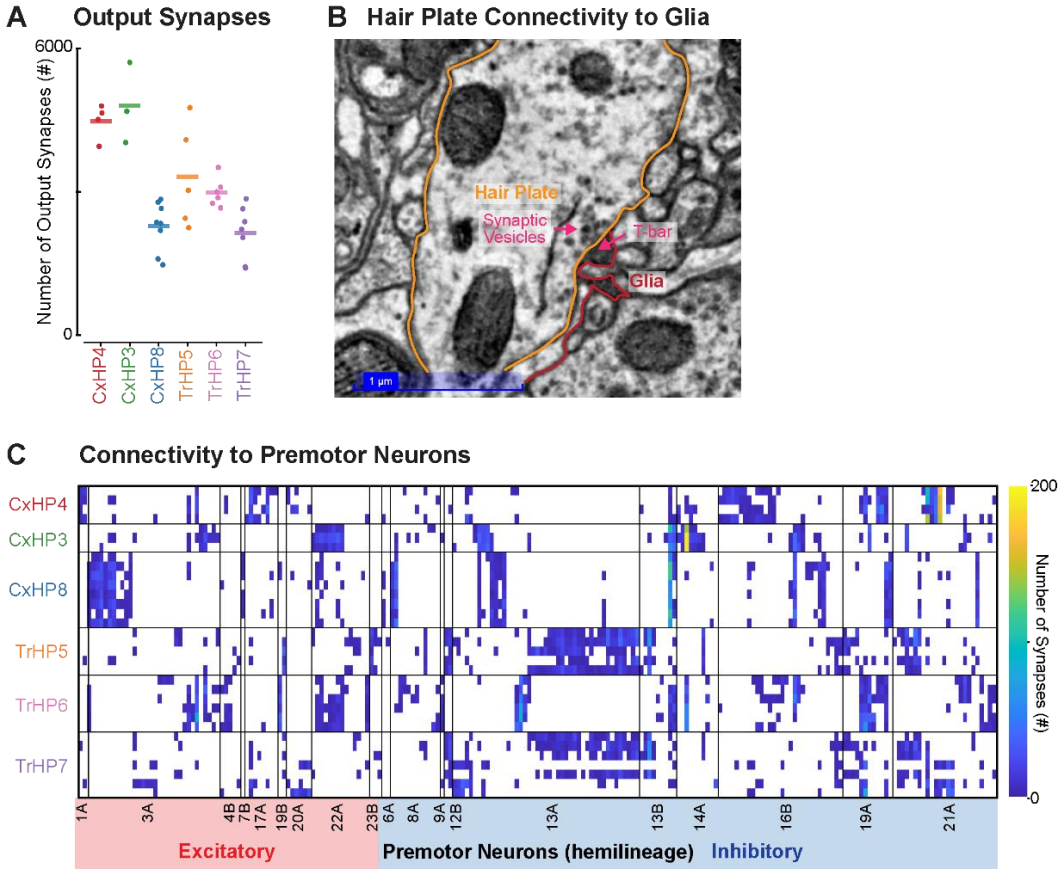

Figure S3.5. Synaptic connectivity of hair plates onto glia and premotor neurons. (**A**) Total number of predicted output synapses of hair plate axons in FANC. Line: mean output synapses; dot: number of output synapses of a single hair plate axon. (**B**) Electron microscopy image illustrating the connectivity between a hair plate axon (orange) and a glia cell (red). Synaptic vesicles and a putative T-bar are labeled. (**C**) Connectivity matrix showing the number of synapses that hair plate axons supply to premotor neurons. Premotor neurons are classified as excitatory (red) or inhibitory (blue) based on their identified hemilineage. Premotor neurons within a hemilineage are arranged according to the proportion of input synapses they receive from each hair plate axon.

Driver Line	Front Leg Proprioceptors										Middle Leg Proprioceptors							Hind Leg Proprioceptors					
	CxHP4	CxHP3	CxHP8	TrHP5	TrHP6	TrHP7	TrHP1	TrCS3 (TrG)	TrCS5 (TrFa)	FeCS11	CxHP4	CxHP8	TrHP5	TrHP6	TrHP7	TrCS3	TrCS2	CxHP4	CxHP8	TrHP5	TrHP6	TrHP7	TrCS3
R48A07 AD: R20C06 DBD	0	0	6	0	0	0	0	0	0	0	0	3	0	0	0	0	0	0	0	0	0	0	0
R93D09 AD: VT061711 DBD	2	0	4	3	0	0	0	3	0	0	0	6	3	3	1	2	0	4	6	3	4	2	0
R93D09 AD: VT009832 DBD	2	2	0	3	2	2	0	0	0	0	2	0	3	2	0	0	1	3	0	3	3	0	0
R93D09 AD: VT040055 DBD	1	0	0	2	0	0	0	2	0	0	2	0	0	0	0	2	0	2	0	0	0	0	2
R93D09 AD: R37G07 DBD	0	0	0	2	1	1	0	0	0	0	1	0	1	0	0	0	0	2	0	0	3	2	0
VT061711 AD: VT045603 DBD	4	0	5	2	0	0	0	3	0	0	3	6	3	2	0	2	0	3	8	2	4	3	3
R93D09 AD: VT038115 DBD	0	0	0	2	2	0	0	0	0	0	0	0	2	0	0	0	0	0	0	2	0	0	0
VT038115 AD: VT040055 DBD	0	0	0	2	0	3	0	0	0	0	N/A	N/A	N/A	N/A	N/A	N/A	N/A	N/A	N/A	N/A	N/A	N/A	N/A
VT0098323 AD: VT061711 DBD	1	0	0	2	0	2	0	2	0	0	N/A	N/A	N/A	N/A	N/A	N/A	N/A	N/A	N/A	N/A	N/A	N/A	N/A
VT0098323 AD: R20C06 DBD	0	0	0	0	0	2	0	3	0	1	N/A	N/A	N/A	N/A	N/A	N/A	N/A	N/A	N/A	N/A	N/A	N/A	N/A
R39B11 AD: VT061711 DBD	0	0	0	3	0	2	0	2	0	3	N/A	N/A	N/A	N/A	N/A	N/A	N/A	N/A	N/A	N/A	N/A	N/A	N/A
R48A07 AD: VT040055 DBD	0	0	0	1	0	1	1	0	0	0	N/A	N/A	N/A	N/A	N/A	N/A	N/A	N/A	N/A	N/A	N/A	N/A	N/A
VT038115 AD: VT061711 DBD	0	0	0	2	0	2	0	0	0	0	N/A	N/A	N/A	N/A	N/A	N/A	N/A	N/A	N/A	N/A	N/A	N/A	N/A
VT0098323 AD: R94E06 DBD	1	0	0	0	0	0	0	0	0	1	N/A	N/A	N/A	N/A	N/A	N/A	N/A	N/A	N/A	N/A	N/A	N/A	N/A
R22D12 AD: VT061711 DBD	2	0	0	0	1	1	0	3	2	3	N/A	N/A	N/A	N/A	N/A	N/A	N/A	N/A	N/A	N/A	N/A	N/A	N/A
R22D12 AD: R94E06 DBD	2	0	4	0	1	0	0	0	0	1	N/A	N/A	N/A	N/A	N/A	N/A	N/A	N/A	N/A	N/A	N/A	N/A	N/A
VT038115 AD: R94E06 DBD	0	0	0	0	0	0	0	0	0	0	N/A	N/A	N/A	N/A	N/A	N/A	N/A	N/A	N/A	N/A	N/A	N/A	N/A
R48A07 AD: R22D12 DBD	4	0	0	0	3	0	0	0	0	0	N/A	N/A	N/A	N/A	N/A	N/A	N/A	N/A	N/A	N/A	N/A	N/A	N/A

R94E06 AD: VT040055 DBD	1	0	0	0	0	3	0	0	0	0	N/A	N/A	N/A	N/A	N/A	N/A	N/A	N/A	N/A	N/A	N/A	N/A	N/A

Table S3.1. Proprioceptor expression of split-GAL4 driver lines in the legs of *Drosophila melanogaster*. The number of cells labeled by the screened split-GAL4 driver lines was determined by counting cells genetically expressing membrane bound GFP and a nuclear reporter (i.e. UAS-mcD8GFP; Redstinger) using confocal imaging. Proprioceptors that did not have their expression checked received a "N/A". The lack of a column for a particular proprioceptive class indicates that either no expression was seen or that proprioceptor was not checked for expression. HP: hair plate; CS: campaniform sensilla.

3.7 References

1. Karashchuk, P., Rupp, K.L., Dickinson, E.S., Walling-Bell, S., Sanders, E., Azim, E., Brunton, B.W., and Tuthill, J.C. (2021). Anipose: A toolkit for robust markerless 3D pose estimation. Cell Rep *36*, 109730. 10.1016/j.celrep.2021.109730.

2. Lobato-Rios, V., Ramalingasetty, S.T., Özdil, P.G., Arreguit, J., Ijspeert, A.J., and Ramdya, P. (2022). NeuroMechFly, a neuromechanical model of adult Drosophila melanogaster. Nature Methods *19*, 620–627. 10.1038/s41592-022-01466-7.

3. Haustein, M., Blanke, A., Bockemühl, T., and Büschges, A. (2024). A leg model based on anatomical landmarks to study 3D joint kinematics of walking in Drosophila melanogaster. bioRxiv, 2024.04.04.588055. 10.1101/2024.04.04.588055.

4. Alexander, R.M. (1989). Optimization and gaits in the locomotion of vertebrates. Physiological Reviews *69*, 1199–1227. 10.1152/physrev.1989.69.4.1199.

5. Cruse, H. (1990). What mechanisms coordinate leg movement in walking arthropods? Trends in Neurosciences *13*, 15–21. 10.1016/0166-2236(90)90057-H.

6. Bidaye, S.S., Bockemühl, T., and Büschges, A. (2018). Six-legged walking in insects: how CPGs, peripheral feedback, and descending signals generate coordinated and adaptive motor rhythms. Journal of Neurophysiology *119*, 459–475. 10.1152/jn.00658.2017.

7. Tuthill, J.C., and Azim, E. (2018). Proprioception. Current Biology *28*, R194–R203. 10.1016/j.cub.2018.01.064.

8. Dietz, V. (2002). Proprioception and locomotor disorders. Nature Reviews Neuroscience *3*, 781–790. 10.1038/nrn939.

9. Proske, U., and Gandevia, S.C. (2012). The Proprioceptive Senses: Their Roles in Signaling Body Shape, Body Position and Movement, and Muscle Force. Physiological Reviews *92*, 1651–1697. 10.1152/physrev.00048.2011.

10. Windhorst, U. (2007). Muscle proprioceptive feedback and spinal networks. Brain Research Bulletin *73*, 155–202. 10.1016/j.brainresbull.2007.03.010.

11. Tuthill, J.C., and Wilson, R.I. (2016). Mechanosensation and Adaptive Motor Control in Insects. Current Biology *26*, R1022–R1038. 10.1016/j.cub.2016.06.070.

12. Burrows, M. (1996). The Neurobiology of an Insect Brain (Oxford University Press).

13. Mamiya, A., Gurung, P., and Tuthill, J.C. (2018). Neural Coding of Leg Proprioception in Drosophila. Neuron *100*, 636-650.e6. 10.1016/j.neuron.2018.09.009.

14. Eidelberg, E., and Woodbury, C.M. (1972). Apparent redundancy in the somatosensory system in monkeys. Experimental Neurology *37*, 573–581. 10.1016/0014-4886(72)90100-8.

15. Burrows, M. (1987). Parallel processing of proprioceptive signals by spiking local interneurons and motor neurons in the locust. J. Neurosci. *7*, 1064–1080. 10.1523/JNEUROSCI.07-04-01064.1987.

16. Kuenzi, F., and Burrows, M. (1995). Central Connections of Sensory Neurones From a Hair Plate Proprioceptor in the Thoraco-Coxal Joint of the Locust. Journal of Experimental Biology *198*, 1589–1601. 10.1242/jeb.198.7.1589.

17. Newland, P.L., Watkins, B., Emptage, N.J., and Nagayama, T. (1995). The Structure, Response Properties and Development of a Hair Plate on the Mesothoracic Leg of the Locust. Journal of Experimental Biology *198*, 2397–2404. 10.1242/jeb.198.11.2397.

18. Pflüger, H.J., Bräunig, P., and Hustert, R. (1981). Distribution and specific central projections of mechanoreceptors in the thorax and proximal leg joints of locusts. Cell and Tissue Research *216*, 79–96. 10.1007/BF00234546.

19. BrÄunig, P., and Hustert, R. (1985). Actions and interactions of proprioceptors of the locust hind leg coxo-trochanteral joint. Journal of Comparative Physiology A *157*, 83–89. 10.1007/BF00611098.

20. BrÄunig, P., and Hustert, R. (1985). Actions and interactions of proprioceptors of the locust hind leg coxo-trochanteral joint. Journal of Comparative Physiology A *157*, 73–82. 10.1007/BF00611097.

21. Wong, R.K., and Pearson, K.G. (1976). Properties of the trochanteral hair plate and its function in the control of walking in the cockroach. Journal of Experimental Biology *64*, 233–249. 10.1242/jeb.64.1.233.

22. Pringle, J.W.S. (1938). Proprioception in Insects: III. The Function of the Hair Sensilla at the Joints. Journal of Experimental Biology *15*, 467–473. 10.1242/jeb.15.4.467.

23. Pearson, K.G., Wong, R.K., and Fourtner, C.R. (1976). Connexions between hair-plate afferents and motoneurones in the cockroach leg. Journal of Experimental Biology *64*, 251–266. 10.1242/jeb.64.1.251.

24. French, A.S., and Sanders, E.J. (1979). The mechanism of sensory transduction in the sensilla of the trochanteral hair plate of the cockroach, Periplaneta americana. Cell and Tissue Research *198*, 159–174. 10.1007/BF00234843.

25. Wendler, G. (1972). Körperhaltung bei der Stabheuschrecke: Ihre Beziehung zur Schwereorientierung und Mechanismen ihrer Regelung. Verhandlungen der Deutschen Zoologischen Gesellschaft, 214–219.

26. Bässler, U. (1977). Sensory control of leg movement in the stick insect Carausius morosus. Biological Cybernetics *25*, 61–72. 10.1007/BF00337264.

27. Graham, D., and Wendler, G. (1981). The reflex behaviour and innervation of the tergo-coxal retractor muscles of the stick insectCarausius morosus. Journal of comparative physiology *143*, 81–91. 10.1007/BF00606071.

28. Cruse, H., Dean, J., and Suilmann, M. (1984). The contributions of diverse sense organs to the control of leg movement by a walking insect. Journal of Comparative Physiology A *154*, 695–705. 10.1007/BF01350223.

29. Schmitz, J. (1986). The depressor trochanteris motoneurones and their role in the coxo-trochanteral feedback loop in the stick insect Carausius morosus. Biological Cybernetics *55*, 25–34. 10.1007/BF00363975.

30. Schmitz, J. (1986). Properties of the feedback system controlling the coxa-trochanter joint in the stick insect Carausius morosus. Biological Cybernetics *55*, 35–42. 10.1007/BF00363976.

31. Büschges, A., and Schmitz, J. (1991). Nonspiking pathways antagonize the resistance reflex in the thoraco-coxal joint of stick insects. Journal of Neurobiology *22*, 224–237. 10.1002/neu.480220303.

32. Smith, S.A., and Shepherd, D. (1996). Central afferent projections of proprioceptive sensory neurons in Drosophila revealed with the enhancer-trap technique. Journal of Comparative Neurology *364*, 311–323. 10.1002/(SICI)1096-9861(19960108)364:2<311::AID-CNE9>3.0.CO;2-8.

33. Dorkenwald, S., Matsliah, A., Sterling, A.R., Schlegel, P., Yu, S., McKellar, C.E., Lin, A., Costa, M., Eichler, K., Yin, Y., et al. (2023). Neuronal wiring diagram of an adult brain. bioRxiv, 2023.06.27.546656. 10.1101/2023.06.27.546656.

34. Azevedo, A., Lesser, E., Mark, B., Phelps, J., Elabbady, L., Kuroda, S., Sustar, A., Moussa, A., Kandelwal, A., Dallmann, C.J., et al. (2022). Tools for comprehensive reconstruction and analysis of Drosophila motor circuits. bioRxiv, 2022.12.15.520299. 10.1101/2022.12.15.520299.

35. Takemura, S., Hayworth, K.J., Huang, G.B., Januszewski, M., Lu, Z., Elizabeth C Marin, Stephan Preibisch, C Shan Xu, John Bogovic, Andrew S Champion, et al. (2023). A Connectome of the Male Drosophila Ventral Nerve Cord. bioRxiv, 2023.06.05.543757. 10.1101/2023.06.05.543757.

36. Phelps, J.S., Hildebrand, D.G.C., Graham, B.J., Kuan, A.T., Thomas, L.A., Nguyen, T.M., Buhmann, J., Azevedo, A.W., Sustar, A., Agrawal, S., et al. (2021). Reconstruction of motor control circuits in adult Drosophila using automated transmission electron microscopy. Cell *184*, 759-774.e18. 10.1016/j.cell.2020.12.013.

37. Schubiger, G. (1968). Anlageplan, Determinationszustand und Transdeterminationsleistungen der männlichen Vorderbeinscheibe vonDrosophila melanogaster. Wilhelm Roux' Archiv für Entwicklungsmechanik der Organismen *160*, 9–40. 10.1007/BF00573645.

38. Petryszak, A., and Fudalewicz-Niemczyk, W. (1994). External proprioceptors on the legs of insects of higher orders. Acta Biologica Cracoviensia. Series Zoologia *36*, 13–22.

39. Hodgkin, H.M., and Bryant, P.J. (1979). Scanning electron microscopy of the adult of Drosophila melanogaster. Genetics and biology of Drosophila 2.

40. Kuan, A.T., Phelps, J.S., Thomas, L.A., Nguyen, T.M., Han, J., Chen, C.-L., Azevedo, A.W., Tuthill, J.C., Funke, J., Cloetens, P., et al. (2020). Dense neuronal reconstruction through X-ray holographic nano-tomography. Nature Neuroscience, 1–7. 10.1038/s41593-020-0704-9.

41. Trimarchi, J.R., Jin, P., and Murphey, R.K. (1999). Controlling the Motor Neuron. In International Review of Neurobiology Neuromuscular Junctions in Drosophila., R. A. H. and P. J. Ronald J. Bradley, ed. (Academic Press), pp. 241–264. 10.1016/S0074-7742(08)60548-6.

42. Oh, S.M., Jeong, K., Seo, J.T., and Moon, S.J. (2021). Multisensory interactions regulate feeding behavior in Drosophila. Proceedings of the National Academy of Sciences *118*, e2004523118. 10.1073/pnas.2004523118.

43. Murphey, R.K., Possidente, D., Pollack, G., and Merritt, D.J. (1989). Modality-specific axonal projections in the CNS of the flies Phormia and Drosophila. Journal of Comparative Neurology *290*, 185–200. 10.1002/cne.902900203.

44. Merritt, D.J., and Murphey, R.K. (1992). Projections of leg proprioceptors within the CNS of the fly Phormia in relation to the generalized insect ganglion. Journal of Comparative Neurology *322*, 16–34. 10.1002/cne.903220103.

45. Lesser, E., Azevedo, A.W., Phelps, J.S., Elabbady, L., Cook, A., Mark, B., Kuroda, S., Sustar, A., Moussa, A., Dallmann, C.J., et al. (2023). Synaptic architecture of leg and wing motor control networks in Drosophila. bioRxiv, 2023.05.30.542725. 10.1101/2023.05.30.542725.

46. Lacin, H., Chen, H.-M., Long, X., Singer, R.H., Lee, T., and Truman, J.W. (2019). Neurotransmitter identity is acquired in a lineage-restricted manner in the Drosophila CNS. Elife *8*. 10.7554/eLife.43701.

47. Dallmann, C.J., Agrawal, S., Cook, A., Brunton, B.W., and Tuthill, J.C. (2023). Presynaptic inhibition selectively suppresses leg proprioception in behaving Drosophila. bioRxiv, 2023.10.20.563322. 10.1101/2023.10.20.563322.

48. Mathis, A., Mamidanna, P., Cury, K.M., Abe, T., Murthy, V.N., Mathis, M.W., and Bethge, M. (2018). DeepLabCut: markerless pose estimation of user-defined body parts with deep learning. Nature Neuroscience *21*, 1281. 10.1038/s41593-018-0209-y.

49. Agrawal, S., Dickinson, E.S., Sustar, A., Gurung, P., Shepherd, D., Truman, J.W., and Tuthill, J.C. (2020). Central processing of leg proprioception in Drosophila. Elife *9*, e60299. 10.7554/eLife.60299.

50. Azevedo, A.W., Dickinson, E.S., Gurung, P., Venkatasubramanian, L., Mann, R.S., and Tuthill, J.C. (2020). A size principle for recruitment of Drosophila leg motor neurons. eLife *9*, e56754. 10.7554/eLife.56754.

51. Pratt, B.G., Lee, S.-Y.J., Chou, G.M., and Tuthill, J.C. (2024). Miniature linear and split-belt treadmills reveal mechanisms of adaptive motor control in walking Drosophila. bioRxiv, 2024.02.23.581656. 10.1101/2024.02.23.581656.

52. Clarac, F., and Cattaert, D. (1996). Invertebrate presynaptic inhibition and motor control. Exp Brain Res *112*, 163–180. 10.1007/BF00227635.

53. Azim, E., and Seki, K. (2019). Gain control in the sensorimotor system. Curr Opin Physiol *8*, 177–187. 10.1016/j.cophys.2019.03.005.

54. Devineni, A.V., and Scaplen, K.M. (2022). Neural Circuits Underlying Behavioral Flexibility: Insights From Drosophila. Frontiers in Behavioral Neuroscience *15*.

55. Gebehart, C., Schmidt, J., and Büschges, A. (2021). Distributed processing of load and movement feedback in the premotor network controlling an insect leg joint. Journal of Neurophysiology *125*, 1800–1813. 10.1152/jn.00090.2021.

56. Lee, S.-Y.J., Dallmann, C.J., Cook, A., Tuthill, J.C., and Agrawal, S. (2024). Divergent neural circuits for proprioceptive and exteroceptive sensing of the Drosophila leg. bioRxiv, 2024.04.23.590808. 10.1101/2024.04.23.590808.

57. Vaxenburg, R., Siwanowicz, I., Merel, J., Robie, A.A., Morrow, C., Novati, G., Stefanidi, Z., Card, G.M., Reiser, M.B., Botvinick, M.M., et al. (2024). Whole-body simulation of realistic fruit fly locomotion with deep reinforcement learning. bioRxiv, 2024.03.11.584515. 10.1101/2024.03.11.584515.

58. Wang-Chen, S., Stimpfling, V.A., Özdil, P.G., Genoud, L., Hurtak, F., and Ramdya, P. (2023). NeuroMechFly 2.0, a framework for simulating embodied sensorimotor control in adult Drosophila. bioRxiv, 2023.09.18.556649. 10.1101/2023.09.18.556649.

59. Lappalainen, J.K., Tschopp, F.D., Prakhya, S., McGill, M., Nern, A., Shinomiya, K., Takemura, S., Gruntman, E., Macke, J.H., and Turaga, S.C. (2023). Connectome-constrained deep mechanistic networks predict neural responses across the fly visual system at single-neuron resolution. bioRxiv, 2023.03.11.532232. 10.1101/2023.03.11.532232.

60. Schindelin, J., Arganda-Carreras, I., Frise, E., Kaynig, V., Longair, M., Pietzsch, T., Preibisch, S., Rueden, C., Saalfeld, S., Schmid, B., et al. (2012). Fiji: an open-source platform for biological-image analysis. Nat Methods *9*, 676–682. 10.1038/nmeth.2019.

61. Maitin-Shepard, J., Baden, A., Silversmith, W., Perlman, E., Collman, F., Blakely, T., Funke, J., Jordan, C., Falk, B., Kemnitz, N., et al. (2021). google/neuroglancer: Version v2.23 (Zenodo). 10.5281/zenodo.5573294 10.5281/zenodo.5573294.

62. Harris, R.M., Pfeiffer, B.D., Rubin, G.M., and Truman, J.W. (2015). Neuron hemilineages provide the functional ground plan for the Drosophila ventral nervous system. eLife *4*, e04493. 10.7554/eLife.04493.

63. Guizar-Sicairos, M., Thurman, S.T., and Fienup, J.R. (2008). Efficient subpixel image registration algorithms. Optics letters *33*, 156–158. 10.1364/OL.33.000156.

64. Moore, R.J.D., Taylor, G.J., Paulk, A.C., Pearson, T., van Swinderen, B., and Srinivasan, M.V. (2014). FicTrac: A visual method for tracking spherical motion and generating fictive animal paths. Journal of Neuroscience Methods *225*, 106–119. 10.1016/j.jneumeth.2014.01.010.

65. Mendes, C.S., Bartos, I., Akay, T., Márka, S., and Mann, R.S. (2013). Quantification of gait parameters in freely walking wild type and sensory deprived Drosophila melanogaster. eLife Sciences *2*, e00231. 10.7554/eLife.00231.

66. DeAngelis, B.D., Zavatone-Veth, J.A., and Clark, D.A. (2019). The manifold structure of limb coordination in walking Drosophila. eLife *8*, e46409. 10.7554/eLife.46409.

67. Wosnitza, A., Bockemühl, T., Dübbert, M., Scholz, H., and Büschges, A. (2013). Inter-leg coordination in the control of walking speed in Drosophila. Journal of Experimental Biology *216*, 480–491. 10.1242/jeb.078139.

68. Strauss, R., and Heisenberg, M. (1990). Coordination of legs during straight walking and turning in Drosophila melanogaster. J. Comp. Physiol. A *167*, 403–412.

Chapter 4.
Concluding remarks

In this dissertation, I described how novel treadmill systems and innovations in deep learning enabled the discovery of fundamental principles of how proprioceptive feedback facilitates adaptive walking. In **Chapter 2**, I presented the linear and split-belt treadmill systems I engineered and highlighted their ability to coerce and perturb walking in flies. Using these systems with modern pose estimation tools[1,2], colleagues and I found that flies on the treadmill walk in a similar manner as freely walking flies, but that the walking of tethered flies is subtly distinct. Moreover, I used the linear treadmill to show that proprioceptive feedback is important for controlling step kinematics across the naturalistic range of walking speeds, which challenged the previous notion that it is only needed at slow walking speeds. Using the split-belt treadmill, I lastly revealed that the middle legs of flies correct for asymmetric perturbations to keep them on a straight walking course. Overall, **Chapter 2** demonstrated how miniature treadmill systems can overcome prior experimental barriers and lead to new discoveries of proprioception's role in adaptive walking, such as controlling step kinematics across all walking speeds.

Additionally, **Chapter 3** combined the FANC connectome a with myriad of experimental approaches to provide insights into how hair plate proprioceptors adaptively control the extremes of leg movement during walking. Using the connectome, I found that different hair plates on the fly front leg are predicted to control distinct aspects of leg movement. Then by using calcium imaging, optogenetics, and my treadmill systems, my colleagues and I validated the prediction that CxHP8, a hair plate on the coxa, facilitates the anterior to posterior transition of leg movement. Thus, the connectivity motifs derived from the connectome, in this case reflex circuit motifs, provide strong functional predictions for proprioceptors in the control of locomotion. Without driver lines to label each hair plate on the fly leg, we used these predictions to understand the contribution of each hair plate in adaptive leg movement. In summary, the connectome has enabled an unparalleled ability to characterize the architecture and ascribe function to proprioceptive circuits.

Although connectomes are powerful in generating testable hypotheses based on neural connectivity, future work should aim to simulate the neural activity within these connectomes. Unlike in *C. elegans*[3], the nervous system of the fruit fly is too large and experimental approaches only enable the characterization of the simultaneous activity of a subset of neurons. However, models that are constrained by the connectome, like one used to predict biophysical properties and neural activity within the fly visual system[4], can be used to bypass these experimental limitations in flies. In the context of proprioception, connectome models can be combined with proprioceptor encoding models[5] to understand how naturalistic movements are represented within proprioceptive circuits. For example, given the encoding properties of hair plates, naturalistic movements of the coxa can be replayed within a connectome-constrained model to determine how hair plate activity influences the activity of neurons within downstream circuits. In addition, connectome-constrained models may reveal the sources of context-dependent modulation onto neural circuits[6], like those which may be modulating the activity of premotor neurons within hair plate reflex circuits. The main obstacle to building these connectome-constrained models is initializing realistic spontaneous activity across neurons. However, once a realistic connectome model is built, it can be rigged up to neuromechanical models of the fruit fly[7,8] to enable closed loop interactions between the body, nervous system, and the environment – a feat that would allow for a deep understanding of how neural circuit function produces rich behavior in complex environments.

Future work should also further develop and use the treadmill systems described in **Chapter 2** to study more aspects of adaptive motor control. Even though the split-belt treadmill can perturb the coordination between the legs, a way to precisely disrupt the movement of a single leg or joint does not exist. Like in cockroaches[9], magnets glued onto different parts of the fly leg or different legs could be used with magnetic fields to perturb single leg movement in walking flies. Moreover, advances in real-time and closed loop tracking algorithms[10] may make it possible to perturb single leg movement during a specific part of the step cycle. With these capabilities, it may be possible to determine how proprioceptive feedback enables flies and other animals to recover walking after unexpected errors in leg movement. In addition to equipping the treadmill with ways to perturb single leg movement, visual arenas should also be incorporated into the treadmill system. Visual feedback has been shown to control walking kinematics in flies[11]. However, as flies walk on the treadmill, there is a mismatch between how fast their legs are moving and the amount of optic flow – picture sprinting on a treadmill in an empty gym; perceptually

nothing changes about the visual scene. After running on a treadmill, humans were shown to experience a visual illusion that made them perceive that they were moving at an accelerated pace[12]. Therefore, a treadmill equipped with visual arenas could make it possible to study the interaction between proprioceptive and visual feedback in walking flies. In summary, these are a few of many improvements that can be made to these treadmill systems to further study the role of proprioception in adaptive walking.

Overall, in my doctoral work, I engineered miniature treadmill systems and exploited advances in deep learning to reveal new ways in which the proprioceptive system contributes to adaptive motor control. Given that these treadmills are cheap and easy to construct, my goal is for them to be adopted by the broader scientific community to facilitate discoveries in the neural control of locomotion. Lastly, I want to thank you, the reader, for taking the time to look over my dissertation, which was hopefully interesting and thought provoking.

References

1. Karashchuk, P., Rupp, K.L., Dickinson, E.S., Walling-Bell, S., Sanders, E., Azim, E., Brunton, B.W., and Tuthill, J.C. (2021). Anipose: A toolkit for robust markerless 3D pose estimation. Cell Rep *36*, 109730. 10.1016/j.celrep.2021.109730.

2. Mathis, A., Mamidanna, P., Cury, K.M., Abe, T., Murthy, V.N., Mathis, M.W., and Bethge, M. (2018). DeepLabCut: markerless pose estimation of user-defined body parts with deep learning. Nature Neuroscience *21*, 1281. 10.1038/s41593-018-0209-y.

3. Nguyen, J.P., Shipley, F.B., Linder, A.N., Plummer, G.S., Liu, M., Setru, S.U., Shaevitz, J.W., and Leifer, A.M. (2016). Whole-brain calcium imaging with cellular resolution in freely behaving Caenorhabditis elegans. Proceedings of the National Academy of Sciences *113*, E1074–E1081. 10.1073/pnas.1507110112.

4. Lappalainen, J.K., Tschopp, F.D., Prakhya, S., McGill, M., Nern, A., Shinomiya, K., Takemura, S., Gruntman, E., Macke, J.H., and Turaga, S.C. (2023). Connectome-constrained deep mechanistic networks predict neural responses across the fly visual system at single-neuron resolution. bioRxiv, 2023.03.11.532232. 10.1101/2023.03.11.532232.

5. Dallmann, C.J., Agrawal, S., Cook, A., Brunton, B.W., and Tuthill, J.C. (2023). Presynaptic inhibition selectively suppresses leg proprioception in behaving Drosophila. bioRxiv, 2023.10.20.563322. 10.1101/2023.10.20.563322.

6. Azim, E., and Seki, K. (2019). Gain control in the sensorimotor system. Curr Opin Physiol *8*, 177–187. 10.1016/j.cophys.2019.03.005.

7. Vaxenburg, R., Siwanowicz, I., Merel, J., Robie, A.A., Morrow, C., Novati, G., Stefanidi, Z., Card, G.M., Reiser, M.B., Botvinick, M.M., et al. (2024). Whole-body simulation of realistic fruit fly locomotion with deep reinforcement learning. bioRxiv, 2024.03.11.584515. 10.1101/2024.03.11.584515.

8. Lobato-Rios, V., Ramalingasetty, S.T., Özdil, P.G., Arreguit, J., Ijspeert, A.J., and Ramdya, P. (2022). NeuroMechFly, a neuromechanical model of adult Drosophila melanogaster. Nature Methods *19*, 620–627. 10.1038/s41592-022-01466-7.

9. Couzin-Fuchs, E., Kiemel, T., Gal, O., Ayali, A., and Holmes, P. (2015). Intersegmental coupling and recovery from perturbations in freely running cockroaches. Journal of Experimental Biology *218*, 285–297. 10.1242/jeb.112805.

10. Kane, G.A., Lopes, G., Saunders, J.L., Mathis, A., and Mathis, M.W. (2020). Real-time, low-latency closed-loop feedback using markerless posture tracking. eLife *9*, e61909. 10.7554/eLife.61909.

11. Creamer, M.S., Mano, O., and Clark, D.A. (2018). Visual Control of Walking Speed in Drosophila. Neuron *100*, 1460-1473.e6. 10.1016/j.neuron.2018.10.028.

12. Pelah, A., and Barlow, H.B. (1996). Visual illusion from running. Nature *381*, 283–283. 10.1038/381283a0.